Copyright
by
Tae Yoon Kim
2006

The Dissertation Committee for Tae Yoon Kim
certifies that this is the approved version of the following dissertation:

Rate-Robustness Tradeoffs in Multicarrier Wireless Communications

Committee:

Jeffrey G. Andrews, Supervisor

Gustavo de Veciana

John E. Gilbert

Robert W. Heath, Jr.

Sriram Vishwanath

Rate-Robustness Tradeoffs in Multicarrier Wireless Communications

by

Tae Yoon Kim, B.S., M.S.

DISSERTATION

Presented to the Faculty of the Graduate School of

The University of Texas at Austin

in Partial Fulfillment

of the Requirements

for the Degree of

DOCTOR OF PHILOSOPHY

THE UNIVERSITY OF TEXAS AT AUSTIN

December 2006

To my family and parents.

Acknowledgments

First of all, I would like to gratefully thank my supervisor, Dr. Jeffrey G. Andrews, for his guidance and support throughout my research at the University of Texas at Austin. He showed me the fundamentals of research and guided me with great insight, broad and profound knowledge, and encouragement.

I am also sincerely grateful to my committee members, Dr. Gustavo de Veciana, Dr. Robert W. Heath, Jr., Dr. Sriram Vishwanath, and Dr. John E. Gilbert, for their invaluable advice and thoughtful comments throughout my graduate studies. Their comments and insights made my research more fruitful. I'm honored to have them on my committee.

I would like to express my thanks to all current and former members in the Wireless Networking and Communications Group for the wonderful friendship and helpful advice, especially my lab members, Jaeweon Kim, Wan Choi, Kabin Huang, Runhua Chen, and Aamir Hasan. I would like to especially thank Changyong Shin, Yung Yi, and Andrew Hunter for their various help and constructive discussions.

Furthermore, I would like to thank the Ministry of Information and Communication of Korea for its financial support during my study at the University of Texas at Austin.

I am especially indebted to my parents, Heasam Kim and Seongja Yang for their sustained love and encouragement throughout my education. All of my

academic successes can be traced back to them.

Finally, I would like to dedicate this dissertation to my wife Youngjoo (Christine) Bien and my sons Daehyun (Brian) and Donghyun (Jayden) for their love, support and encouragement. Without them, it would have been impossible to accomplish this.

Rate-Robustness Tradeoffs in Multicarrier Wireless Communications

Publication No. _____

Tae Yoon Kim, Ph.D.
The University of Texas at Austin, 2006

Supervisor: Jeffrey G. Andrews

Emerging wireless communication systems exploit various resources to increase their robustness and data rate. Since these resources are limited, there is a tradeoff between the need for robust communication and the desire for high throughput. The aim of this dissertation is to study and optimally balance this tradeoff for a few important cases in multicarrier communications.

First, multi-code code division multiple access (CDMA) techniques tradeoff the number of supportable subscribers with the per subscriber data rate. However, the interference scales linearly with the data rate of each user since they use multiple codes. To resolve this interference problem, a novel multi-code multicarrier CDMA system is proposed, and this system clearly outperforms previous systems in terms of bit error probability and user capacity. This shows that flexible data rates can be successfully balanced with robustness in a multiuser multi-rate CDMA system by carefully choosing the data rates number of subcarriers.

Second, in multiple-input multiple-output orthogonal frequency division multiplexing (MIMO-OFDM), pilots are used to estimate the channel, but in addition to consuming bandwidth, they reduce the transmitted energy for data symbols under a fixed transmit power constraint. This suggests a tradeoff between the power allowed to data symbols and the accuracy of channel estimation. The optimal pilot-to-data power ratio (PDPR) for maximizing a capacity lower bound is formulated and derived for four likely pilot patterns and two different channel conditions. The optimal PDPR shows about 10%∼30% higher capacity lower bound than equal power allocation.

Third, and closely related to the second contribution, adaptive M-QAM, spectral efficiency, and symbol error rate (SER) are considered since these are respectively the dominant modulation type and quality metrics in emerging standards. The effect of the system structure on the PDPR is analytically shown, and the optimal PDPR for minimizing the average SER and maximizing the spectral efficiency is derived for two well-known linear receivers; zero-forcing and minimum mean-square error. The distributions of the SNR (including channel estimation error) for these receivers are derived and used to find the optimal PDPR. Exact guidelines are provided for the power allocation between data and pilot symbols for these cases.

Table of Contents

Acknowledgments v

Abstract vii

List of Figures xiii

Chapter 1. Introduction 1

1.1 Multicarrier Communications 1

1.2 The Rate-Robustness Tradeoff 5

1.2.1 Data Rate and Interference Robustness Tradeoff in Multicarrier CDMA with a Multi-code Scheme 8

1.2.2 Pilot-Data Power Allocation Tradeoff in OFDM 8

1.3 Contributions and Organization of the Dissertation 9

Chapter 2. Variable Data Rate and Interference Robustness Tradeoff 12

2.1 Introduction 12

2.2 System Model and Time-Frequency Signaling Gain 15

2.3 System Analysis 18

2.3.1 Signal Description 18

2.3.2 Analysis of the Output of the Matched Filter 20

2.3.3 Probability of Symbol Error for the case of an M-ary Signal using an Orthogonal Code Sequence ($M \geq 2$) 23

2.3.4 Probability of Symbol Error for the case of an M-ary Signal using Non-orthogonal Code Sequences ($M \geq 2$) 25

2.4 Performance Comparison for MC-MC-CDMA 26

2.5 Chapter Summary 32

Chapter 3. Power Allocation Tradeoff in MIMO Multicarrier Systems - Theoretical Capacity **34**

3.1 Introduction . . . 34
3.2 System Description . . . 37
3.3 PDPR for Static Channels . . . 39
3.3.1 Channel Estimation with Different Pilot Patterns . . . 40
3.3.2 Maximizing a Capacity Lower Bound . . . 44
3.3.3 Optimal PDPR of IPP, OPP, and SPP-1 . . . 47
3.3.4 Optimal PDPR of SPP-2 . . . 49
3.4 PDPR for Dynamic Channels . . . 51
3.4.1 Interpolated Symbols . . . 52
3.4.1.1 MMSE Frequency Interpolation . . . 53
3.4.1.2 MMSE Time Interpolation . . . 54
3.4.2 Maximizing the Capacity Lower Bound . . . 55
3.4.3 Optimal PDPR . . . 56
3.5 Results and Interpretation . . . 57
3.5.1 Ergodic Capacity with the Optimal PDPR for Static Channels 58
3.5.2 Ergodic Capacity with the Optimal PDPR for Dynamic Channels . . . 61
3.5.3 PDPR for Practical Systems . . . 64
3.6 Chapter Summary . . . 66

Chapter 4. Power Allocation Tradeoff in M-QAM MIMO Multicarrier Systems - Practical Performance **68**

4.1 Introduction . . . 68
4.2 System Model and Channel Estimation . . . 70
4.2.1 System Model . . . 70
4.2.2 LS Channel Estimation . . . 72
4.2.3 MMSE Channel Estimation . . . 75
4.3 SNR Analysis with PDPR . . . 76
4.3.1 Average SNR of ZF Receiver with LS Channel Estimation . . 76
4.3.2 Average SNR of MMSE Receiver with MMSE Channel Estimation . . . 80
4.4 Effect of the PDPR on MIMO-OFDM with a Linear Receiver . . . 82

4.4.1 Optimal PDPR of Minimizing Average SER of Non-adaptive M-QAM Modulation . . . 82
4.4.1.1 ZF Receiver . . . 83
4.4.1.2 MMSE Receiver . . . 84
4.4.2 Optimal PDPR for Adaptive Modulation . . . 85
4.4.2.1 ZF Receiver . . . 89
4.4.2.2 MMSE Receiver . . . 90
4.5 Numerical Results . . . 90
4.5.1 Effect of the PDPR on the Average SER of M-QAM MIMO-OFDM . . . 90
4.5.2 Effect of the PDPR on Adaptive Modulation . . . 92
4.5.3 Validating the Optimal PDPR in a Practical Channel Model . 95
4.6 Chapter Summary . . . 98

Chapter 5. Conclusion **100**
5.1 Future Research . . . 103

Appendices **106**

Appendix A. Derivation of the Decision Variable: the Output of the Matched Filter **107**

Appendix B. Channel Estimation and Interpolation Error Analysis **110**
B.1 MMSE Time Interpolation . . . 110
B.2 Channel Estimation Error Covariance of the Dynamic Channel Case 111

Appendix C. SNR Lower Bound of MMSE Receiver with MMSE Channel Estimation **113**
C.1 Derivation of the k^{th} Stream SNR of the MMSE Receiver . . . 113
C.2 Proof of Lemma 4.1 in Section 4.3.2 . . . 114
C.3 α_X, β_X, and γ_X Values for the Approximated Distribution of the SNR Lower Bound in Section 4.3.2 . . . 116

Appendix D. Differentiation of S and Finding the Optimal α **117**
D.1 Differentiation of S . . . 117
D.2 Finding α^* from $\partial S/\partial z$ . . . 118

Bibliography **119**

Vita **135**

List of Figures

1.1 MC-CDMA and OFDM transceiver block diagram 3

1.2 Rate-robustness tradeoffs in wireless communications 6

2.1 Transmitter and receiver structure of the MC-MC-CDMA system . . 16

2.2 Simulation results for BER versus SNR for MC-CDMA, MC-SC-CDMA, and MC-MC-CDMA with various M. All these systems occupy the same total bandwidth, and the MC-MC-CDMA system uses orthogonal code sequences since $M \leq N_c$. 27

2.3 The comparison of SER by analysis and SER by simulation for M-ary ($M = 2, M = 16$) orthogonal code sequence cases in $K = 16$ independent subcarrier channels 29

2.4 The comparison of SER upper bound by analysis and SER by simulation for the MC-MC-CDMA system using non-orthogonal code sequence sets. $M = 16$, $N_c = 8$, $K = 32$, $N_u = 10$ 30

2.5 The BER versus the number of users for the MC-CDMA system and the MC-MC-CDMA system. 31

2.6 The received (pre-despreading) SINR versus M with various N_u and SNR. It can be seen that the value of M does not change the received SINR. 32

3.1 MIMO-OFDM structure with pilot signals 38

3.2 Description of independent, orthogonal and scattered pilot patterns . 42

3.3 Pilot and interpolation structure for the dynamic channel case 52

3.4 Capacity lower bound versus pilot power for 2×2 MIMO-OFDM systems with three different pilot patterns, K=64, P=4, L=4 59

3.5 Capacity lower bound with optimal PDPR versus SNR for 2×2 and 4×4 MIMO-OFDM systems, K=64, P=4, L=4 59

3.6 Capacity upper and lower bound versus SNR for 2×2 MIMO-OFDM system with the optimal PDPR and equal power, K=64, P=4, L=4 . 62

3.7 Capacity lower bound versus pilot power for 2×2 MIMO-OFDM for dynamic channel, veh. speeds=1,30,60km/h, K=64, P=4, L=4, N=10, SNR=20dB 63

3.8 Capacity lower bound versus pilot power for 4×4 MIMO-OFDM for dynamic channel, veh. speeds=1,30,60km/h, K=64, P=4, L=4, N=10, SNR=20dB 63
3.9 Capacity lower bound versus SNR for 4×4 MIMO-OFDM with the optimal PDPR and equal power, veh. speeds = 1, 60km/h, K=64, P=4, L=4, N=10 65
3.10 Optimal pilot power percentage versus vehicle speed for 2×2 and 4×4 MIMO-OFDM, K=64, P=4, L=4, N=10, SNR=20dB 65
3.11 Maximum average effective SNR versus vehicle speed for 2×2 and 4×4 MIMO-OFDM, K=64, P=4, L=4, N=10, SNR=20dB 66

4.1 Adaptive MIMO-OFDM structure 71
4.2 Pilot pattern 72
4.3 Effect of the number of pilot symbols and the number of channel taps on BER performance of 2×2 MIMO-OFDM with LS/ZF and QPSK. $P = 4$ 73
4.4 Channel estimation error versus noise variance 86
4.5 SER versus percentage of pilot power for 2×2 QPSK MIMO-OFDM with LS/ZF and MMSE/MMSE cases. 91
4.6 SER versus SNR with optimal PDPR and equal power of 2×2 MIMO-OFDM with LS/ZF. Comparison between the analysis and simulation. 93
4.7 SER versus SNR with optimal PDPR and equal power of 2×2 MIMO-OFDM with MMSE/MMSE. Comparison between the analysis and simulation. 93
4.8 Average spectral efficiency versus SNR of 2×2 MIMO-OFDM with LS/ZF. 94
4.9 Average spectral efficiency versus SNR of 2×2 MIMO-OFDM with MMSE/MMSE. 94
4.10 Average spectral efficiency versus the number of pilot symbols ($P \geq L$) for 2×2 MIMO-OFDM with LS/ZF. 95
4.11 Comparison between the analysis and simulation results with TU channels: spectral efficiency vs. SNR (TU channel) 96
4.12 Comparison between the analysis and simulation results with TU channels: spectral efficiency vs. PDPR (TU channel) 97

Chapter 1

Introduction

Emerging wireless communication systems exploit many resources such as power, bandwidth, and spatial channels in order to increase their robustness and achievable data rate. Various schemes such as spreading, error control coding, multicarrier modulation, and multiple antennas can be used to exploit these resources. However, since these resources are limited, there is a tradeoff between the need for robust communication and the desire for high throughput. The communication system designer needs to consider this tradeoff in the light of the available configurations of the system and the channel characteristics.

1.1 Multicarrier Communications

Multicarrier modulation is a method of transmitting broadband data by splitting it into several components, and sending each of these components over separate carrier signals in order to ease channel equalization at the receiver [8, 29, 43, 57, 73, 84]. While the composite signal generally has a broad bandwidth, each individual carrier is narrowband. Even the bandwidth of several narrowband carriers is typically less than the coherence bandwidth of the channel. Therefore, the narrowband signals do not experience frequency selective fading.

Multicarrier modulation was first used in analog military communications in the 1950s. Recently, multicarrier modulation has attracted attention as a means of enhancing the bandwidth of wireless communications with physical limitations. The technology lends itself to digital television, and is used as a method of obtaining high data rates in asymmetric digital subscriber line (ADSL) systems and emerging wireless communication standards such as 3GPP-LTE, IEEE 802.11a/g, IEEE 802.16e, and IEEE 802.11n [8, 24, 35, 95, 104, 113, 117].

Orthogonal frequency division multiplexing (OFDM) and multicarrier code division multiple access (MC-CDMA) are two popular multicarrier technologies in recent wireless communications standards, and their transceiver block diagrams are shown in Fig. 1.1.

The principles and some of the benefits of OFDM have been known since the 1960s [15]. European Telecommunications Standards Institute (ETSI) digital audio broadcasting (DAB) is the first OFDM based standard [27]. When the symbol duration is relatively long compared to channel delay spread, the system suffers less inter-symbol interference (ISI) caused by multipath. Thus it is more effective to transmit a number of low rate streams in parallel than a single high rate stream. OFDM achieves this by splitting the high-rate data stream into many low-rate parallel substreams and transmitting on multiple orthogonal subcarriers. This makes the effects of the channel roughly constant (flat) over any given subchannel [13, 19, 36, 54, 107, 118]. It also greatly simplifies the design of both the transmitter and the receiver, and allows for high spectral efficiency. Furthermore, a guard period is inserted between consecutive transmitted symbols, in the form

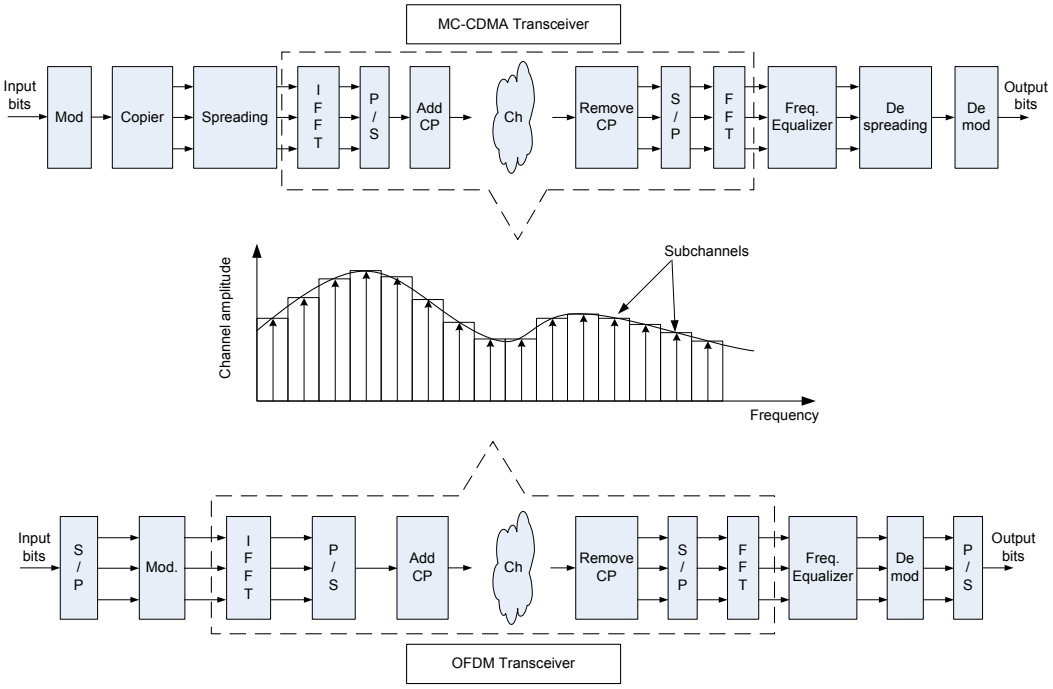

Figure 1.1: MC-CDMA and OFDM transceiver block diagram

of cyclic prefix (CP). As a result, OFDM can effectively compensate for multipath impairment without any loss of orthogonality between allocated subchannels over frequency-selective fading channels [70]. OFDM has attracted increasing interest due to its robustness against the frequency selectivity and its resource allocation capability to multiple users [65, 111, 119]. Therefore, it is considered to be the probable modulation method in next-generation wireless communication standards [28, 35, 52].

The term MC-CDMA has been used to represent three different technologies such as multicarrier CDMA, multicarrier direct sequence, and multitone CDMA [16, 20, 43, 84, 112, 123]. In this dissertation, the acronym will assume the conno-

tations of multicarrier CDMA [43, 122]. In MC-CDMA, the different users share the same bandwidth at the same time with the data separated by the application of different user-specific spreading sequences. All users transmit data symbols simultaneously over several narrowband subchannels, and these subchannels are multiplied by the chips of the user-specific spreading sequence in the frequency domain as shown in Fig. 1.1. The performance benefits of MC-CDMA are achieved by combining across carriers to maximize frequency diversity benefits. This also results in lower interference from other cells.

The multicarrier modulation technique has a number of advantages over single carrier modulation. The following are some of the advantages followed by some disadvantages.

-Advantages:

- Since the frequency selective fading channel is divided into a number of narrowband subchannels as shown in Fig. 1.1, the symbol rate on each subcarrier (low rate sub-stream) is much less than the original data symbol rate (high rate data stream). Thus, the effects of delay spread such as ISI significantly decrease, and the channel equalizer can be simplified (1-tap per subchannel) at the receiver by using a longer CP than the maximum delay spread of the wireless channel.

- Less susceptibility than single-carrier systems to interference caused by impulse noise

- Simple digital realization is possible by using digital signal processing (FFT).

-Disadvantages:

- A low efficiency of the power amplifier due to high peak-to-average power ratio (PAPR).
- Loss in spectral efficiency due to the guard interval.
- Spectral regrowth of the signal outside the useful signal bandwidth.

1.2 The Rate-Robustness Tradeoff

The rate-robustness tradeoff in wireless communications is caused by the scarcity of resources. There are various rate-robustness tradeoffs related to different resources and their usage as shown in Fig. 1.2. A natural question that arises is how the available resources in wireless communication systems should be optimally used in order to tradeoff the need for robust communication and the desire for very high throughput.

One of these rate-robustness tradeoff problems is the spatial diversity versus multiplexing tradeoff in multiple-input multiple-output (MIMO) systems. Recently, there have been a number of studies [25, 46, 47, 83, 102, 110, 127] that deal with how spatial diversity and multiplexing gains can be utilized by considering the fundamental tradeoff between rate and robustness in MIMO systems. Different antennas see different multipath characteristics or different fading characteristics and this can be used to generate a more reliable received signal, as in [34, 92, 109]. Also, in MIMO systems, the bit stream to be transmitted can be demultiplexed into

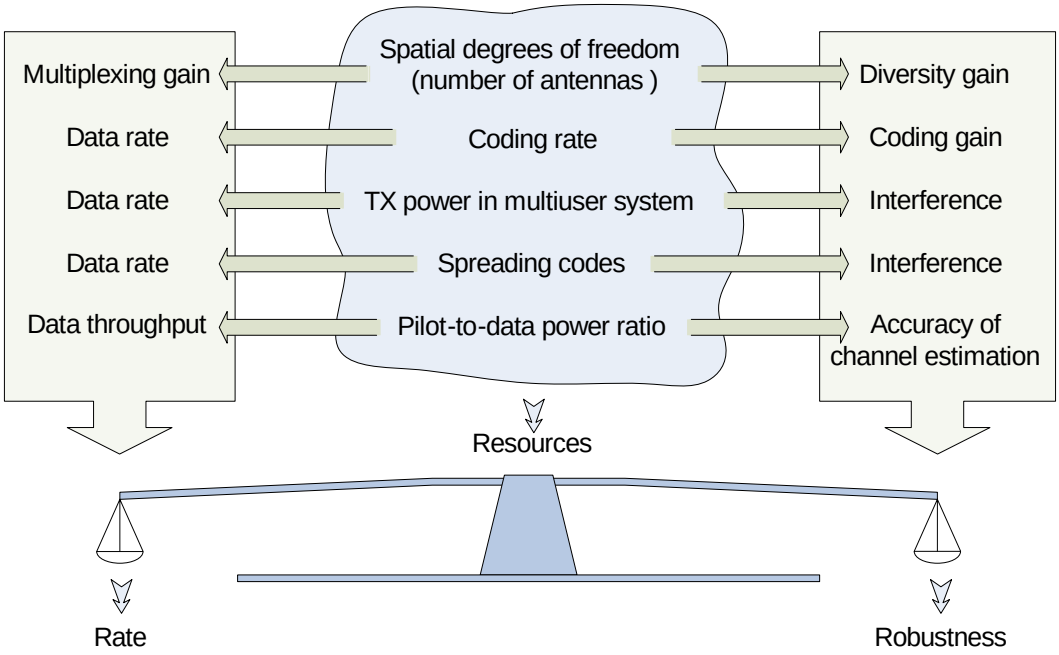

Figure 1.2: Rate-robustness tradeoffs in wireless communications

the number of transmit antennas and transmitted simultaneously from each transmit antenna. Then, at the receiver, those substreams can be extracted from the received signal using the knowledge of the channel and combined to yield the original bit stream. This is spatial multiplexing, and it offers a linear increase in the transmission rate for the same bandwidth with no additional power expenditure [30, 49, 91]. Spatial multiplexing focuses on data rate whereas spatial diversity focuses on the robustness of MIMO systems. The tradeoff between spatial diversity and multiplexing is a more complicated measure than maximal spatial diversity gain or maximal spatial multiplexing gain alone.

Error-correcting codes (ECCs) can be used to improve the robustness of the

system. An ECC is an algorithm for expressing a sequence of numbers such that any errors that are introduced can be detected and corrected (within certain limitations) based on the remaining numbers. Error correction involves the addition of redundant bits that are used to aid in correcting any bits received in error. Shannon's channel coding theorem states that there always exists a coding scheme that enables information to be transmitted over any given channel with arbitrarily small error probability provided the data rate (including that due to redundant bits) over the channel is less than the channel capacity (as defined by the classical Shannon theorem). Over the last four decades a number of powerful and efficient codes have been designed [72]. ECCs with coding rate r introduce $1/r$ redundant symbols for every data symbol, and hence nominally reduce the transmitted data rate by a factor $r \leq 1$, where $r = 1$ is a trivial case. Thus, there is a tradeoff between rate and robustness when ECCs are used. The coded sequence consumes time, frequency, or space as a resource according to which domain is used for encoding information data [45, 74, 79, 108, 109].

When we allocate transmit power to each user in a multiuser environment, the rate-robustness tradeoff again comes into play [18, 53, 89, 103]. In a multiuser environment, the multiuser interference is increased as we allocate more power to each user. Therefore, multiuser interference such as inter-cell interference and intra-cell interference should be handled to optimize system performance.

Besides these examples of the rate-robustness tradeoffs in wireless systems, we can find two other rate-robustness tradeoff problems in multicarrier systems which are caused by the utilization of the frequency domain. The data rate and

interference robustness tradeoff in multicarrier CDMA with a multi-code scheme and the pilot-data power allocation tradeoff in OFDM are two of these tradeoffs as shown in Fig. 1.2.

1.2.1 Data Rate and Interference Robustness Tradeoff in Multicarrier CDMA with a Multi-code Scheme

The first rate-robustness tradeoff in multicarrier systems that will be considered occurs when the multicarrier system is used in conjunction with a multi-code scheme to support higher and variable data rates. Specifically for multicarrier systems, several works such as [12, 31, 32] have attempted to utilize resources such as spreading gain in order to support a wide variety of data rates and improve system reliability. However, the systems in [12, 32] have a multi-code interference problem: the systems experience more interference with increasing data rate since each data stream is treated as an independent user. Thus, there is a tradeoff between providing higher data rates and the amount interference generated by high-rate users, and this tradeoff should be investigated in a system design to improve system performance. In this dissertation, this data rate and interference robustness tradeoff in variable rate multicarrier systems is studied under a novel multi-code multicarrier CDMA system (MC-MC-CDMA), proposed in this dissertation, in order to overcome the shortcomings of prior systems.

1.2.2 Pilot-Data Power Allocation Tradeoff in OFDM

In OFDM, pilot symbols are used to estimate the channel, but in addition to consuming bandwidth, they reduce the transmitted energy for data symbols un-

der a fixed transmit power constraint. This suggests a tradeoff between the power allocated to data symbols and the accuracy of channel estimation [2, 6, 48, 76, 86, 96]. This tradeoff depends on which is more crucial for system performance, i.e., whether the improvement in channel estimation error or the increase in data rate is more valuable. Also, this pilot and data power allocation problem is related to the channel condition and the structure of pilot symbols, for example the number of pilot symbols in one OFDM symbol, the pilot symbol placement, and pilot transmitting patterns in MIMO systems. In this dissertation, the data rate versus channel estimation accuracy tradeoff is investigated to find the optimal balancing power allocation for MIMO-OFDM systems for two different models: theoretical capacity and practical performance (SER) .

1.3 Contributions and Organization of the Dissertation

The main contribution of this dissertation is to investigate the tradeoff between the data rate and robustness in order to achieve a robust high data rate multicarrier system design. In this pursuit, three principle innovations based on the aforementioned rate-robustness tradeoff are developed.

Chapter 2 presents the first contribution of this dissertation: the tradeoff between variable data rates and interference robustness in multi-code systems which utilize spreading gain is investigated by proposing and analyzing a novel MC-MC-CDMA system. The proposed MC-MC-CDMA system can support variable data rates without the interference scaling problem of multi-code systems and obtains both time and frequency domain gains. The results show the availability of data

rate flexibility in a single antenna multicarrier CDMA system without any sacrifice in performance, and to the contrary, can actually allow improved robustness, flexibility, and capacity.

The second contribution, presented in Chapter 3, deals with the power allocation tradeoff in MIMO multicarrier systems based on theoretical capacity. In MIMO multicarrier systems, channel knowledge is required to make use of the diversity or multiplexing gain. The characteristics of the channel are closely related to the diversity performance; e.g., higher selectivity channel gain gives more diversity [124, 125]. Therefore, accurate channel estimation is critical in MIMO multicarrier systems. Among the various resources in MIMO multicarrier systems the power assignment for data and pilot symbols shows the tradeoff between the raw data rate and the accuracy of the channel estimation when the total transmit power is fixed. Pilot symbols facilitate channel estimation, but in addition to consuming bandwidth, they reduce the transmitted energy available for data symbols (per OFDM symbol) under a fixed total transmit power condition. Thus, in Chapter 3, the power tradeoff in MIMO-OFDM systems is investigated to maximize the system capacity lower bound for four likely pilot patterns with low and high mobility. From the analysis, it is shown that different pilot patterns can achieve different maximum capacity lower bounds, and the capacity lower bound of a typical MIMO-OFDM system can be increased by simply using the optimal pilot-to-data power ratio (PDPR) without using any additional resource. Moreover, the optimal PDPR varies not only with system parameters such as the number of antennas, the number of pilot and data symbols, the number of channel taps, and SNR, but also

with the vehicle speed. However it is proven that the variation of the optimal PDPR with the vehicle speed is small.

The third contribution of this dissertation, closely related to the second contribution, is optimally balancing pilot and data power in adaptive M-QAM MIMO multicarrier systems based on practical system performance, which is presented in Chapter 4. Spectral efficiency and SER of adaptive M-QAM are considered as quality metrics. M-QAM is considered since it is respectively the dominant modulation type in current and emerging standards. Since the achievable performance of the system depends on the receiver type, the distributions of SNR with channel estimation error for two well-known linear receivers, ZF and MMSE, are derived and used to find the optimal PDPR for minimizing the average SER and maximizing the spectral efficiency. The results show that the amount of boosting power of pilot symbols in practical systems should be decided based on the system configuration, for example, the receiver type and the channel estimation method, since the optimal PDPR depends on them.

In Chapter 5, the contributions of this dissertation are summarized alongside future research topics.

It seems intuitive that allocating all resources to data rate will give high raw data rate but poor reliability of communications, whereas allocating all resources to robustness is excessively conservative. A major goal of this dissertation is to study and optimally balance this tradeoff for multicarrier communication systems in order to provide guidelines on how to design them.

Chapter 2

Variable Data Rate and Interference Robustness Tradeoff

This chapter presents the data rate-interference tradeoff in multicarrier systems. This is one of the rate-robustness tradeoffs in multicarrier wireless communications. The goal of this chapter is to investigate this tradeoff to provide a means for many variable-rate users to simultaneously access a channel while remaining relatively robust to the interference caused by other users.

2.1 Introduction

Future wireless systems such as fourth generation (4G) cellular will need flexibility to provide subscribers with a variety of services such as voice, data, images, and video. Because these services have widely different data rates and traffic profiles, future generation systems will have to accommodate a wide variety of data rates. CDMA has proven very successful for large scale cellular voice systems, but there is some skepticism about whether CDMA will be well-suited to non-voice traffic [94]. This has motivated research on multi-code CDMA systems which allow variable data rates [50, 51, 99] by allocating multiple codes, and hence varying degrees of capacity to different users. Meanwhile, MC-CDMA has emerged as a

powerful alternative to conventional direct sequence CDMA (DS-CDMA) in mobile wireless communications [4, 42, 43, 105, 122, 123], and has been shown to have superior performance to single-carrier CDMA in multipath fading. This chapter proposes and analyzes a new multiple access and modulation technique: a combined multi-code multicarrier CDMA system for exploiting the best aspects of each of these earlier systems to achieve high data rate while remaining robust to the multiple access interference.

Multi-rate transmission for single-carrier CDMA systems in AWGN channels has been previously considered in the literature, e.g. [78, 87]. It is also an important part on third generation cellular standards, namely CDMA2000 1xEV-DO [1] and 1xEV-DV [80], known sometimes as HDR [7]. HDR supports diverse data rates using many codes with different spreading factors. However, in this case, the code assignment is limited by the number of orthogonal codes for the short spreading factor, and multipath can be very problematic for the higher data rates since the spreading factor is short. Unlike the HDR system, the proposed system does not require variable spreading factors. It uses the same code book to support various data rates for different users.

Multi-code techniques such as the proposed system tradeoff the number of supportable subscribers with the per subscriber data rate. Said another way, the number of simultaneous higher data rate users in a multi-code CDMA system will be less than the number of equal data rate users in a traditional CDMA system. A variation of the multi-code scheme, which supports variable data rates by varying the set of code sequences assigned to each of the users, has been proposed in [99,

100]. The users communicate their data by choosing one sequence from their code set to transmit over the common channel. Also, in [100] the performance of multi-code CDMA was considered only in an AWGN channel.

There have been to my knowledge two previous studies on multi-rate transmission for multicarrier direct sequence CDMA (MC-DS-CDMA) systems [12, 31]. The study of multi-rate transmission for MC-DS-CDMA systems based on the concepts of multi-code access and variable-spreading gain code access was first presented in [31]. In multi-rate MC-DS-CDMA, the data stream of a user with data rate M is first multiplexed into M different serial streams with a base data rate, and each serial stream is treated as an individual user. Each of the M serial streams is then converted into P parallel sub-streams and spread by the same spreading code with a constant spreading factor. Moreover, the system in [31] has M times more interference per user, because each of the M data streams is treated as an independent user. Therefore, the system of [31] experiences more interference as the data rate increases, even with a fixed number of users. Also, multi-rate transmission for frequency spread multicarrier CDMA has been studied in [32]. In the multi-rate multicarrier CDMA system in [32], the subcarriers are divided into M groups according to the required data rate. Therefore, when the number of subcarrier is fixed, the spreading gain in frequency domain for each data is decreased with increasing data rate. The single-carrier multi-code CDMA system in [99] addresses this interference scaling problem by using just one code sequence instead of spreading each of the M multiplexed data streams so that the interference does not increase linearly with the data rate. However, this system [99] does not achieve the frequency

diversity benefits of multicarrier modulation.

This chapter proposes a multicarrier CDMA system with multi-code that outperforms both [31] and [99]. The proposed MC-MC-CDMA system achieves the advantages of both systems: (i) variable data rates without interference scaling and (ii) enhanced robustness to multipath fading channels. Moreover, the proposed system gains in both the time and frequency domain to exploit the diversity and interference averaging properties of multicarrier modulation and CDMA. The bit error probability of the proposed system is derived analytically and the improvement of the proposed system over an MC-CDMA system is shown through both analysis and simulations in a frequency selective fading channel.

2.2 System Model and Time-Frequency Signaling Gain

The proposed MC-MC-CDMA system depicted in Fig. 2.1 uses a set of M codes called the *code sequence set* for M-ary modulation. Each user has the same code sequence set which represents an information data symbol of $\log_2 M$ bits. The size of the code sequence set depends on the required data rate. In the usual CDMA case, the size of the code sequence set is 2, i.e. there are two sequences in the set, one to represent a '0' and the other to represent a '1'. In the proposed system, each user has a set of M code sequences, where $\log_2 M$ is the ratio of the required data rate to the base data rate (1 bit/symbol). Therefore, if the data rate is to be made $\log_2 M$ times the base data rate, the size of the code sequence set is M and each M-ary data symbol is mapped to one of the code sequences of length N_c. This code length N_c is fixed over all different values of M. Thus, varying

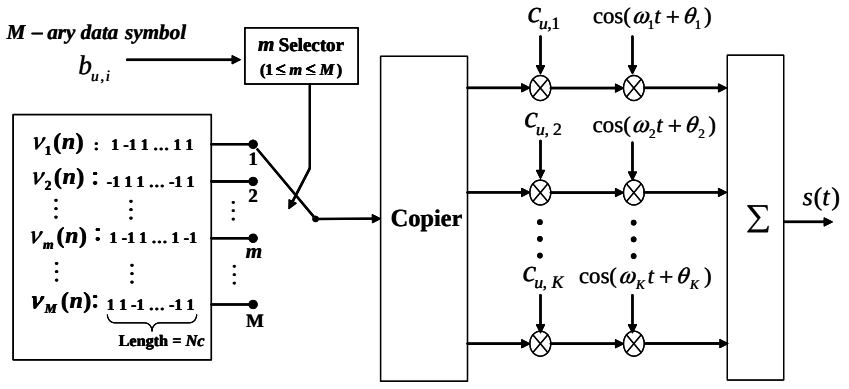

(a) Transmitter

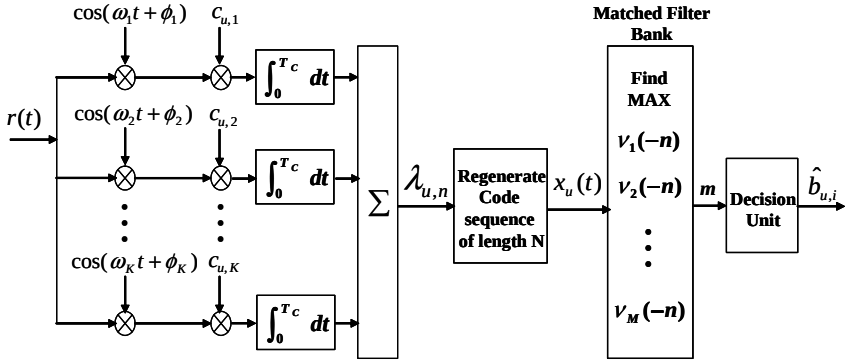

(b) Receiver

Figure 2.1: Transmitter and receiver structure of the MC-MC-CDMA system

the data rate does not change the code length N_c, but it does change the size of the code sequence set M. If orthogonal code sequences are used, the performance advantages of orthogonal modulation are attained. However, in order to maintain linear independence between the code sets, it is required that $M \leq N_c$. If non-orthogonal code sequences are used, then M can be greater than N_c, naturally at the expense of the distance between code symbols.

As shown in Fig. 2.1(a), an M-ary symbol selects one of M pre-mapped

code sequences for transmission. Each code sequence has a time domain length of N_c. Each bit of the length N_c code sequence is copied onto the K subcarrier branches and multiplied with the user-specific scrambling code of the corresponding branch, $c_{u,k}$. Note that the $c_{u,k}$ are independent of time so that the spreading at this stage is only in frequency, allowing users to choose specific codes that have low cross-correlations with other user's codes. Each of these branches then modulates one of the K orthogonal subcarriers and the results are summed. As in popular OFDM, this process can be implemented using a size K Inverse FFT to replace the subcarrier multiplication and summation. Unlike OFDM, which uses serial to parallel conversion, in multicarrier CDMA the same information bit is replicated on all subcarriers to achieve a spreading gain for multiple access. Also, a cyclic prefix is not typically employed in multicarrier CDMA because self-ISI is a minor effect compared to multiple access interference.

A multicarrier CDMA system with spreading only in the frequency domain is generally referred to as an MC-CDMA system, while a multicarrier system with spreading only in the time domain is usually called MC-DS-CDMA. As shown in Section 2.2 and Fig. 2.1, the proposed MC-MC-CDMA system has two-dimensional gain in both the time and frequency domains by using a multi-code signal and multicarrier modulation, respectively. Two-dimensional spreading exploits both time and frequency diversity and thus can simultaneously combat frequency selective fading and multiple-access interference (MAI) from the advantages of multicarrier modulation and CDMA.

The total gain with two-dimensional signaling is the product of the time

domain gain which comes from the orthogonality between code sequences and the frequency spreading gain. Within a fixed total bandwidth, the two-dimensional gain can be adapted to the user load and radio link conditions such as Doppler spread, delay spread, and channel gain.

It may be noted that two-dimensional gain in the time and frequency domain is similar in principle to the MC-DS-CDMA system recently proposed in [122]. By using a frequency spreading code sequence, both systems can distinguish users while assigning the same time domain spreading codes to each user. MC-MC-CDMA improves upon MC-DS-CDMA in its handling of variable rates, and more efficient spreading codes. The latter property is due to the selection of one of M information-bearing codewords rather than multiplying a fixed codeword by the incoming data bit.

2.3 System Analysis

2.3.1 Signal Description

To formalize the analysis of the MC-MC-CDMA system, consider that each user has the same code sequence set which can be written as

$$\Omega = \{\nu_m(n) | 1 \leq m \leq M\}, \tag{2.1}$$

where $\nu_m(n)$ is a m^{th} code sequence in the set Ω and n is a time index. User u's i^{th} M-ary data symbol $b_{u,i}$ is mapped to one of the code sequences in Ω. Thus the i^{th} transmit sequence of user u before multicarrier modulation can be written as

$$S_{u,i}(n) \quad = \quad \nu_{b_{u,i}}(n) \tag{2.2}$$

$$S_{u,i}(t) \quad = \quad \sum_{n=0}^{N_c-1} S_{u,i}(n) f_r(t - nT_b - iT_s), \tag{2.3}$$

where $S_{u,i}(n)$ is the n^{th} bit in the i^{th} code sequence of user u, T_b is the bit duration of the code sequence, T_s is the symbol duration ($T_s = N_c T_b$), N_c is the length of code sequence, and $f_r(t)$ is the normalized rectangular waveform defined as

$$f_r(t) = \begin{cases} \frac{1}{\sqrt{T_b}}, & 0 \le t \le T_b \\ 0, & \text{elsewhere} \end{cases} \tag{2.4}$$

According to the block diagram of the MC-MC-CDMA transmitter shown in Fig. 2.1(a), the transmitted BPSK signal of user u can be written as

$$s_u(t) = \sum_{i=-\infty}^{\infty} \sum_{k=1}^{K} \sum_{n=0}^{N_c-1} S_{u,i}(n) f_r(t - nT_b - iT_s) c_{u,k}(N_c i + n) \cos(\omega_k t + \theta_{u,k}) \tag{2.5}$$

where $c_{u,k}(N_c i + n)$ is the k^{th} chip of the n^{th} bit in the i^{th} code sequence of user u, ω_k is the k^{th} carrier frequency, $\theta_{u,k}$ is the random phase of the k^{th} subcarrier of user u and uniformly distributed over [0,2π], and K is the number of subcarriers.

To suppress the out-of-band interference, it may be necessary to remove the side lobes by filtering at the transmitter. In practical systems, pulse shaping filter such as raised cosine filter is used. In (2.5), $f_r(t)$ is used as the rectangular pulse shaping filter for each information bit before IFFT operation. Thus, sinc functions are located at each subcarrier in the frequency domain. Since the frequency separation between the neighboring carriers is $1/T_b$, the carriers are orthogonal on chip duration. Therefore, with assumption of perfect synchronization and no frequency offset, there is no overlap between different subcarrier signals at each subcarrier frequency due to zero crossing. Moreover, pulse shaping for entire bandwidth after FFT operation is assumed to be ideally used [4, 42].

In the receiver of Fig. 2.1(b), a size K FFT is applied to the input. The output of the FFT is then despread to generate each bit of the received code sequence. The N_c regenerated bits compose one code sequence, and the regenerated code is the input of the matched filter bank to detect the transmitted symbol. The N_c despread bits form a degenerated code sequence, which is correlated with each of the possible M code sequences. The sequence that gives maximum correlation is then mapped back into an M-ary symbol. The use of this narrowband multicarrier scheme provides frequency diversity for multipath mitigation so that no RAKE receiver is required, and a greater percentage of the received energy is actually collected for detection.

2.3.2 Analysis of the Output of the Matched Filter

In this section, the output of the matched filter is analyzed. Because the MC-MC-CDMA transmitted waveform consists of a large number of narrowband subcarriers, the channel model can be reasonably approximated as a frequency selective Rayleigh fading channel where each subcarrier experiences flat Rayleigh fading. Different channel model can be considered instead of a Rayleigh fading channel. However, the reason for considering a Rayleigh fading channel is that the BER performance of the proposed scheme can be easily compared with other schemes through analysis by using this channel. The subchannels can be written as

$$h_{u,k}(t) = g_{u,k}(t)e^{j\psi_{u,k}(t)} \tag{2.6}$$

which is a complex Gaussian random variable with zero mean and variance σ^2, characterized by a Rayleigh distributed amplitude attenuation $g_{u,k}(t)$, and a phase

shift $\psi_{u,k}(t)$. While in practice there would be some correlation between adjacent subchannels, it is assumed here that $h_{u,k}(t)$ are uncorrelated and identically distributed for different u and k.

If there are N_u active users, the received signal of the synchronous system is

$$r(t) = \sum_{i=-\infty}^{\infty} \sum_{u=1}^{N_u} \sum_{k=1}^{K} \sum_{n=0}^{N_c-1} g_{u,k}(t) S_{u,i}(n) f_r(t - nT_b - iT_s) \times c_{u,k}(N_c i + n) \cos\left(\omega_k t + \phi_{u,k}(t)\right) + n(t), \quad (2.7)$$

where $\phi_{u,k}(t) = \theta_{u,k} + \psi_{u,k}(t)$ and $n(t)$ is the additive white Gaussian noise with zero mean and power spectral density N_o. The amplitude attenuation and phase shift is considered to be constant over the time interval $[0,T_b)$.

From Fig. 2.1(b) and (2.7), the matched filter output at the receiver can be derived. Assume that the user 1 is the desired user and the 0^{th} transmitted M-ary symbol of the desired user is m which represents an M-ary data symbol $b_{1,0}$, then the 0^{th} output of the filter matched to the code m of user 1 is

$$Z_{1,m} = \int_0^{T_s} x_1(t) \sum_{n=0}^{N_c-1} \nu_m(n) f_r(t - nT_b) dt, \quad (2.8)$$

where the demodulated code sequence of user 1 $x_1(t)$ is

$$x_1(t) = \sum_{j=0}^{N_c-1} \lambda_{1,j} f_r(t - jT_b), \quad (2.9)$$

$$\lambda_{1,j} = \frac{1}{T_b} \int_{jT_b}^{(j+1)T_b} r(t) \sum_{q=1}^{K} c_{1,q}(j) \cos(\omega_q t + \phi_{1,q}(j)) \alpha_{1,q} dt. \quad (2.10)$$

In this chapter, equal gain combining (EGC) is considered, because of its simplicity as the receiver does not require the estimation of the channel gain factor. Thus,

$\alpha_{1,q} = 1$ for all q. As shown in Appendix A, the matched filter output (2.8) can be written as [4, 42, 105]

$$Z_{1,m} = D_{1,m} + I_{1,m} + J_{1,m} + \eta, \tag{2.11}$$

where $D_{1,m}$ is the desired signal for user 1, $I_{1,m}$ is the same carrier interference from other users, $J_{1,m}$ is other carrier interference from other users, and η is the AWGN term with variance $N_o K N_c/4T_b$. The desired signal $D_{1,m}$ is

$$D_{1,m} = \frac{1}{2}\sum_{n=0}^{N_c-1} \nu_m(n)\nu_{b_{1,0}}(n) \sum_{q=1}^{K} g_{1,q}(0). \tag{2.12}$$

In (2.11), the same carrier interference term $I_{1,m}$ can be written as

$$\begin{aligned} I_{1,m} &= \frac{1}{2}\sum_{u=2}^{N_u}\sum_{k=1}^{K}\sum_{n=0}^{N_c-1} g_{u,k}(0)\nu_m(n)\nu_{b_{u,0}}(n) \\ &\qquad \times c_{u,k}(n)c_{1,k}(n)\cos(\phi_{u,k}(n) - \phi_{1,k}(n)), \end{aligned} \tag{2.13}$$

and other carrier interference term $J_{1,m}$ can be written as

$$\begin{aligned} J_1 &= \frac{1}{2T_b}\sum_{n=0}^{N_c-1}\sum_{u=2}^{N_u}\sum_{k=1}^{K}\sum_{\substack{q=1\\q\neq k}}^{K} g_{u,k}(0)\nu_m(n)\nu_{b_{u,0}}(n)c_{u,k}(n)c_{1,q}(n) \\ &\qquad \times \int_0^{T_b} \cos((\omega_k - \omega_q)t + \phi_{u,k}(t) - \phi_{1,q}(t))dt. \end{aligned} \tag{2.14}$$

As shown in Appendix A, $I_{1,m}$ and $J_{1,m}$ have zero mean and variance

$$\mathrm{var}(I_{1,m}) = \frac{1}{4}(N_u - 1)KN_c\sigma^2, \tag{2.15}$$

$$\mathrm{var}(J_{1,m}) = \frac{\sigma^2 N_c(N_u - 1)}{8\pi^2}\sum_{k=1}^{K}\sum_{\substack{q=1\\q\neq k}}^{K}\frac{1}{(k-q)^2}, \tag{2.16}$$

respectively. Therefore, assuming that the transmitted code sequence is known, the mean and variance of $Z_{1,m}$, the statistics of output of the filter matched to the transmitted code sequence at time 0 is as follows:

$$E(Z_{1,m}) = \frac{1}{2}\sum_{n=0}^{N_c-1}\sum_{k=1}^{K} g_{1,k}(0), \tag{2.17}$$

and

$$\text{var}(Z_{1,m}) = \frac{1}{4}(N_u-1)KN_c\sigma^2 + \frac{\sigma^2 N_c(N_u-1)}{8\pi^2}\sum_{k=1}^{K}\sum_{\substack{q=1\\q\neq k}}^{K}\frac{1}{(k-q)^2} + \frac{N_o K N_c}{4T_b}. \tag{2.18}$$

Now the probability of error for orthogonal and non-orthogonal code sequences are separately derived.

2.3.3 Probability of Symbol Error for the case of an M-ary Signal using an Orthogonal Code Sequence ($M \geq 2$)

If the Gaussian approximation is used for MAI and perfect subcarrier channel knowledge is assumed, the PDF of the output of the matched filter corresponding to the transmitted code sequence m for the desired user 1 is

$$P_{Z_{1,m}}(x) = \frac{1}{\sqrt{2\pi\text{var}(Z_{1,m})}}\exp\left(-\frac{(x-E(Z_{1,m}))^2}{2\text{var}(Z_{1,m})}\right), \tag{2.19}$$

where $E(Z_{1,m})$ and $\text{var}(Z_{1,m})$ are shown in (2.17) and (2.18). For simplicity, let's assume that the transmitted code sequence m is 1. The symbol error probability for the case of an M-ary orthogonal code sequence conditioned on the collection of subcarrier channels $P_{e,M-orthogonal|g}$ is

$$P_{e,M-orthogonal|g} = 1 - \int_{-\infty}^{\infty} P(z > Z_{1,2}, \ldots, z > Z_{1,M}|Z_{1,1} = z)P_{Z_{1,1}}(z)dz, \tag{2.20}$$

where $Z_{i,m}$ is the output of the matched filter corresponding to the code sequence m for user i, $m = 1, \ldots M$. Since the $\{Z_{i,m}\}$ are statistically independent, the joint probability function $P(z > Z_{1,2}, z > Z_{1,3}, \ldots, z > Z_{1,M} | Z_{1,1} = z)$ can be a product of $M - 1$ marginal probabilities as follows,

$$P(z > Z_{1,m} | Z_{1,1} = z) = \int_{-\infty}^{z} P_{Z_{1,m}}(x) dx, \tag{2.21}$$

where the PDF of the output of the matched filter corresponding to the code sequence m ($i \neq 1$) is

$$P_{Z_{1,m}}(x) = \frac{1}{\sqrt{2\pi \text{var}(Z_{1,m})}} \exp\left(-\frac{x^2}{2\text{var}(Z_{1,m})}\right). \tag{2.22}$$

These probabilities are all same for $m = 2, \ldots M$. Then, the symbol error probability for the case of an M-ary orthogonal code sequence conditioned on the collection of subcarrier channels can be obtained as

$$\begin{aligned}
&P_{e,M-orthogonal|g} \\
&= 1 - \int_{-\infty}^{\infty} \left[P(z > Z_{1,m} | Z_{1,1} = z)\right]^{M-1} P_{Z_{1,1}}(z) dz \\
&= 1 - \frac{1}{\sqrt{2\pi \text{var}(Z_{1,1})}} \int_{-\infty}^{\infty} \left(\int_{-\infty}^{z} \frac{1}{\sqrt{2\pi \text{var}(Z_{1,m})}} \exp\left(-\frac{x^2}{2\text{var}(Z_{1,m})}\right) dx \right)^{M-1} \\
&\qquad \times \exp\left(-\frac{(z - E(Z_{1,1}))^2}{2\text{var}(Z_{1,1})}\right) dz, \qquad \text{where } m \neq 1
\end{aligned} \tag{2.23}$$

The symbol error probability can be evaluated by Monte Carlo integration over the channel realization $\{g_{u,l}\}$. The symbol error probability conditioned on the collection of subcarrier channels (2.23) is the same when any one of the other $M-1$ code sequence is transmitted. Since all the M code sequence are equally likely, the

symbol error probability given in (2.23) is the average probability of a symbol error conditioned on the collection of subcarrier channels.

For $M = 2$, The symbol error probability conditioned on the collection of subcarrier channels can be simplified to

$$P_{e,Binary-orthogonal|g} = Q\left(\frac{E(Z_{1,1})}{\sqrt{2\text{var}(Z_{1,1})}}\right). \tag{2.24}$$

2.3.4 Probability of Symbol Error for the case of an M-ary Signal using Non-orthogonal Code Sequences ($M \geq 2$)

For an M-ary signal using non-orthogonal code sequences, the average symbol error probability conditioned on the collection of subcarrier channels $P_{e,M|g}$ can be expressed as

$$P_{e,M|g} = \frac{1}{M}\sum_{m=1}^{M} P_{e,m|g}, \tag{2.25}$$

where $P_{e,m|g}$ is the probability of error conditioned on the collection of subcarrier channels for the code sequence ν_m. The probability of error $P_{e,m|g}$ is upper-bounded as

$$P_{e,m|g} \leq \sum_{\substack{s=1 \\ s\neq m}}^{M} P_{e,M=2|g}(\nu_s, \nu_m), \tag{2.26}$$

where $P_{e,M=2|g}(\nu_s, \nu_m)$ is the probability of error conditioned on the collection of subcarrier channels for a binary communication system using two non-orthogonal code sequences ν_s and ν_m. The binary error probability $P_{e,M=2|g}(\nu_s, \nu_m)$ is

$$P_{e,M=2|g}(\nu_s, \nu_m) = Q\left(\frac{1}{2}\sqrt{\frac{d_{sm}^2}{\text{var}(Z_{1,m})}}\right), \tag{2.27}$$

where $d_{sm}^2 = \|\widehat{S}_s - \widehat{S}_m\|^2$.

From (2.9),(2.10), the two sequences $\widehat{S}_s$ and $\widehat{S}_m$ after passing through the channel and demodulator are

$$\widehat{S}_j = \sum_{n=0}^{N_c-1}\left(\frac{1}{T_b}\int_{nTc}^{(n+1)T_b} r(t)\sum_{q=1}^{K} c_{i,q}(n)\cos(\omega_q t + \phi_{i,q}(n))\alpha_{i,q}dt\right) f_r(t-nT_b), \quad \text{for } j \in \{s,m\}, \qquad (2.28)$$

where i is the user index, and $r(t)$ is the received signal. Thus, the symbol error probability conditioned on the collection of subcarrier channels for an M-ary non-orthogonal code sequence is upperbounded as [93]

$$P_{e|g,M} \leq \frac{1}{M}\sum_{m=1}^{M}\sum_{\substack{s=1 \\ s\neq m}}^{M} Q\left(\frac{1}{2}\sqrt{\frac{d_{sm}^2}{\mathrm{var}(Z_{1,m})}}\right), \qquad (2.29)$$

which can be evaluated by Monte Carlo integration over the channel realizations $\{g_{u,k}\}$.

As shown in (2.29), the symbol error probability for the case of the non-orthogonal code sequence depends on the distance between code sequences in the code sequence set, as would be expected.

2.4 Performance Comparison for MC-MC-CDMA

In this section, the numerical BER performance of MC-MC-CDMA is compared to competing systems, and some properties of MC-MC-CDMA are observed. For the MC-MC-CDMA system, the chosen parameters are $N_c = 16$ for the length of the code sequence, $K = 16$ for the number of subcarriers, and $M = 2, 4, 8, 16$ for

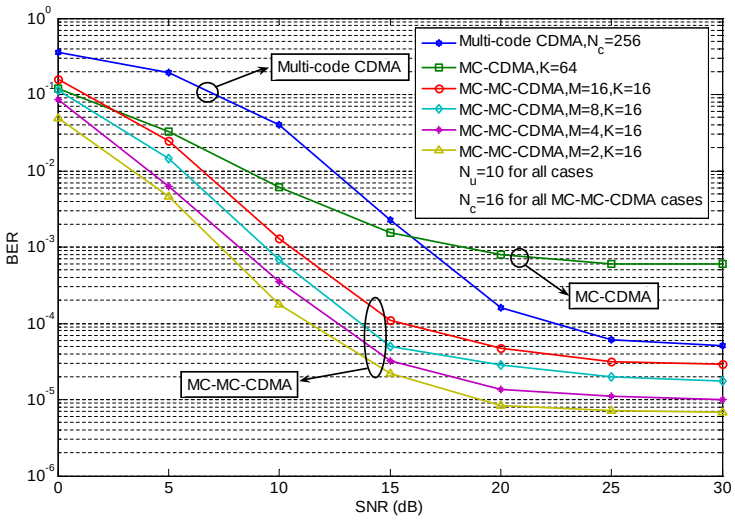

Figure 2.2: Simulation results for BER versus SNR for MC-CDMA, MC-SC-CDMA, and MC-MC-CDMA with various M. All these systems occupy the same total bandwidth, and the MC-MC-CDMA system uses orthogonal code sequences since $M \leq N_c$.

the M-ary symbols. The frequency selective Rayleigh fading channel is considered for the simulation. It is assumed that the channel on each subcarrier can be considered as flat fading and the receiver has perfect channel knowledge to detect the transmitted signal.

Fig. 2.2 shows the BER performance of the MC-MC-CDMA system with various M, the MC-CDMA system [42], and the multi-code single-carrier CDMA (MC-SC-CDMA) system [99]. In order to fairly compare the performance of these systems which have different subcarrier channel bandwidths, the number of subcarriers in each system is fixed to make the total bandwidth equal for all three systems. For example, when the length of the code sequence $N_c = M = 16$, the MC-MC-

CDMA system transmits 16 bits within one symbol time (4 information bits). That means the MC-MC-CDMA system uses 4 times more bandwidth compared to an MC-CDMA system with the same data rate. Therefore, 16 subcarriers are used for the MC-MC-CDMA system and 64 subcarriers are used for the MC-CDMA system. For the MC-SC-CDMA system, the length of the code sequence is 256. Moreover, all three systems have the same data rate. Since the length of the code sequence N_c is 16, the maximum supportable data rate is 4 bits/symbol. Thus, both multi-code CDMA and the MC-CDMA systems have the same information rate of 4 bits/symbol. In this way, all three systems use the same total bandwidth and the same data rate in the simulation. As can be seen, the proposed MC-MC-CDMA system performs better than the MC-CDMA system. By using multicarrier modulation, the MC-MC-CDMA system also easily outperforms the MC-SC-CDMA system in a frequency selective fading channel. Due to the gain which comes from orthogonality between code sequences and frequency spreading gain, the proposed MC-MC-CDMA system shows better performance than MC-CDMA and MC-SC-CDMA systems. The performance can be adjusted to different channel conditions, since the time-frequency spreading tradeoff can be controlled accordingly.

In Fig. 2.3, the analytical expressions and the simulation results in a Rayleigh fading channel for the orthogonal code sequence case are compared. Here, $M = 2$ and 16, and $N_u = 10$. The performance is better for $M = 2$, because the 16-ary MC-MC-CDMA system uses more code sequences than the binary MC-MC-CDMA system. In the same $N_c = 16$ dimensional signal space, it results in a smaller distance between code sequences than for the $M = 2$ case. The plot shows that the

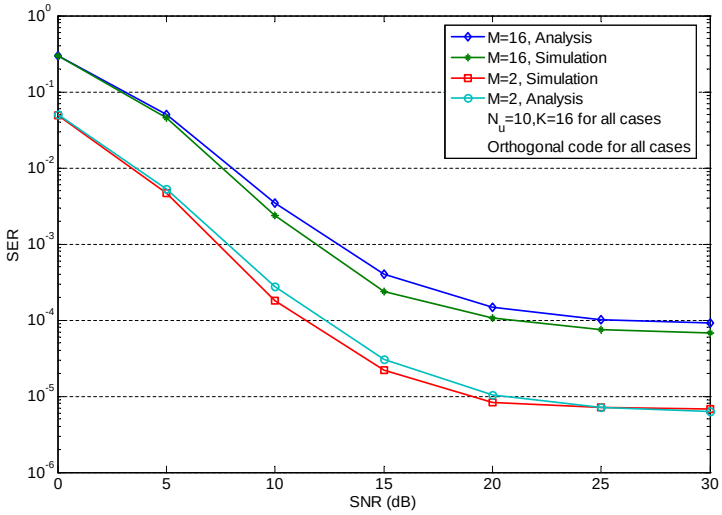

Figure 2.3: The comparison of SER by analysis and SER by simulation for M-ary ($M = 2, M = 16$) orthogonal code sequence cases in $K = 16$ independent subcarrier channels

analytical derivations agree closely with the simulation results for the orthogonal code sequence case.

Fig. 2.4 shows the analytical upper bound on symbol error probability and the simulation results for the MC-MC-CDMA system using non-orthogonal code sequences with various average code distances, as derived in Section 2.3.4. Here, $M = 16$, $N_c = 8$, $K = 32$, and $N_u = 10$. The code sequence set is randomly generated. In Fig. 2.4, d represents the average distance between code sequences:

$$\mathrm{d} = \frac{1}{(M-1)(M-1)} \sum_{m=1}^{M} \sum_{\substack{s=1 \\ s \neq m}}^{M} \|v_m - v_s\|, \qquad v_i \in \Omega, \quad i = 1, \cdots, M. \tag{2.30}$$

It is shown that the simulation results fall in under the analytical upper bound, as expected. The upper bound is relatively tight. As shown in Section 2.3.4, for the

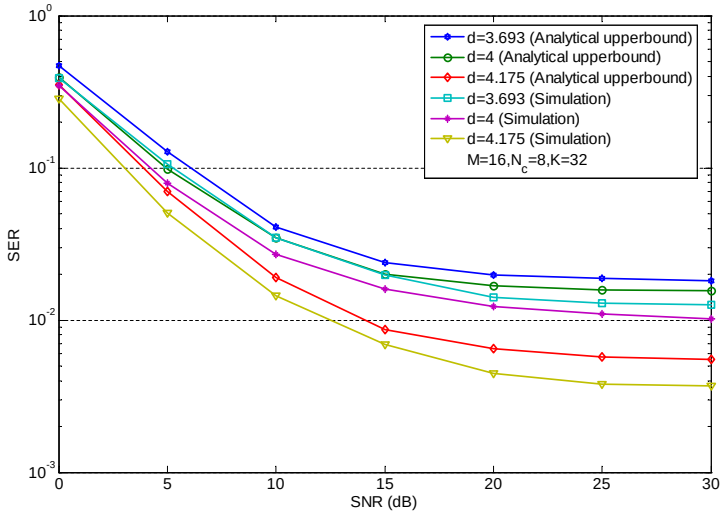

Figure 2.4: The comparison of SER upper bound by analysis and SER by simulation for the MC-MC-CDMA system using non-orthogonal code sequence sets. $M = 16$, $N_c = 8$, $K = 32$, $N_u = 10$

non-orthogonal code sequence, the symbol error probability upper bound depends on the distance between code sequences. Naturally, as the average distance between code sequences is decreased, the upper bound is increased.

The BER performance versus the number of users for both systems with an SNR of 10dB is shown in Fig. 2.5. At the same BER, data rate per user, and consumed bandwidth, the MC-MC-CDMA system can support more users than the MC-CDMA system. For example, at a BER of 3×10^{-3}, the number of users supported by the MC-MC-CDMA system is about 13, while it is about 7 for the MC-CDMA system. These are both uncoded systems with a total spreading gain of 64.

Fig. 2.6 shows the received (pre-despreading) signal-to-interference-plus-

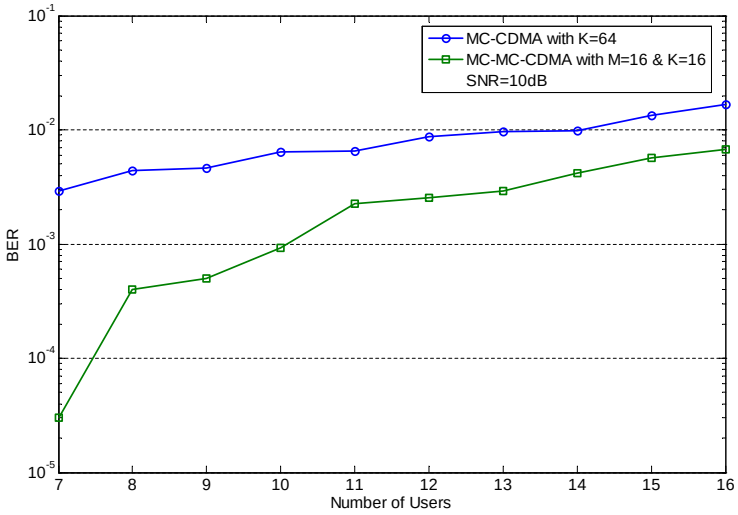

Figure 2.5: The BER versus the number of users for the MC-CDMA system and the MC-MC-CDMA system.

noise ratio (SINR) versus M with various numbers of users N_u and SNR. In this system, the mean of all interference power is assumed to be equal. As shown in Fig. 2.6, the received SINR of the MC-MC-CDMA system varies according to the variation of N_u and SNR, but not M. Since the length of the code sequence N_c is fixed over all different value of M, the received SINR is not changed according to M as shown in Fig. 2.6. It means that the proposed MC-MC-CDMA system can support higher data rate without increasing the interference unlike the multi-rate multicarrier CDMA system [31].

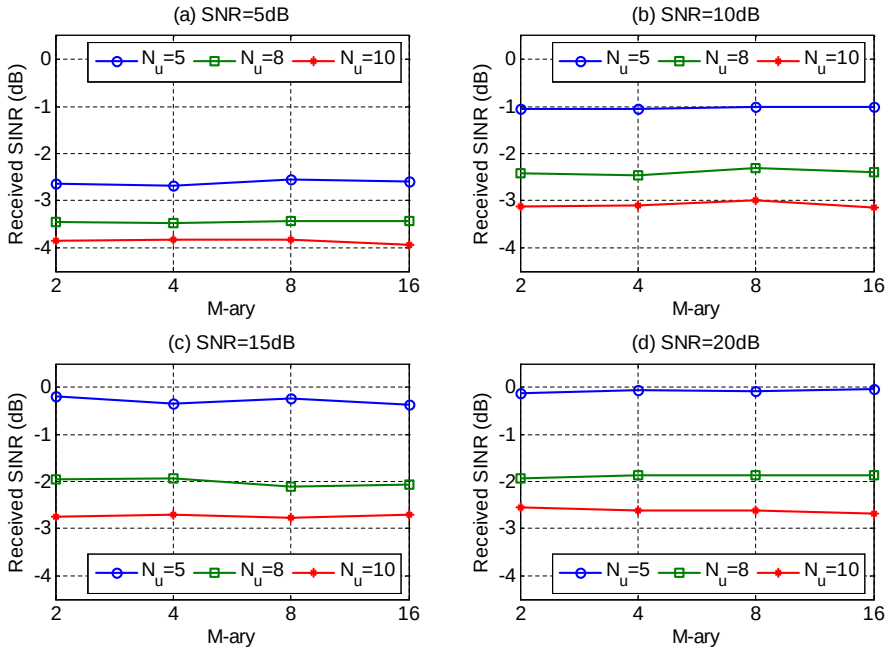

Figure 2.6: The received (pre-despreading) SINR versus M with various N_u and SNR. It can be seen that the value of M does not change the received SINR.

2.5 Chapter Summary

In this chapter, multi-code multicarrier CDMA was shown to be a promising method for supporting variable data rates for a large number of users in future cellular systems by addressing the interference scaling problem with enhanced robustness to multipath fading channels. By using the multi-code concept, the MC-MC-CDMA system achieves two-dimensional gain as well as frequency diversity. In addition, various data rates can easily be supported by changing the size of the code sequence set. With the same total bandwidth, both analytical and simulation results showed that the proposed MC-MC-CDMA system clearly outperforms mul-

ticarrier CDMA and single carrier multi-code CDMA in terms of bit error probability and user capacity in a frequency selective Rayleigh fading channel. This shows that data rate flexibility can be achieved in a multicarrier CDMA system without any sacrifice in performance, but rather offers improved robustness, flexibility, and capacity.

Chapter 3

Power Allocation Tradeoff in MIMO Multicarrier Systems - Theoretical Capacity

3.1 Introduction

OFDM is one of the most important physical layer technologies for high data rate wireless communications due to its robustness to frequency selective fading, high spectral efficiency, and low computational complexity. OFDM can be used in conjunction with a MIMO transceiver to increase the diversity gain and/or the system capacity [3, 9, 71, 90, 106, 121]. MIMO-OFDM is considered the key physical layer technology in emerging high-data rate systems such as 3GPP-LTE, IEEE 802.16e (WiMAX), and IEEE 802.11n [24, 35, 52, 97].

In MIMO-OFDM systems, channel state information (CSI) is essential at the receiver in order to coherently detect the received signal and to perform diversity combining or spatial interference suppression. To attain instantaneous CSI at the receiver, pilot-symbol-aided or decision-directed channel estimation must be used to track the variations of the frequency selective fading channel [68, 69]. Pilot symbols facilitate channel estimation, but in addition to consuming bandwidth, they reduce the transmitted energy for data symbols per OFDM symbol under a fixed total transmit power condition. This suggests a tradeoff between the power allowed to data

symbols and the accuracy of the channel estimation when the total transmit power is fixed. Pilot symbols can be transmitted in various ways in MIMO-OFDM systems including independent (time-multiplexed), scattered (frequency-multiplexed), or orthogonal (code-multiplexed) pilot patterns [21]. In this chapter, the PDPR for MIMO-OFDM systems with these different pilot patterns is optimized from a Shannon capacity point of view. The results herein allow system designers to have a well-justified basis for allocating more power to pilot symbols, despite the fact that they do not carry actual information themselves.

To date, there have been several previous studies on the problem of optimizing pilot signals for wireless communication systems [86, 114], but there have been far fewer studies for MIMO-OFDM. Optimizing the PDPR for DS/CDMA systems has been considered in [101] for the single user case. In multiuser cases, the optimal PDPR for the DS/CDMA uplink with multiuser detection has been examined in [48]. Both works optimized the PDPR of DS/CDMA systems with respect to the bit error rate (BER) performance. For OFDM systems with a SISO, optimizing training tones for minimizing the mean-square error (MSE) in channel estimates has been proposed in [85], optimal placement and power of pilot signals for maximizing capacity has been analyzed in [2, 75, 86], and the BER-minimizing pilots for OFDM systems were derived in [10]. Also, in [11], the training signal design problem for single carrier SISO system with adaptive modulation has been studied including channel estimation and prediction errors.

For MIMO systems, some recent research has begun to develop guidelines for appropriate pilot signal design. For single-carrier MIMO systems, the effects

of pilot-assisted channel estimation were analyzed in [96], and an optimal training signal was developed in [44]. Both papers optimize the training signal to maximize the capacity lower bound. In [77], the pilot signal is optimized for block transmissions with MIMO systems to maximize the capacity lower bound. However, only the scattered pilot pattern is considered assuming that pilot symbols are transmitted at every OFDM symbol time. The problem of optimizing training tones for MIMO-OFDM systems has been addressed in [6] with the mobility. The metric for optimization in [6] was the MSE of the channel estimation with pilot symbols in every OFDM symbol. The effect of feedback error on the information throughput has been studied in [5], which also studied training signal design for MIMO systems including feedback error.

In this chapter, the PDPR of MIMO-OFDM systems is optimized by directly maximizing a capacity lower bound while considering the effects of imperfect channel estimation. The analysis shows that the correlation between different channel links in the estimated channel can be removed by using different pilot patterns which are termed as independent, scattered, and orthogonal, and an optimal PDPR is derived for each of those cases. The analysis is begun with a static channel, which can also be interpreted as a block fading channel. For the scattered pilot pattern, two different scenarios are considered: (i) transmit pilot symbols only at the first of M_t OFDM symbol times (SPP-1), (ii) transmit pilot symbols at every OFDM symbol time (SPP-2) [77]. The analysis for the static channel case can be viewed as a generalization of prior results on SISO-OFDM [2], as the results reduce to that special case when only one antenna is present at both the transmitter and receiver.

A dynamic channel case with high mobility is also considered. There have been no studies, to my knowledge, on the relative power ratios between pilot and data symbols for maximizing the capacity of MIMO-OFDM systems accounting for the channel interpolation error due to Doppler effects. The importance of considering the dynamic channel case is that the block fading model is invalid at high vehicular speed, since each OFDM symbol experiences a different channel. Moderate mobility is assumed; namely, the channel varies over a block of OFDM symbols but is invariant during one OFDM symbol duration. Note that this level of mobility is insufficient to cause a doubly-selective channel [55, 56, 98]. As will be explained, independent and orthogonal pilot patterns cannot properly estimate the mobile MIMO channel, while the scattered pilot pattern can. Moreover, in emerging standards pilot symbols are transmitted periodically rather than in every OFDM symbol, and interpolation techniques are used over two pilot-inserted OFDM symbols. For dynamic channels, the optimal PDPR can be determined by considering both channel estimation and interpolation error over the Doppler Spectrum.

3.2 System Description

The system under consideration is depicted in Fig. 3.1, which shows a spatial multiplexing MIMO-OFDM system with M_t transmit antennas and M_r receive antennas. The number of subcarriers is K, and the number of nonzero taps of the impulse response is L for each channel. Suppose the received signal in the frequency domain is denoted by the $M_rK \times 1$ vector $\mathbf{y} = [\ \mathbf{y}_1^T \ \cdots \ \mathbf{y}_{M_r}^T\ ]^T$ where $\mathbf{y}_j = [\ y_j(1) \ \cdots \ y_j(K)\ ]^T$ and $y_j(k)$ is the received signal on the k^{th} subcarrier of

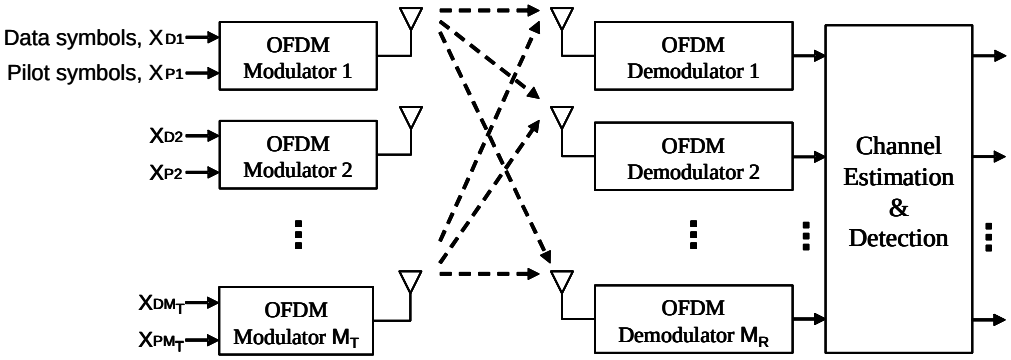

Figure 3.1: MIMO-OFDM structure with pilot signals

the j^{th} receive antenna. The received signal at the j^{th} receive antenna is given by

$$\mathbf{y}_j = \sum_{i=1}^{M_t} \mathbf{x}_i \mathbf{W}_K \mathbf{h}_{i,j} + \mathbf{n}_j = \mathbf{X}\mathbf{F}\mathbf{h}_j + \mathbf{n}_j, \tag{3.1}$$

where $\mathbf{X} = [\ \mathbf{x}_1 \cdots \mathbf{x}_{M_t}\ ]$ is the transmit symbol matrix where $\mathbf{x}_i = \text{diag}\,(x_i(k))_{k=1}^{K}$, the function diag(·) is used as follows

$$\text{diag}\,(\mathbf{A}_i)_{i=0}^{M-1} = \begin{bmatrix} \mathbf{A}_0 & & \mathbf{0} \\ & \ddots & \\ \mathbf{0} & & \mathbf{A}_{M-1} \end{bmatrix}, \tag{3.2}$$

where $\mathbf{A}_i$ can be a series of matrices or scalars, $\mathbf{h}_j = [\ \mathbf{h}_{1,j}^T \ \cdots \ \mathbf{h}_{M_t,j}^T\ ]^T$ is the channel impulse response matrix at j^{th} receive antenna where $\mathbf{h}_{i,j} = [\ h_{i,j}(1) \cdots h_{i,j}(L)\ ]^T$ and $h_{i,j}(l)$ denotes the channel response of the l^{th} path from the i^{th} transmit antenna to the j^{th} receive antenna, and $\mathbf{n}_j = [\ n_j(1), \ldots, n_j(K)\ ]^T$ is additive white Gaussian noise (AWGN) which is zero mean Gaussian with covariance $\sigma_n^2\mathbf{I}$. The subcarrier index sets for the data and pilot symbols are $\mathcal{D}$ and $\mathcal{P}$, respectively, and the number of the data and pilot symbols are D and P. Let $\mathbf{x}_{d,i}$ and $\mathbf{x}_{p,i}$ be the diagonal matrix of data and pilot symbols transmitted from the i^{th} transmit antenna;

in other words, $\mathbf{x}_{d,i} = \text{diag}\,(x_i(k))_{k\in\mathcal{D}}$ and $\mathbf{x}_{p,i} = \text{diag}\,(x_i(k))_{k\in\mathcal{P}}$, where k is the subcarrier index. When $\text{E}[\mathbf{x}_{d,i}\mathbf{x}_{d,i}^{\text{H}}] = \sigma_d^2\mathbf{I}_D$, $\mathbf{x}_{p,i}\mathbf{x}_{p,i}^{\text{H}} = \sigma_p^2\mathbf{I}_P$, and $\mathbf{I}_a$ is an $(a \times a)$ identity matrix, the PDPR is defined as follows.

Definition 3.1. *The PDPR is the ratio between the average power of each pilot and data tone:*

$$\eta = \frac{\text{trace}\left(\mathbf{x}_{p,i}\mathbf{x}_{p,i}^{\text{H}}\right)/P}{\text{trace}\left(\text{E}\left[\mathbf{x}_{d,i}\mathbf{x}_{d,i}^{\text{H}}\right]\right)/D} = \frac{\sigma_p^2}{\sigma_d^2}. \tag{3.3}$$

Finally, let the DFT matrix for data subchannels and pilot subchannels be $\mathbf{W}_d \in C^{D\times L}$ and $\mathbf{W}_p \in C^{P\times L}$. Those DFT matrices are generated by selecting rows from $\mathbf{W}_K$ according to the index sets $\mathcal{D}$ and $\mathcal{P}$.

3.3 PDPR for Static Channels

In this section, the static channel case is considered. When mobility is restricted, the channel can be considered constant over some number of OFDM symbols. In this case, the estimated channel does not require time-interpolation, so only FFT-based interpolation over frequency domain is considered. Moreover, four likely pilot patterns; independent (IPP), orthogonal (OPP), and two scattered (SPP1, SPP2) pilot patterns can be used to estimate MIMO-OFDM channel which requires estimating multiple spatial links, and the optimal PDPR for each of them is obtained for this static channel case.

3.3.1 Channel Estimation with Different Pilot Patterns

It is assumed that the channel is estimated by using a MMSE estimator using pilot symbols as in [44] and the taps of $\mathbf{h}_{i,j}$ are independent and identically distributed (i.i.d.) complex Gaussian random variables with zero mean and variance equal to $\frac{1}{L}$. Since there are many scatterers near a receiver, each (narrowband) channel can be modeled as a Rayleigh fading channel. It is possible to investigate the effect of channel model on balancing PDPR by using different channel models. However, I focused on the pilot pattern and structure. The received signal for channel estimation is composed of the signals on subcarriers reserved for pilot symbols, and can be expressed as follows,

$$\begin{aligned} \mathbf{y}_p &= [\ \mathbf{y}_{p,1}^T \quad \mathbf{y}_{p,2}^T \quad \cdots \quad \mathbf{y}_{p,M_r}^T\ ]^T \\ &= \mathbf{Z}\mathbf{h} + \mathbf{n}_p, \end{aligned} \tag{3.4}$$

where $\mathbf{y}_{p,j} = \mathrm{vec}\left(y_j(q)\right)_{q\in\mathcal{P}}$, $\mathbf{h} = [\ \mathbf{h}_1^T \quad \cdots \quad \mathbf{h}_{M_r}^T\ ]^T$, $\mathbf{Z} = \mathbf{I}_{M_r} \otimes \mathbf{X}_p\mathbf{F}_p$ where $\otimes$ is the Kronecker product, $\mathbf{F}_p = \mathbf{I}_{M_t} \otimes \mathbf{W}_p$, $\mathbf{W}_p \in C^{P\times L}$ is a DFT matrix generated by selecting rows from a DFT matrix $\mathbf{W}_K \in C^{K\times L}$ according to the index sets $\mathcal{P}$, $\mathbf{X}_p = [\ \mathbf{x}_{p,1} \quad \cdots \quad \mathbf{x}_{p,M_t}\ ]$, $\mathbf{N}_p = [\ \mathbf{n}_{p,1}^T \quad \cdots \quad \mathbf{n}_{p,M_r}^T\ ]^T$, $\mathbf{n}_{p,j} = \mathrm{vec}\left(n_j(k)\right)_{k\in\mathcal{P}}$, and $\mathrm{vec}\,(a_k)$ is a function which creates a vector with elements a_k.

From (3.4) and the channel assumption ($\mathrm{E}\left[\mathbf{h}\mathbf{h}^{\mathrm{H}}\right] = \frac{1}{L}\mathbf{I}_L$), the estimated channel can be expressed as

$$\begin{aligned} \hat{\mathbf{h}}_p &= \mathbf{Z}^{\mathrm{H}}(\mathbf{Z}\mathbf{Z}^{\mathrm{H}} + L\sigma_n^2\mathbf{I}_{PM_r})^{-1}\mathbf{Y}_p \\ &= (\mathbf{I}_{M_r} \otimes \mathbf{F}_p^{\mathrm{H}}\mathbf{X}_p^{\mathrm{H}})\left[(\mathbf{I}_{M_r} \otimes \mathbf{X}_p\mathbf{F}_p\mathbf{F}_p^{\mathrm{H}}\mathbf{X}_p^{\mathrm{H}}) + L\sigma_n^2\mathbf{I}_{PM_r}\right]^{-1}\mathbf{Y}_p \end{aligned} \tag{3.5}$$

by using $(\mathbf{A} \otimes \mathbf{B})(\mathbf{C} \otimes \mathbf{D}) = \mathbf{AC} \otimes \mathbf{BD}$. Then, the estimated channel at the j^{th} receive antenna is

$$\hat{\mathbf{h}}_{p,j} = (\mathbf{F}_p^{\mathrm{H}} \mathbf{X}_p^{\mathrm{H}}) \cdot (\sum_{s=1}^{M_t} \mathbf{x}_{p,s} \mathbf{W}_p \mathbf{W}_p^{\mathrm{H}} \mathbf{x}_{p,s}^{\mathrm{H}} + L\sigma_n^2 \mathbf{I}_P)^{-1} \cdot (\mathbf{X}_p \mathbf{F}_p \mathbf{h}_j + \mathbf{n}_{p,j}), \tag{3.6}$$

where $\mathbf{n}_{p,j}$ is the AWGN noise in frequency domain at the j^{th} receive antenna. Thus, the estimated channel between i^{th} transmit antenna and j^{th} receive antenna using the MMSE channel estimator can be expressed as

$$\hat{\mathbf{h}}_{i,j} = \mathbf{U}_i(\mathbf{X}_p \mathbf{F}_p \mathbf{h}_j + \mathbf{n}_{p,j}) = \sum_{m=1}^{M_t} \mathbf{U}_i \mathbf{x}_{p,m} \mathbf{W}_p \mathbf{h}_{m,j} + \mathbf{U}_i \mathbf{n}_{p,j}, \tag{3.7}$$

where $\mathbf{U}_i = \mathbf{W}_p^{\mathrm{H}} \mathbf{x}_{p,i}^{\mathrm{H}} \left(\sum_{s=1}^{M_t} \mathbf{x}_{p,s} \mathbf{W}_p \mathbf{W}_p^{\mathrm{H}} \mathbf{x}_{p,s}^{\mathrm{H}} + L\sigma_n^2 \mathbf{I}_P \right)^{-1}$. As shown in (3.7), the estimated channel between i^{th} transmit antenna and j^{th} receive antenna has components related not only to $\mathbf{h}_{i,j}$ but also $\mathbf{h}_{m,j}$ $(m \neq i)$. Moreover, it has the term $\sum_{s=1}^{M_t} \mathbf{x}_{p,s} \mathbf{W}_p \mathbf{W}_p^{\mathrm{H}} \mathbf{x}_{p,s}^{\mathrm{H}}$ which sums the power of pilot symbols from all transmit antennas, and decreases the performance of channel estimation. This is because pilot symbols on the same subcarriers are transmitted from all transmit antennas at the same time.

Three pilot transmit schemes that eliminate this interference are considered in order to allow better channel estimation as shown in Fig. 3.2. Independent, orthogonal, and scattered pilot patterns guarantee the orthogonality between signals from different transmit antennas in time, frequency, and code domain, respectively. The motivation for considering different pilot patterns is that for various reasons, different practical systems employ different pilot patterns. For example, in the IEEE 802.16e standard [52], pilot symbols for 2 different transmit antennas are allocated

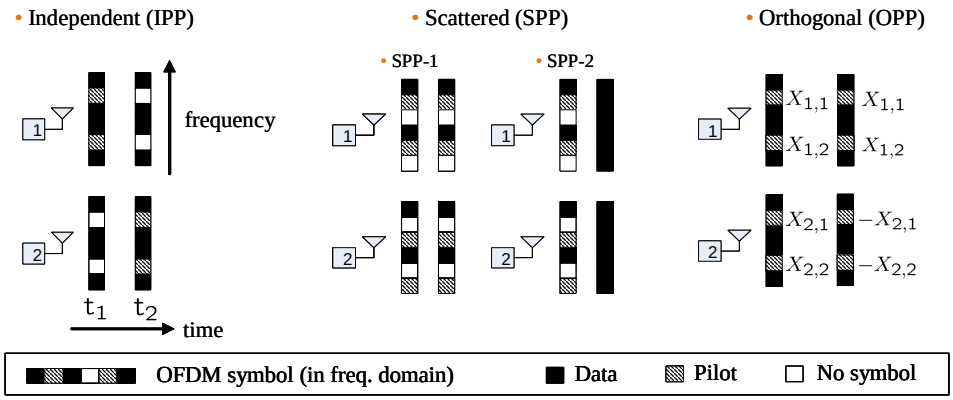

Figure 3.2: Description of independent, orthogonal and scattered pilot patterns

in different symbols (i.e. IPP). For 3 and 4 transmit antennas, pilot symbols for different antennas are allocated in the time and frequency domain, which is a combination of IPP and SPP. In the technical specification of the IEEE802.11n (TGn Sync) proposal [82], orthogonal codes are generated for the pilot symbols of different transmit antennas in MIMO-OFDM HT (high throughput) mode, like OPP. Therefore, independent, orthogonal, and scattered pilot patterns are considered in practical MIMO-OFDM systems, which provides motivation for deriving and comparing the optimal PDPR of each those patterns.

Moreover, the scattered scheme uses more subcarriers for pilot symbols and null symbols during each OFDM symbol time, when it transmits pilot symbols at every OFDM symbol time. It thus requires the channel to be constant over just one OFDM symbol, rather than M_t OFDM symbols. Therefore, it is better for a high Doppler channel scenario, i.e. a fast fading channel. Alternatively, in slowly fading channels, it might be possible to send several OFDM symbols without pilot symbols. Thus, the pilot symbols can be transmitted either at every OFDM symbol

time (SPP-1) or only at the first OFDM symbol time over M_t OFDM symbol times (SPP-2). In this chapter, both configurations will be considered for the scattered pattern.

With the three different pilot patterns and the estimated channel in (3.7), the channel estimation error ($\tilde{\mathbf{h}}_p = \mathbf{h}_p - \hat{\mathbf{h}}_p$) covariance can be found through analysis and simplified as follows,

$$\begin{aligned} \mathrm{E}\left[\tilde{\mathbf{h}}_p \tilde{\mathbf{h}}_p^{\mathrm{H}}\right] &= \frac{1}{L}\left(\mathbf{I}_{LM_tM_r} - \sum_{i=1}^{M_t} \mathbf{Z}^{\mathrm{H}}(\mathbf{Z}\mathbf{Z}^{\mathrm{H}} + L\sigma_n^2\mathbf{I}_{PM_r})^{-1}\mathbf{Z}\right), \\ &= \frac{1}{L}\mathbf{I}_{M_rM_t} \otimes \left(\mathbf{I}_L + \frac{M_t^{\xi}\sigma_p^2}{L\sigma_n^2}\mathbf{W}_p^{\mathrm{H}}\mathbf{W}_p\right)^{-1}, \end{aligned} \tag{3.8}$$

where ξ is 0 for IPP/SPP and 1 for OPP, and $\mathbf{X}_p$ in $\mathbf{Z}$ depends on each pilot pattern of IPP, OPP, and SPP.

From (3.8), it can be found that the channel estimation error covariance is lower bounded when $\mathbf{W}_p^{\mathrm{H}}\mathbf{W}_p$ is a multiple of the identity matrix. The reason for this is that lower bound of the channel MSE can be achieved when this condition is satisfied. In [2, 77], it has been shown that by maximizing the capacity lower bound with respect to the pilot placement while fixing the pilot and data power tradeoff, an upper bound on the capacity lower bound which is a function of only pilot and data power tradeoff can be achieved. And this upper bound on the capacity lower bound is obtained by minimizing the channel MSE, and this MSE lower bound can be achieved when $\mathbf{W}_P^H\mathbf{W}_P$ in the channel MSE is a diagonal matrix. Since the diagonal element of $\mathbf{W}_P^H\mathbf{W}_P$ is P, $\mathbf{W}_P^H\mathbf{W}_P$ has to be $P\mathbf{I}$. And it is easy to find that when $D = mP$ ($m \geq 1$) and $P \geq L$, all of the following placements satisfy this

condition [2]:

$$\mathcal{P} = \{i, i + m + 1, i + 2(m + 1), \ldots, i + (P - 1)(m + 1)\} \tag{3.9}$$

where i can be any integer between 1 and $m + 1$. Using more pilot symbols reduces the available power for data symbols, so once $\mathbf{W}_p^{\mathrm{H}}\mathbf{W}_p$ is a multiple of the identity matrix and $P \geq L$, the minimum possible value L is chosen for the number of required pilot symbols. It will be shown in Section 3.3.3 that additional pilot symbols above L does not result in an additional capacity gain. With this placement and number of pilot symbols, the optimal PDPR which maximizes the capacity lower bound can be found.

3.3.2 Maximizing a Capacity Lower Bound

In this section, a lower bound on capacity is found and the relationship between the capacity lower bound and the PDPR is shown. The reason for considering a capacity lower bound rather than the capacity is that it is difficult to obtain an exact closed form for capacity including PDPR effects. In this chapter, the optimal PDPR is obtained by maximizing the worst case capacity which is the capacity lower bound expressed as the closed form in this chapter. A considerable amount of related research uses the capacity lower bound as a criterion [2, 44, 77]. The capacity is the maximum of the mutual information between the known signals and the unknown signal over the distribution of the transmitted data signal [44]. The received signal at the j^{th} receive antenna in the frequency domain is given by

$$\mathbf{y}_j = \mathbf{H}_j\mathbf{x}_d + \mathbf{n}_j$$

$$= \hat{\mathbf{H}}_j \mathbf{x}_d + \underbrace{\tilde{\mathbf{H}}_j \mathbf{x}_d + \mathbf{n}_j}_{\mathbf{y}_E}, \tag{3.10}$$

where $\mathbf{H}_j = [\ \mathbf{H}_{1,j} \ \cdots \ \mathbf{H}_{M_t,j}\ ]$, $\mathbf{H}_{i,j} = \text{diag}\left(\mathbf{W}_K \mathbf{h}_{i,j}\right)$, $\mathbf{x}_d = [\ \text{vec}\,(x_1(k))_k^T \cdots \text{vec}\,(x_{M_t}(k))_k^T\ ]^T$, $\text{vec}\,(a_k)_k$ is a function which creates a row vector with elements a_k. $\mathbf{H}_j = \hat{\mathbf{H}}_j - \tilde{\mathbf{H}}_j$, and $\tilde{\mathbf{H}}_j$ is the channel estimation error in frequency domain. When $\mathbf{x}_d \sim \mathcal{CN}\left(0, \sigma_d^2 \mathbf{I}\right)$, the capacity lower bound can be obtained as follows [44],

$$\begin{aligned} C_{lb} &= \inf_{p(\mathbf{y}_E)} \sup_{p(\mathbf{x}_d)} I\left(\mathbf{y}_d; \mathbf{x}_d | \hat{\mathbf{H}}\right) \\ &= \frac{1}{K} \mathrm{E}\left[\log_2 \det\left(\mathbf{I}_{DM_r} + \sigma_d^2 \mathbf{R}_{\mathbf{y}_E}^{-1} \hat{\mathbf{H}} \hat{\mathbf{H}}^H\right)\right] \end{aligned} \tag{3.11}$$

where $I\left(\mathbf{y}_d; \mathbf{x}_d | \hat{\mathbf{H}}\right)$ is the mutual information between the received $\mathbf{y}_d$ and transmitted $\mathbf{x}_d$, given the estimated channel, and $p(\mathbf{y}_E)$ and $p(\mathbf{x}_d)$ are the probability distribution of $\mathbf{y}_E$ and $\mathbf{x}_d$, respectively, $\mathbf{R}_{\mathbf{y}_E}$ is the covariance matrix of $\mathbf{y}_E$, and $\mathbf{H} = [\ \mathbf{H}_1^T \ \ \mathbf{H}_2^T \ \cdots \ \mathbf{H}_{M_t}^T\ ]^T$. With the optimal pilot placements in Section 3.3.1 and the assumption that P is a factor of K and $P \geq L$, the matrix $\mathbf{W}_p^{\mathrm{H}} \mathbf{W}_p$ becomes the identity matrix. Through the mathematical analysis, the covariance matrix of $\mathbf{y}_E$ can be expressed as

$$\begin{aligned} \mathbf{R}_{\mathbf{y}_E} &= \sigma_d^2 \mathrm{E}\left[\text{diag}\left(\tilde{\mathbf{H}}_j \tilde{\mathbf{H}}_j^{\mathrm{H}}\right)_{j=1}^{M_r}\right] + \sigma_n^2 \mathbf{I}_{DM_r} \\ &= \sigma_d^2 \cdot \text{diag}\left(\sum_{i=1}^{M_t} \text{diag}\left(\mathbf{W}_d \bar{\mathbf{I}}_{i,j} \mathrm{E}\left[\tilde{\mathbf{h}}_p \tilde{\mathbf{h}}_p^{\mathrm{H}}\right] \bar{\mathbf{I}}_{i,j}^{\mathrm{H}} \mathbf{W}_d^{\mathrm{H}}\right)\right)_{j=1}^{M_r} + \sigma_n^2 \mathbf{I}_{DM_r} \\ &= \left(\frac{L\sigma_d^2 M_t}{M_t^\kappa P \gamma_p + L} + \sigma_n^2\right) \mathbf{I}, \end{aligned} \tag{3.12}$$

where κ is 0 for IPP and SPP, 1 for OPP, and $\gamma_p = \sigma_p^2 / \sigma_n^2$. $\bar{\mathbf{I}}_{i,j}$ is used for convenience in expression. $\bar{\mathbf{I}}_{i,j} = [\ \mathbf{0}_{(i-1)L+M_r(j-1)L} \ \ \mathbf{I}_L \ \ \mathbf{0}\ ]$, the size of $\mathbf{I}_i$ is $(L \times LM_tM_r)$, and

$\mathbf{0}_{(i-1)L+M_r(j-1)L}$ is an $(L \times ((i-1)L + M_r(j-1)L))$ all zero matrix. For the scattered pilot pattern, two possible scenarios are considered as mentioned in Section 3.3.1. However, the analysis of the capacity lower bound for the time when pilot symbols are transmitted is the same for both cases.

When the PDPR is changed, the estimated channel matrix also varies. Therefore, the effective SNR and the estimated channel matrix should be considered together for maximizing the capacity lower bound. However, after normalizing the estimated channel matrix, the capacity lower bound can be maximized by maximizing only the effective SNR, because the effective SNR is the only term including the PDPR effect after normalization [44, 77]. The estimated channel can be normalized as $\bar{\mathbf{H}} = \frac{1}{\sigma_{\hat{\mathbf{H}}}}\hat{\mathbf{H}}$. The estimated channel $\hat{\mathbf{H}}$ is zero mean, thus the variance can be obtained as

$$\begin{aligned} \sigma^2_{\hat{\mathbf{H}}} &= \mathrm{E}[\mathrm{tr}(\hat{\mathbf{H}}\hat{\mathbf{H}}^{\mathrm{H}})] \\ &= M_r M_t D - \frac{M_r M_t L D}{M_t^{\kappa} P \gamma_p + L}. \end{aligned} \tag{3.13}$$

Then, the capacity lower bound can be written as

$$C_{lb} = \frac{1}{K}\mathrm{E}\left[\log_2 \det\left(\mathbf{I}_{DM_r} + \rho_{\mathrm{eff}}\bar{\mathbf{H}}\bar{\mathbf{H}}^{\mathrm{H}}\right)\right], \tag{3.14}$$

$$\rho_{\mathrm{eff}} = \frac{D P M_r M_t^{(\kappa+1)} \sigma_d^2 \sigma_p^2}{\sigma_n^2(M_t^{\kappa} P \sigma_p^2 + L(\sigma_d^2 M_t + \sigma_n^2))}, \tag{3.15}$$

where the size of the estimated channel matrix and D are different according to the pilot patterns due to their different number of subcarriers for data symbols. In the case of the scattered pilot pattern, this capacity lower bound is for the OFDM symbol time when pilot symbols are transmitted. As shown in (3.14), the capacity

lower bound can be maximized only by maximizing the effective SNR ρ_{eff} using the optimal PDPR. If we consider a single-input single-output system by setting M_t and M_r equal to 1, (3.14) is similar to the effective SNR in [2].

3.3.3 Optimal PDPR of IPP, OPP, and SPP-1

Let α denote the fraction of total transmit power that is allocated to data symbols, then σ_d^2 and σ_p^2 in the effective SNR can be expressed with α and p_{tot} which is the total transmit power. Thus, the effective SNR can be written as

$$\rho_{\text{eff}} = \frac{\alpha(1-\alpha)DP_{tot}^2 M_r}{\sigma_n^2(\alpha P_{tot}(LM_t^{\chi} - D) + D(P_{tot} + LM_t^{\chi}\sigma_n^2))}, \tag{3.16}$$

where χ is 0 for IPP and OPP, 1 for SPP-1. Then, the optimal PDPR that maximizes the capacity lower bound of MIMO-OFDM system with IPP, OPP, and SPP-1 can be obtained as following theorem.

Theorem 3.1. *Under the assumption that P is a factor of D and $P \geq L$, the optimal PDPR that maximizes the capacity lower bound of MIMO-OFDM system with IPP, OPP, and SPP-1 is given by*

$$\eta_{opt} = \begin{cases} \frac{DM_t^{\xi}}{P} & \text{if } LM_t^{\chi} = D \\ \frac{\sqrt{LM_t^{\chi} D(LM_t^{\chi}\sigma_n^2 + P_{tot})(P_{tot} + \sigma_n^2 D)M_t^{\xi}}}{P(P_{tot} + LM_t^{\chi}\sigma_n^2)} & \text{otherwise} \end{cases} \tag{3.17}$$

where ξ is 1 for IPP, 0 for OPP and SPP-1, and χ is 0 for IPP and OPP, 1 for SPP-1.

Proof. To find the optimal α, solving the optimization problems by finding $\max \rho_{\text{eff}}$ subject to the total power constraints is required. Now, for IPP, OPP, and SPP-1 cases, the α which maximizes the effective SNR over $0 < \alpha < 1$ can be found by

differentiating ρ_{eff} and setting it equal to zero. Thus, if it is assumed that P is a factor of D and $P \geq L$, the optimal fraction of total transmit power that is allocated to data symbols is given by

$$\begin{aligned} \alpha_{max} &= \arg\max_{0<\alpha<1} \rho_{\text{eff}} \\ &= \begin{cases} \frac{1}{2} & \text{if } LM_t^{\chi} = D \\ \frac{-\gamma + \sqrt{\beta\gamma + \gamma^2}}{\beta} & \text{otherwise} \end{cases} \end{aligned} \tag{3.18}$$

where $\beta = P_{tot}(LM_t^{\chi} - D)$, $\gamma = D(P_{tot} + LM_t^{\chi}\sigma_n^2)$. Then, with the definition of PDPR, the optimal PDPR can be found by using the optimal α. □

From (3.16) and $K = D + M_t^{\chi} P$, the effect of the number of pilot symbols on the effective SNR can be found as follows,

$$\rho_{\text{eff}}(P) - \rho_{\text{eff}}(P+1) > 0 \qquad \forall P \geq L, \tag{3.19}$$

where $\rho_{eff}(P)$ is the effective SNR when the number of pilot symbols is P. This means, as noted earlier, that there is no additional gain when $P \geq L$, so $P = L$.

In the case of SPP-2, the channel value which is estimated at the first OFDM symbol time with the PDPR in (3.17) can be used for the remaining $(M_t - 1)$ OFDM symbol times. Even though this is a suboptimal solution for the SPP-2 configuration, it has much lower complexity than the optimal solution. Moreover, the lower bound with this suboptimal method shows similar results to the optimal solution, as shown in Section 3.3.4.

3.3.4 Optimal PDPR of SPP-2

In the configuration of SPP-2, pilot symbols are transmitted only at the first OFDM symbol time (T_1) during M_t OFDM symbol times. During the remaining $M_t - 1$ OFDM symbol times (T_2), data symbols can be transmitted on subcarriers which is used for pilot symbols at the first OFDM symbol time with using the same channel information estimated at first OFDM symbol time. Then the capacity lower bound of this scattered pilot pattern can be expressed as following.

$$C_{lb} = \frac{1}{M_t} E\left[C_{lb,1} + (M_t - 1)C_{lb,2}\right], \tag{3.20}$$

where $C_{lb,1}$ and $C_{lb,2}$ are capacity lower bound at T_1 and T_2, respectively, and are given as

$$C_{lb,m} = \frac{1}{K} \log_2 \det\left(\mathbf{I}_{D_m M_r} + \rho_{\text{eff},m} \bar{\mathbf{H}} \bar{\mathbf{H}}^{\text{H}}\right), \qquad \text{for } m = 1,2 \tag{3.21}$$

where $D_1 = D$ and $D_2 = K$, $\rho_{\text{eff},1}$ is the effective SNR for scattered pilot pattern in (3.14) and $\rho_{\text{eff},2}$ is given by

$$\rho_{\text{eff},2} = \frac{(1-\alpha) K P_{tot}^2 M_r}{\sigma_n^2(\alpha P_{tot}(LM_t - K) + K(P_{tot} + LM_t\sigma_n^2))}. \tag{3.22}$$

Due to the structure of $\bar{\mathbf{H}}$ and by using the singular value decomposition (SVD), the capacity lower bound (3.21) can be expressed as follows,

$$\begin{aligned} C_{lb,1} &= \frac{1}{K} \log_2 \prod_{k_1 \in \mathcal{D}_{SPP}} \det\left(\mathbf{I} + \rho_{\text{eff},1} \bar{\mathbf{H}}(k_1) \bar{\mathbf{H}}^{\text{H}}(k_1)\right) \\ &= \frac{1}{K} \log_2 \prod_{k_1 \in \mathcal{D}_{SPP}} \det\left(1 + \rho_{\text{eff},1} \mathbf{\Lambda}(k_1)\right) \end{aligned}$$

$$= \frac{1}{K}\log_2 \prod_{k_1\in\mathcal{D}_{SPP}} \prod_{j_1\in\mathcal{M}} \left(1+\rho_{\text{eff},1}\lambda_{k_1,j_1}\right), \tag{3.23}$$

where $\mathcal{M} = \{1, \cdots, M_r\}$, $\mathcal{D}_{SPP}$ is an index set of subcarriers for data symbols of the scattered pilot pattern, $\mathbf{\Lambda}(k_1)$ is a vector containing the singular values $\{\lambda_{k_1,1}, \cdots, \lambda_{k_1,M_r}\}$ of $\bar{\mathbf{H}}(k_1)\bar{\mathbf{H}}^{\text{H}}(k_1)$, and $\bar{\mathbf{H}}(k_1)$ is the $(M_r \times M_t)$ normalized estimated channel matrix for the k_1^{th} subcarrier. With the same procedure and defining $\prod_{a,b}$ as $\prod_{a\in\mathcal{A}} \prod_{b\in\mathcal{B}}$, $C_{lb,2}$ can be expressed as

$$C_{lb,2} \quad = \quad \frac{1}{K}\log_2 \prod_{k_2,j_2} \left(1+\rho_{\text{eff},2}\lambda_{k_2,j_2}\right), \tag{3.24}$$

where $k_2 \in \mathcal{K}$, $j_2 \in \mathcal{M}$, $\mathcal{K} = \{1, \ldots, K\}$ is an index set of all K subcarriers. Thus, from (3.20), the capacity lower bound of SPP-2 is given by

$$\begin{aligned} C_{lb} &= \frac{1}{KM_t}\left[\log_2 \prod_{k_1,j_1}\left(1+\rho_{\text{eff},1}\lambda_{k_1,j_1}\right) + (M_t-1)\log_2 \prod_{k_2,j_2}\left(1+\rho_{\text{eff},2}\lambda_{k_2,j_2}\right)\right], \\ &= \frac{1}{KM_t}E\Bigg[\underbrace{\log_2 \prod_{k_1,j_1}\left(1+\rho_{\text{eff},1}\lambda_{k_1,j_1}\right)\left(1+\rho_{\text{eff},2}\lambda_{k_1,j_1}\right)^{(M_t-1)}}_{(3.25)-A} \\ &\qquad \underbrace{\times \prod_{k_3,j_2}\left(1+\rho_{\text{eff},2}\lambda_{k_3,j_2}\right)^{(M_t-1)}}_{(3.25)-B}\Bigg], \end{aligned} \tag{3.25}$$

where $k_3 \in \mathcal{P}_{SPP}$. (3.25)-B is an additional capacity gain by transmitting data symbols on subcarriers which are used for pilot symbols at the first OFDM symbol time. The whole available transmit power is allocated to data symbols during $(M_t - 1)$ OFDM symbol times, and this gain can be found from $\rho_{\text{eff},2}$ in (3.25). The optimal PDPR can be found by finding α which maximizes C_{lb} in (3.25) as follows,

$$\alpha_{opt} = \arg\max_{0<\alpha<1} C_{lb}. \tag{3.26}$$

Even though this optimization can be solved for any number of antennas by differentiating C_{lb}, there is no general closed form of the solution for the arbitrary number of antennas cases. Moreover, the complexity of solving this problem is very high. For example, even for the 2×2 MIMO case, the equation is the product of $2K$ terms.

3.4 PDPR for Dynamic Channels

In this section, moderate mobility is considered such that the channel is varying over consecutive OFDM symbols but invariant during one OFDM symbol duration so that it is insufficient to cause doubly-selective fading channel [55, 56, 98]. As shown in the previous section, SPP-2 shows higher capacity lower bound than other pilot patterns in static channels, because the power allocation in SPP-2 is a 2 dimensional problem while it is a 1 dimensional problem in other patterns. Thus, there are more degrees of freedom with SPP-2, and it results in a higher capacity lower bound. Moreover, since the channel varies over OFDM symbols in dynamic channels, OPP does not guarantee the orthogonality in pilot structure and results in worse performance. In the case of IPP, channel estimation and interpolation can be done for each antenna separately, but still it is an 1 dimensional problem over M_t OFDM symbol time. Thus, SPP is considered in this dynamic channel case. In case of SPP-1, the optimal PDPR and overall analysis are the same as in static channels, since pilot symbols are transmitted every OFDM symbol. However, in the case of SPP-2, interpolation is required in time and frequency. Due to the excellent performance of the SPP-2 structure in static channels, in this section the efficacy of this pattern is analyzed with MMSE interpolation in time and frequency as shown

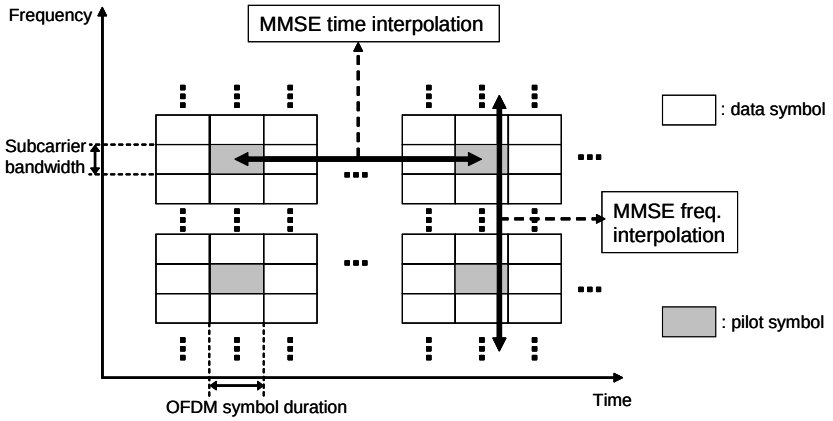

Figure 3.3: Pilot and interpolation structure for the dynamic channel case

in Fig. 3.3.

3.4.1 Interpolated Symbols

First, channel estimation over pilot symbols is required. The least-squares (LS) channel estimation is considered in this chapter. Since the channel estimation is interpolated over time and frequency, one spatial link channel is considered in this analysis part instead of whole MIMO channel. The LS estimated frequency channel response over pilot symbol subcarriers is given by

$$\hat{\mathbf{H}}_P^{m_r,m_t} = \mathbf{H}_P^{m_r,m_t} + \frac{\mathbf{n}}{\sigma_p}, \tag{3.27}$$

where $\mathbf{s}_p$ is a vector of pilot symbols transmitted at one (m_t^{th}) transmit antenna. Since pilot symbols are transmitted over certain time-frequency locations, interpolation is required to obtain the channel estimate for data symbols. MMSE interpolation is considered in both the time and frequency domain. In this chapter, the estimated channel is interpolated over the frequency domain, then the interpolation in time is

performed to obtain a channel estimate for the data symbols in non-pilot-inserted OFDM symbols. A joint 2D interpolation can show better system performance than separate time and frequency interpolation. However, the joint 2D interpolation has higher complexity than the separate time and frequency interpolation due to requiring the cross correlation of frequency and time. Thus, the separate time and frequency interpolation scheme is considered to investigate the optimal PDPR with practical pilot structure.

3.4.1.1 MMSE Frequency Interpolation

In a pilot-assisted OFDM symbol, the channel estimate over the pilot tones can be interpolated to provide a channel estimate for the data symbols. Since it is assumed that the channel is varying during a block of OFDM symbols but invariant during one OFDM symbol duration, Doppler does not affect the frequency interpolation. The estimated channel using MMSE frequency interpolation is given by

$$\hat{\mathbf{H}}_F^{m_r,m_t} = \mathbf{R}_{FP}\left(\mathbf{R}_{PP} + \frac{\sigma_n^2}{\sigma_p^2}\mathbf{I}\right)^{-1}\hat{\mathbf{H}}_P^{m_r,m_t}, \tag{3.28}$$

where $\mathbf{R}_{FP} = E\left[\mathbf{H}_F^{m_r,m_t}(\mathbf{H}_P^{m_r,m_t})^H\right]$ and $\mathbf{R}_{PP} = E\left[\mathbf{H}_P^{m_r,m_t}(\mathbf{H}_P^{m_r,m_t})^H\right]$. With the matrix inversion lemma and $E\left[\mathbf{h}^{m_r,m_t}(\mathbf{h}^{m_r,m_t})^H\right] = \frac{1}{L}\mathbf{I}$,

$$\begin{aligned}\hat{\mathbf{H}}_F^{m_r,m_t} &= \frac{\gamma_p}{P\gamma_p + L}\mathbf{F}\mathbf{F}_P^H\hat{\mathbf{H}}_P^{m_r,m_t} \\ &= \mu P\mathbf{H}^{m_r,m_t} + \mu\mathbf{F}\mathbf{F}_P^H\frac{\mathbf{n}_P}{\sigma_p},\end{aligned} \tag{3.29}$$

where $\mu = \frac{\gamma_p}{P\gamma_p+L}$. Thus, the frequency interpolated frequency domain channel response of k^{th} subcarrier is given by

$$\hat{\mathbf{H}}_F^{m_r,m_t}(k) = \mu P \mathbf{H}^{m_r,m_t}(k) + \mu \frac{\mathbf{N}'(k)}{\sigma_p}, \tag{3.30}$$

where $\mathbf{N}' = \mathbf{F}\mathbf{F}_P^H \mathbf{n}_P$.

3.4.1.2 MMSE Time Interpolation

Since the channel is varying over successive OFDM symbols, the data symbols in subsequent OFDM symbols undergo different but correlated channels. Let N be the number of OFDM symbols between two pilot-inserted OFDM symbols. Then, the channel estimation values for data symbols on the k^{th} subcarrier in $N-1$ non-pilot-inserted OFDM symbols can be obtained by interpolating the frequency interpolated channel estimation values on the k^{th} subcarrier in two pilot-inserted OFDM symbols. To exploit the time correlation of channel which is related to the Doppler effect, the MMSE time interpolation is considered.

From Appendix B.1, the time interpolated k^{th} subcarrier channel response of N OFDM symbols is given by

$$\hat{\mathbf{H}}_{FT,k}^{m_r,m_t} = \mathbf{G}_k \hat{\mathbf{C}}_{P,k}, \tag{3.31}$$

where

$[\mathbf{G}_k]_{i,j} = g_{i,j}$ where j=1,2

$$= \begin{cases} \psi\left(\varepsilon \mathrm{J}_0(2\pi f_d(i-1)T_s) - \mu^2 P^2 \mathrm{J}_0(2\pi f_d(N-1)T_s)\mathrm{J}_0(2\pi f_d(N-i)T_s)\right), \\ \qquad\qquad\qquad\qquad\qquad\qquad\qquad\qquad \text{for } j = 1 \\ \psi\left(\varepsilon \mathrm{J}_0(2\pi f_d(N-i)T_s) - \mu^2 P^2 \mathrm{J}_0(2\pi f_d(N-1)T_s)\mathrm{J}_0(2\pi f_d(i-1)T_s)\right), \\ \qquad\qquad\qquad\qquad\qquad\qquad\qquad\qquad \text{for } j = 2 \end{cases} \tag{3.32}$$

$$\varepsilon = \mu^2 P^2 + \frac{\mu^2 \omega_k}{\gamma_P}, \tag{3.33}$$

$$\psi = \frac{\mu P}{|\varepsilon^2 - \mu^4 P^4 \mathrm{J}_0(2\pi f_d(N-1)T_s)^2|}. \tag{3.34}$$

As shown in Appendix B.1 and (3.32) the Clark's model is used to see the effect of Doppler on balancing PDPR. Thus, a temporal correlation function is modeled as a Bessel function. Since the channel temporal correlation similarly decreases for different channel models, the results with different channel models can be expected to have similar trends. Also, given a temporal correlation function for a different channel model, the developed frame work can be used for that channel model (using the temporal correlation function instead of a Bessel function).

3.4.2 Maximizing the Capacity Lower Bound

With the time-frequency interpolated channel estimation in (3.31), the capacity lower bound of this pilot structure with Doppler effect can be obtained as follows,

$$C_{lb} = \frac{1}{KN}\mathrm{E}\left[\sum_{n=1}^{N} \log_2 \det\left(\mathbf{I} + \sigma_d^2 \mathbf{R}_{\mathbf{y}_{E,n}}^{-1} \hat{\mathbf{H}}_{FT}(n) \hat{\mathbf{H}}_{FT}^H(n)\right)\right], \tag{3.35}$$

where $\mathbf{R}_{\mathbf{y}_{E,n}} = E\left[\mathbf{y}_E(n)\mathbf{y}_E^H(n)\right]$, $\mathbf{y}_E(n) = \tilde{\mathbf{H}}(n)\bar{\mathbf{X}}(n) + \mathbf{n}$, and $\hat{\mathbf{H}}_{FT}(n)$ has the same structure as $\hat{\mathbf{H}}$ in (3.11). Then, the capacity lower bound can be obtained as following lemma.

Lemma 3.1. *A capacity lower bound of MIMO-OFDM with pilot-based MMSE time and frequency interpolation is*

$$\mathrm{C}_{lb} = \frac{1}{KN}\mathrm{E}\left[\sum_{n=1}^{N}\log_2\det\left(\mathbf{I}+\boldsymbol{\rho}_{\mathrm{eff}}(n)\bar{\mathbf{H}}(n)\bar{\mathbf{H}}^{\mathrm{H}}(n)\right)\right], \tag{3.36}$$

$$\boldsymbol{\rho}_{\mathrm{eff}}(n) = \sigma_d^2\sigma^2_{\hat{\mathbf{H}}_{FT}(n)}\left(\mathrm{diag}(\boldsymbol{\Lambda}_{m_r,n})_{m_r=1}^{M_r}\right)^{-1}. \tag{3.37}$$

Proof. The channel estimation error covariance matrix can be obtained as (B.8) in Appendix B.2, and we can normalize $\hat{\mathbf{H}}_{\mathbf{FT}}(n)$ as $\bar{\mathbf{H}}(n) = \frac{1}{\sigma_{\hat{\mathbf{H}}_{FT}(n)}}\hat{\mathbf{H}}_{\mathbf{FT}}(n)$, as shown in Section 3.3.2, where the variance is given by

$$\begin{aligned}\sigma^2_{\hat{\mathbf{H}}_{FT}(n)} &= \mathrm{E}[\mathrm{tr}(\hat{\mathbf{H}}_{FT}(n)\hat{\mathbf{H}}_{FT}(n)^{\mathrm{H}})] \\ &= M_rM_t\sum_{k=1}^{K_n}\Big(g^2_{n,1}\mu^2P^2 + g^2_{n,2}\mu^2P^2 + 2g_{n,1}g_{n,2}\mu^2P^2\mathrm{J}(1,N) \\ &\qquad + (g^2_{n,1}+g^2_{n,2})\frac{\mu^2\omega_k}{\gamma_P}\Big),\end{aligned} \tag{3.38}$$

where

$$K_n = \begin{cases} K, & n = 2,\ldots,N-1 \\ K - M_tP, & n = 1, N \end{cases} \tag{3.39}$$

Then, the capacity lower bound can be obtained as (3.37) □

3.4.3 Optimal PDPR

Let α denote the fraction of total transmit power that is allocated to data symbols as in Section 3.3.3. The effective SNR value of each subcarrier is different due to the frequency domain interpolation error. $\boldsymbol{\omega} = [\omega_1,\ldots,\omega_K]$ is a vector having the same element every $m+1$ elements where $D = mP$ (i.e. $\omega_i = \omega_{i+m+1}$). However, since the pilot structure in Section 3.3.1 is considered, all the elements

of $\boldsymbol{\omega}$ are same (i.e $\omega_k = \omega_1$ for all k). Therefore, the capacity lower bound can be maximized by maximizing the effective SNR as in the static channel case. Thus, the effective SNR to be maximized is given by

$$\rho_{\text{eff}}(n) = \frac{\sigma_d^2 M_r M_t K_n \left(g_{n,1}^2 \mu^2 P^2 + g_{n,2}^2 \mu^2 P^2 + 2 g_{n,1} g_{n,2} \mu^2 P^2 \mathrm{J}(1,N) + (g_{n,1}^2 + g_{n,2}^2) \frac{\mu^2 \omega_1}{\gamma_P} \right)}{(M_t \sigma_d^2 \xi_1(n) + \sigma_n^2)}, \tag{3.40}$$

As shown in Section 3.3.4, the capacity lower bound can be expressed as

$$C_{lb} = \frac{1}{KN} E \left[\sum_{n=1}^{N} \log_2 \prod_{k_n, m_r} (1 + \rho_{\text{eff}}(n) \lambda_{k_n, m_r}) \right], \tag{3.41}$$

where $k_n \in \mathcal{K}_n$ and $\mathcal{K}_n$ is a data subcarrier index set of the n^{th} OFDM symbol. Then the optimal PDPR can be obtained by finding α which maximizes C_{lb} in (3.41) as $\alpha_{opt} = \arg\max_{0<\alpha<1} C_{lb}$, when it is assumed that P is a factor of D and $P \geq L$. It is difficult to find the closed form of the solution due to the correlation between λ_{k_{n1}, m_r} and λ_{k_{n2}, m_r} for $n1 \neq n2$, $n1, n2 \in \{1, \ldots, N\}$. This problem can be readily solved by numerical search and the results are shown in Section 3.5.2.

3.5 Results and Interpretation

In this section, the capacity lower bound of pilot-assisted MIMO-OFDM systems with the optimized PDPR is demonstrated under two different channel conditions using Monte Carlo simulations. For the simulation, it is assumed that $L = 4$, $P = 4$, $K = 64$, and the OFDM symbol duration (T_s) is $60\mu s$. In the case of dynamic channels, 1~60km/h vehicle speed is considered so that my assumption of

a varying channel over a block of OFDM symbols and an invariant channel during one OFDM symbol is reasonable.

3.5.1 Ergodic Capacity with the Optimal PDPR for Static Channels

Fig. 3.4 shows the ergodic capacity lower bound of a 2×2 MIMO-OFDM system with four different pilot patterns according to the percentage of pilot power for 2 different SNR cases (SNR=6,16dB). It is assumed that the channel is constant over M_t OFDM symbol periods. The capacity of IPP and OPP show the same results. At each SNR, the capacity lower bound has maximum value when the percentage of pilot power is about 0.18 for IPP/OPP, about 0.28 for SPP-1, and about 0.35 for SPP-2. The capacity decreases as the pilot power is either decreased or increased from the optimal percentages due to poor channel estimation and low transmit power for data symbols, respectively. In case of SPP-2, if more power to pilot symbols is allocated than the optimal percentage of SPP-1, it will result in a lower capacity lower bound than that of SPP-1 at the first OFDM symbol time. However, a higher capacity lower bound can be obtained over the remaining (M_t-1) OFDM symbol times which results in a higher ergodic capacity lower bound for SPP-2. An overall observation is that the capacity is not especially sensitive to the PDPR as long as it is in a certain region. For example, a quasi-optimal region is about $0.1 \sim 0.3$ in 2×2 MIMO-OFDM systems with IPP/OPP.

The ergodic capacity with the optimal PDPR for 2×2 and 4×4 MIMO-OFDM systems with four different pilot patterns are shown in Fig. 3.5. Suboptimal SPP-2 is the case when the optimal PDPR of SPP-1 for SPP-2 configuration is used.

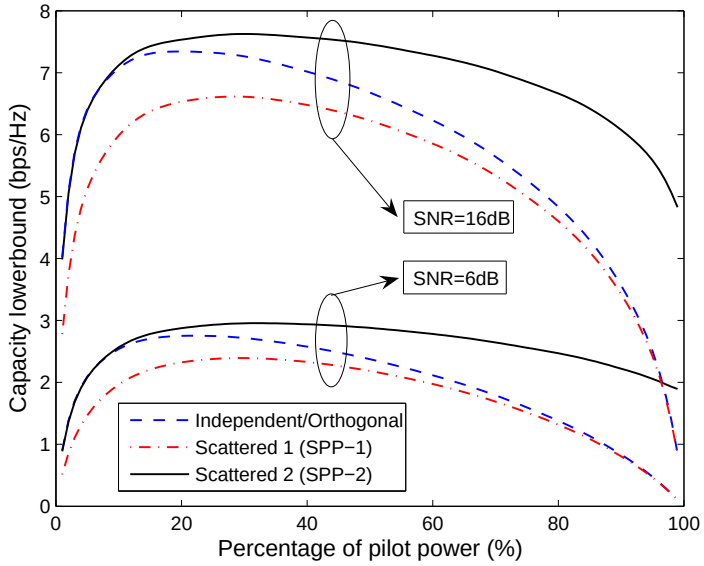

Figure 3.4: Capacity lower bound versus pilot power for 2×2 MIMO-OFDM systems with three different pilot patterns, K=64, P=4, L=4

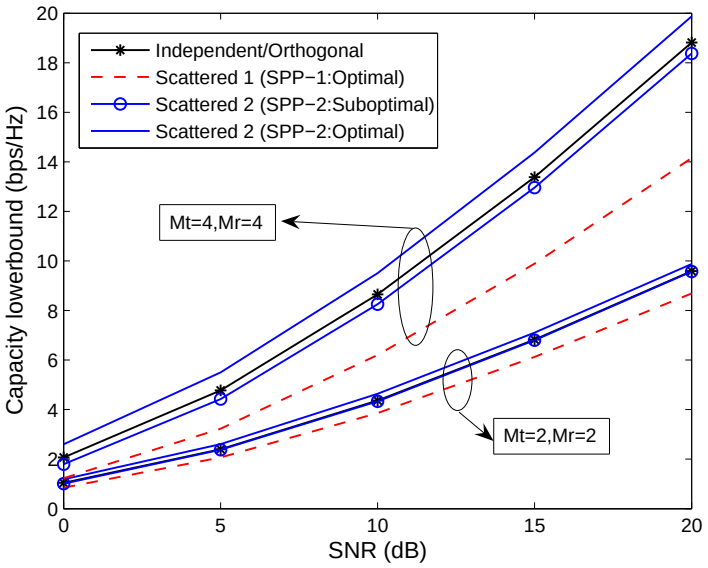

Figure 3.5: Capacity lower bound with optimal PDPR versus SNR for 2×2 and 4×4 MIMO-OFDM systems, K=64, P=4, L=4

In Fig. 3.5, the ergodic capacity lower bounds of IPP, OPP, and suboptimal SPP-2 are similar and higher than the optimal SPP-1. However, they are lower than the capacity lower bound of the optimal SPP-2. In the case of the 2x2 MIMO-OFDM, the gap between the optimal and suboptimal solutions is very small. The optimal solution shows about 1dB gain over the suboptimal solution for 4×4 MIMO-OFDM. The gap can be larger for systems that have more transmit and receive antennas, but, for reasonable numbers of antennas (i.e. 2, 3, 4), the suboptimal solution shows similar performance and lower complexity compared to the optimal solution.

From Section 3.3.2, for a fixed power $P_x = tr(E[\mathbf{x}_d \mathbf{x}_d^H])$, the mutual information between transmitted information symbols and received symbols is given by $I(\mathbf{y}_d; \mathbf{x}_d|\hat{\mathbf{H}})$. The ergodic channel capacity is given by

$$C = \frac{1}{K} E\left[\max_{p(\mathbf{x}_d), P_x} I(\mathbf{y}_d; \mathbf{x}_d|\hat{\mathbf{H}})\right] \qquad (bits/sec/Hz). \tag{3.42}$$

Then, when the channel estimate is perfect, an upper bound on capacity can be obtained for a Gaussian distributed $\mathbf{x}_d$ as [77]

$$C_{upper} = \frac{1}{K} E\left[\log\det\left(\mathbf{I} + \frac{P_x}{\sigma_n^2}\mathbf{H}\mathbf{H}^H\right)\right]. \tag{3.43}$$

This upper bound of the average capacity is a benchmark for the maximum achievable rate.

Fig. 3.6 shows the capacity upper bound and lower bound for 2×2 MIMO-OFDM systems considering four different pilot patterns. As previously defined, the upper bound case is when the channel estimate is perfect. Thus, it shows the maximum achievable capacity. As shown in this figure, the capacity lower bound

with equal power allocation shows capacity loss due to having channel estimation error and using pilot symbols. Using the optimal PDPR, the capacity lower bound is increased toward the capacity upper bound. For example, in 2×2 MIMO-OFDM systems with SNR=10dB, the capacity lower bound can be increased about 40%, 30%, and 19% for IPP/OPP, SPP-1, and SPP-2, respectively. It implies that higher data rates are achievable by simply using this optimal PDPR.

3.5.2 Ergodic Capacity with the Optimal PDPR for Dynamic Channels

Figs. 3.7, 3.8, and 3.9 show the results for dynamic channels. In this case, the number of non-pilot-inserted OFDM symbols between pilot-inserted symbols is 8 (i.e. $N = 10$). Fig. 3.7 and 3.8 show the capacity lower bound of a 2×2 and 4×4 MIMO-OFDM systems with 3 different vehicle speeds. The optimal PDPR and equal power points are marked with squares and circles, respectively. As shown in these figures, the optimal PDPR changes according to the vehicle speed due to the effect of the Doppler shift on channel estimation and interpolation. However, the optimal points between the different vehicle speed cases are very close. With the optimal PDPR, capacity lower bound is much higher than in the equal power case (i.e. no pilot power boosting) as shown in the static channels. Moreover, there is broad range of PDPR showing similar capacity to the optimal capacity case. Thus, the smaller PDPR value can be used to achieve similar capacity lower bound with the optimal value while reducing the peak transmit power of the transmitter.

Fig. 3.9 compares the capacity lower bound of two different vehicle speed with the optimal PDPR and the equal pilot and data power. As shown in this figure,

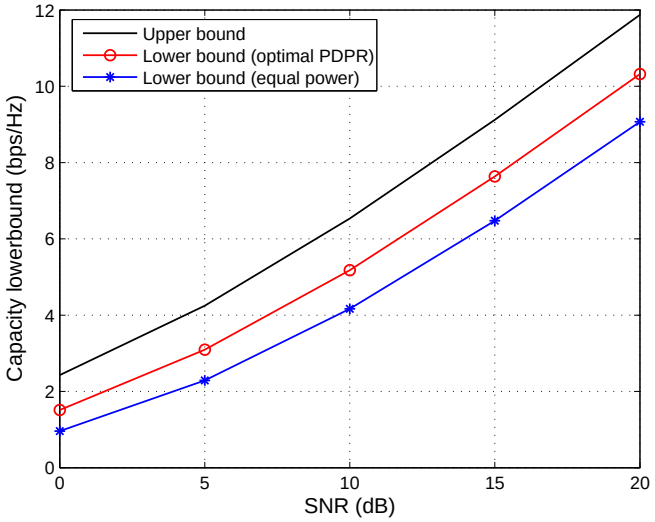

(a) SPP-1 case

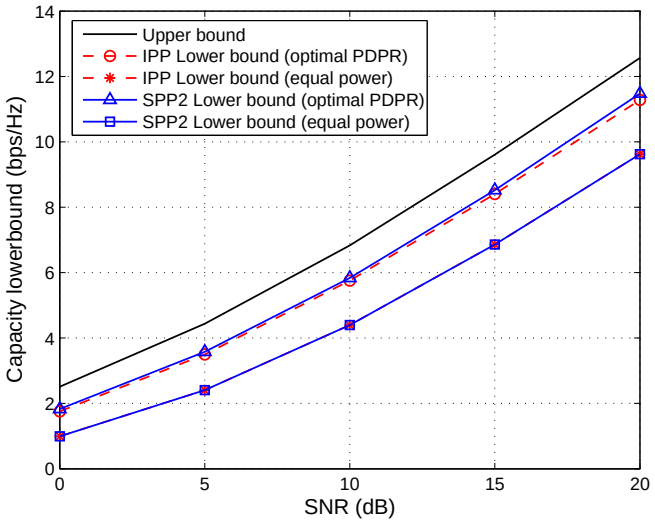

(b) IPP/OPP and SPP-2 cases

Figure 3.6: Capacity upper and lower bound versus SNR for 2×2 MIMO-OFDM system with the optimal PDPR and equal power, K=64, P=4, L=4

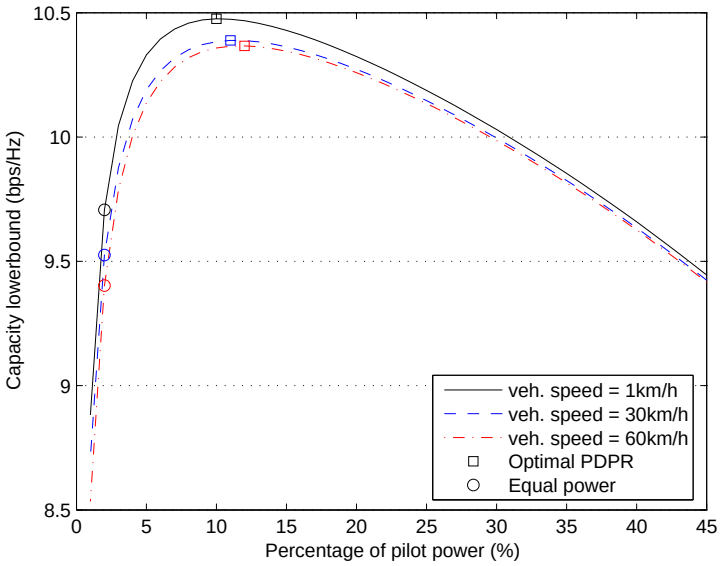

Figure 3.7: Capacity lower bound versus pilot power for 2×2 MIMO-OFDM for dynamic channel, veh. speeds=1,30,60km/h, K=64, P=4, L=4, N=10, SNR=20dB

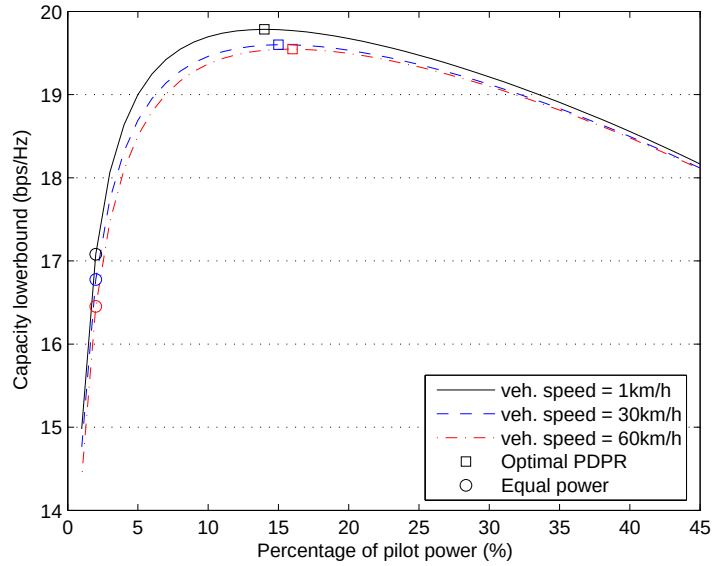

Figure 3.8: Capacity lower bound versus pilot power for 4×4 MIMO-OFDM for dynamic channel, veh. speeds=1,30,60km/h, K=64, P=4, L=4, N=10, SNR=20dB

with the optimal PDPR, 19% and 21% higher capacity can be achieved than the equal power case for 1km/h and 60km/h vehicle speeds, respectively. It can be found that the optimal PDPR results in not only a higher capacity lower bound than the equal power case but also smaller capacity loss due to the higher speed.

Fig. 3.10 shows the optimal pilot power percentage according to different vehicle speeds. The optimal PDPR is varied according to the vehicle speed, but its variation is small. This is because the Doppler effect with the considered vehicle speed region affects the channel estimation and interpolation error, but its effect is not severe. This can be confirmed by Fig. 3.11 which shows the maximum average effective SNR according to different vehicle speeds. As the vehicle speed increases, the maximum average effective SNR per antenna is decreased due to higher channel estimation and interpolation error with higher Doppler effect. However, the variation is very small. It shows that the Doppler effect with the considered vehicle speed region is not severe, and the SNR loss due to high Doppler is reduced when the optimal PDPR is used.

3.5.3 PDPR for Practical Systems

Maximizing the capacity lower bound might be an inappropriate solution in some practical wireless communications systems. For example, the optimal PDPR in this chapter might be a suboptimal solution for minimizing the average error rate, especially for the SPP-2 case since different objective functions (log or exponential) can give different results when they are optimized over a block of OFDM symbols. However, in practical systems, channel coding schemes such as a turbo coding are

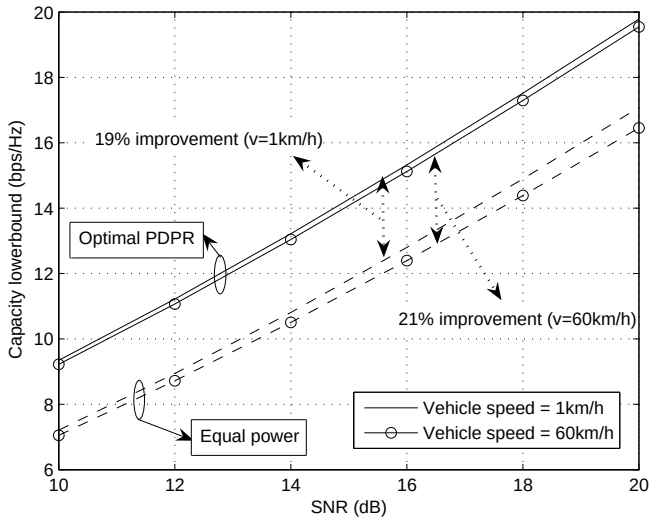

Figure 3.9: Capacity lower bound versus SNR for 4×4 MIMO-OFDM with the optimal PDPR and equal power, veh. speeds = 1, 60km/h, K=64, P=4, L=4, N=10

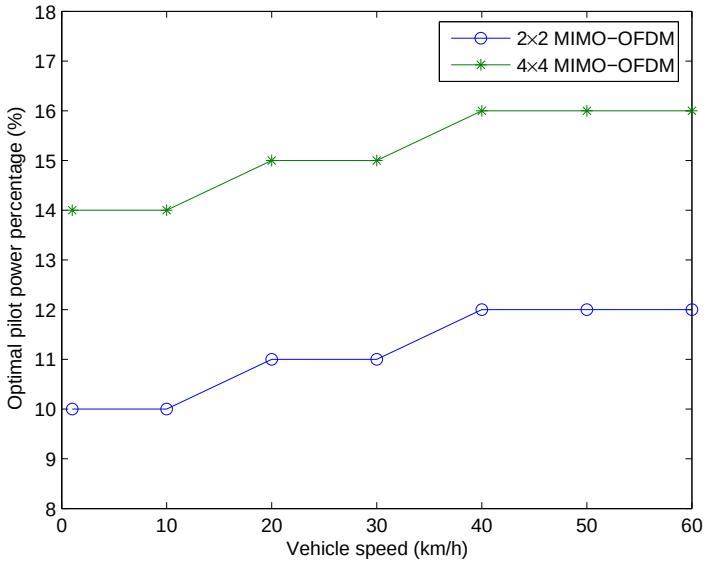

Figure 3.10: Optimal pilot power percentage versus vehicle speed for 2×2 and 4×4 MIMO-OFDM, K=64, P=4, L=4, N=10, SNR=20dB

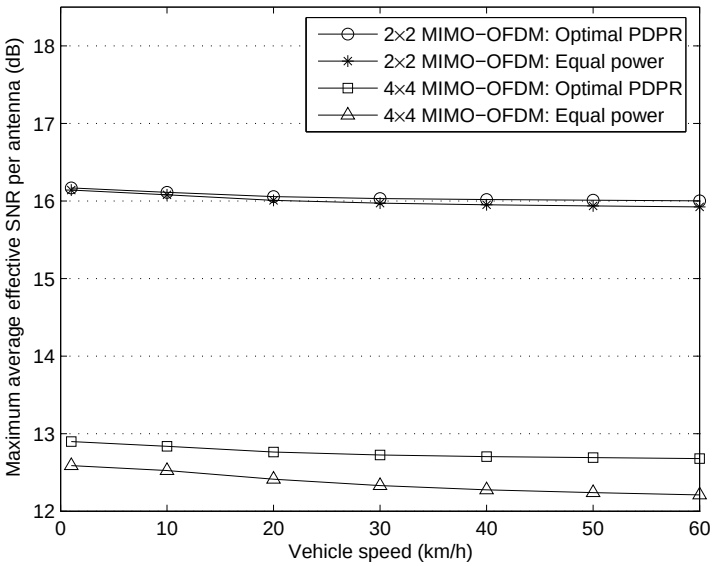

Figure 3.11: Maximum average effective SNR versus vehicle speed for 2×2 and 4×4 MIMO-OFDM, K=64, P=4, L=4, N=10, SNR=20dB

used to obtain capacity approached performance. Also, adaptive modulation and MIMO scheme can be used to achieve higher spectral efficiency. So, from a system view point, considering capacity as a criterion is valuable even for a practical system. The balancing PDPR problems in other performance measures such as the average error rate will be investigated in next chapter to see the relation with the optimal PDPR obtained from this chapter.

3.6 Chapter Summary

In this chapter, the optimal PDPR in MIMO-OFDM for maximizing a capacity lower bound was formed and analyzed for two different channel conditions and four likely pilot patterns. There is a tradeoff between the power for data sym-

bols and the accuracy of the channel estimation in MIMO-OFDM systems when the total transmit power is fixed. From the analysis, it is shown that the capacity lower bound of a typical MIMO-OFDM system can be increased about 10%~30% compared with the case of equal power allocation by simply using the optimal PDPR; this is a "free" gain that consumes no other system resources. By comparing the SPP-1 and SPP-2 cases, it is found that the optimal PDPR should be designed according to the system configuration. Also, it is found that the optimal PDPR varies with the vehicle speed, but the variation is small.

Chapter 4

Power Allocation Tradeoff in M-QAM MIMO Multicarrier Systems - Practical Performance

As shown in Chapter 3, the theoretical capacity of the MIMO-OFDM system can be maximized by balancing the pilot and power tradeoff. In this chapter, this tradeoff problem is studied in more practical system models to investigate the feasibility of adapting the obtained solution to practical systems.

4.1 Introduction

In recent high-speed communication standards, adaptive modulation is used to provide higher spectral efficiency over time and/or frequency varying channels [14, 17, 38, 39, 88, 115, 116, 120, 129, 130]. To adapt the modulation to the channel conditions, tracking the variations of the frequency selective fading channel is crucial [68, 69]. In these standards, pilot symbol power is often boosted to improve the overall system performance by enhancing the channel estimation accuracy (e.g. 2.5 dB in the IEEE 802.16e-2005 [52]), and its substantial improvement in theoretical capacity is shown in previous chapter. A question that arises is whether the optimal PDPR obtained in a theoretical capacity viewpoint is also the optimal solution for practical system performance, and if not, what is the optimal solution for this case.

In this chapter, this tradeoff problem is defined, quantified, and explored from the viewpoint of practical system performance.

Since the optimal PDPR depends on the system structure and its objective, finding the optimal PDPR has previously been considered for a few systems and objectives: for maximizing a lower bound on ergodic capacity for MIMO frequency-selective fading channels [77] and the MIMO single carrier system [44], for minimizing the channel MSE of MIMO-OFDM systems [6], and for minimizing the BER of a transmit-beamformer with variable-rates adaptive modulation [129]. However, minimizing the MSE does not consider the tradeoff between the accuracy of channel estimation and the data symbol power, and the average error rate and spectral efficiency are more relevant criteria for evaluating the achievable performance of adaptive MIMO-OFDM systems than a Shannon capacity lower bound [44, 77], due to the ubiquitous finite modulation orders (i.e. M-QAM). In [22, 23], the pilot design problem for MIMO and SIMO with adaptive modulation has been studied for maximizing spectral efficiency. However, in MIMO systems [22], orthogonal space time block coding scheme and linear receiver for the STBC scheme were considered. The received SNR for both MIMO and SIMO with MRC can be obtained in a same manner. Thus, the problem in MIMO is the same as the problem in SIMO with MRC in [23]. Moreover, they found the optimal solution by numerical search.

The performance of MIMO-OFDM with adaptive modulation depends on the distribution of the SNR and the receiver type. Many receiver types can be used for MIMO-OFDM systems such as linear (ZF and MMSE) and non-linear (max-

imum likelihood (ML) and MMSE successive interference cancellation (MMSE-SIC)) receivers. However, the complexity of non-linear receivers is usually too high to implement in a practical MIMO-OFDM system. Thus, in order to provide a framework for finding optimal PDPR in MIMO-OFDM systems, the average SER and spectral efficiency are considered for two well-known receiver types, ZF and MMSE. The optimal PDPR for M-QAM based MIMO-OFDM systems with ZF and MMSE linear receivers is derived, in terms of minimizing average SER and maximizing average spectral efficiency. The results find the optimal PDPR by deriving the distribution of the output SNR of different linear receivers including the effect of the pilot-based channel estimation, which has not been done previously. The key insights are that pilot power boosting should be optimized by considering system structures such as pilot, modulation order, and receiver type.

4.2 System Model and Channel Estimation

4.2.1 System Model

A spatial multiplexing MIMO-OFDM system with M_t transmit antennas and M_r receive antennas is considered with M-QAM, and shown in Fig. 4.1. The LS and MMSE methods are considered for channel estimation, and ZF and MMSE receivers are used according to whether or not the channel estimation requires the noise statistics. At each transmit antenna, data and pilot symbols are modulated on a set of subcarriers by the OFDM modulator with total K subcarriers. $\mathcal{K} = \{1, \ldots, K\}$ is a subcarrier index set. The number of nonzero taps of the impulse response is L for each channel. $\mathcal{D}$ and $\mathcal{P}$ are the subcarrier index sets for the data and pilot

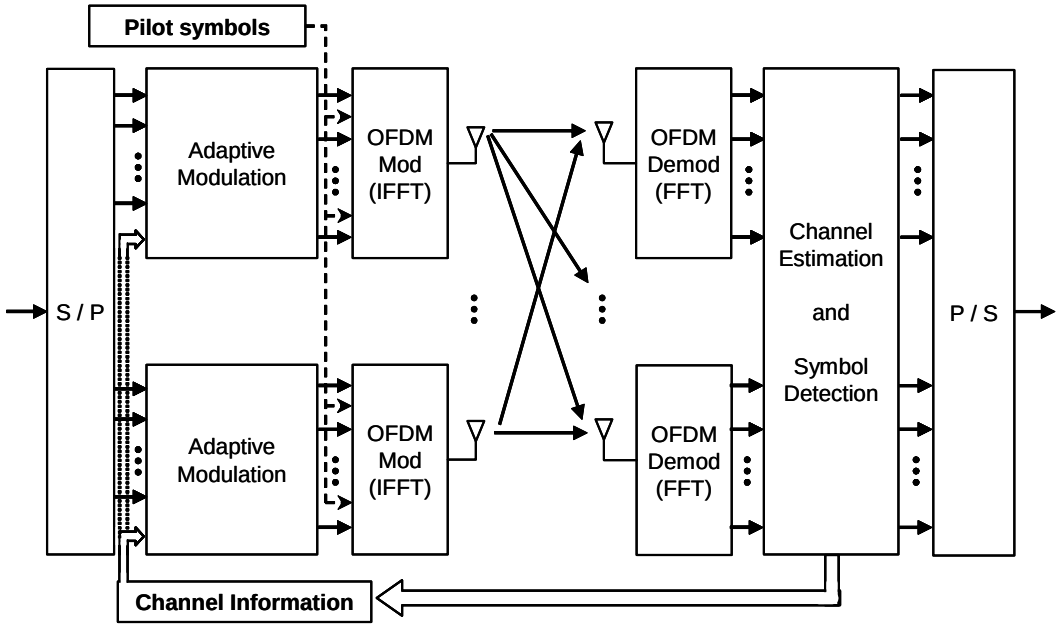

Figure 4.1: Adaptive MIMO-OFDM structure

signals, respectively. $\mathbf{s}_{d,i} = \text{vec}\,(s_i(k))_{k\in\mathcal{D}}$ and $\mathbf{s}_{p,i} = \text{vec}\,(s_i(k))_{k\in\mathcal{P}}$ are the vector of data and pilot symbols, where $s_i(k)$ is a transmit signal on the k^{th} subcarrier of the i^{th} transmit antenna, and $\text{vec}\,(a_k)_k$ is a function which creates a vector with elements a_k. The PDPR is defined in Definition 3.1.

Suppose the received signal in the frequency domain is denoted by the $M_rK \times 1$ vector

$$\mathbf{y} = \frac{1}{\sqrt{M_t}}\mathbf{H}\mathbf{s} + \mathbf{n}, \tag{4.1}$$

where $\mathbf{y} = [\mathbf{y}_j^T, \ldots, \mathbf{y}_{M_r}^T]^T$, $\mathbf{y}_j = \text{vec}(y_j(q))_{q\in\mathcal{K}}$, $\mathbf{H} = [\mathbf{H}_1^T, \ldots, \mathbf{H}_{M_t}^T]^T$, $\mathbf{H}_j = [\mathbf{H}_{1,j}$, $\ldots, \mathbf{H}_{M_t,j}]$, $\mathbf{H}_{i,j} = \text{diag}(H_{i,j}(1), \cdots, H_{i,j}(K)) = \text{diag}(\mathbf{W}_K\mathbf{h}_{i,j})$, $H_{i,j}(k)$ is the frequency channel response of the k^{th} subcarrier from the i^{th} transmit antenna to the j^{th} receive antenna, $\mathbf{W}_K$ is a $(K \times L)$ DFT matrix, $\mathbf{s} = [\mathbf{s}_1^T, \ldots, \mathbf{s}_{M_t}^T]^T$, $\mathbf{s}_i = \text{vec}(s_i(k))_{k\in\mathcal{K}}$, $\mathbf{n}$

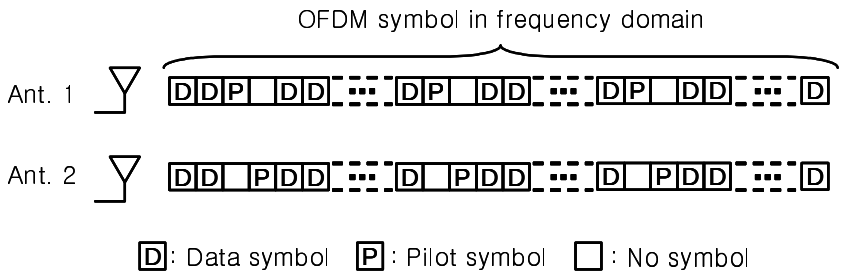

Figure 4.2: Pilot pattern

is a $(M_r K \times 1)$ AWGN vector which is zero mean Gaussian with covariance $\sigma_n^2 \mathbf{I}$. Finally, let the DFT matrix for data subchannels and pilot subchannels be $\mathbf{W}_d \in \mathbb{C}^{D \times L}$ and $\mathbf{W}_p \in \mathbb{C}^{P \times L}$. Those DFT matrices are generated by selecting rows from $\mathbf{W}_K$ according to the index sets $\mathcal{D}$ and $\mathcal{P}$.

4.2.2 LS Channel Estimation

The LS estimate of the channel $\mathbf{h}$, assuming $\mathbf{Z}^H\mathbf{Z}$ has full rank, is given by

$$\hat{\mathbf{h}} = \sqrt{M_t}\left(\mathbf{Z}^H\mathbf{Z}\right)^{-1}\mathbf{Z}^H\mathbf{y}, \tag{4.2}$$

where $\mathbf{Z} = \mathbf{I}_{M_r} \otimes \mathbf{SF}$ where $\mathbf{I}_{M_r}$ is an identity matrix of size $(M_r \times M_r)$ and $\otimes$ is the Kronecker product. $\mathbf{F} = \mathbf{I}_{M_t} \otimes \mathbf{W}_p$, $\mathbf{S} = [\mathrm{diag}(\mathbf{s}_1), \ldots, \mathrm{diag}(\mathbf{s}_{M_t})]$, $\mathbf{h} = [\ \mathbf{h}_1^T \ \cdots \ \mathbf{h}_{M_r}^T\ ]^T$, $\mathbf{h}_j = [\ \mathbf{h}_{1,j}^T \ \cdots \ \mathbf{h}_{M_t,j}^T\ ]^T$ is the channel impulse response matrix at j^{th} receive antenna where $\mathbf{h}_{i,j} = [\ h_{i,j}(1) \ \cdots \ h_{i,j}(L)\ ]^T$, and $h_{i,j}(l)$ denotes the channel response of the l^{th} path from the i^{th} transmit antenna to the j^{th} receive antenna. It is assumed that the taps of $\mathbf{h}_{i,j}$ are independent and identically distributed (i.i.d.) complex Gaussian random variables with zero mean and $\frac{1}{L}\mathbf{I}$ variance.

Since multiple channels exist in MIMO systems, the received signal will

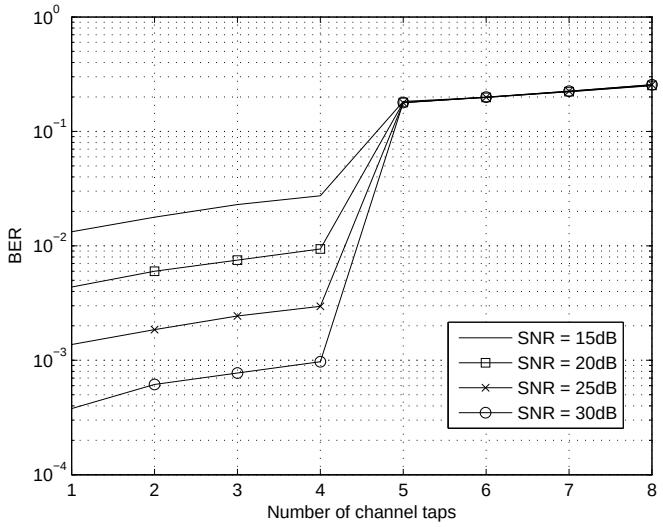

Figure 4.3: Effect of the number of pilot symbols and the number of channel taps on BER performance of 2×2 MIMO-OFDM with LS/ZF and QPSK. $P = 4$

be a superposition of the signal from each transmit antenna distorted by a number of channels. In this chapter, pilot symbols are transmitted on different subcarriers for different antennas, and zeros are transmitted on the subcarriers which are used for the pilot symbols of other transmit antennas as shown in Fig. 4.2. Thus, each transmit antenna has different subcarrier index set $\mathcal{P}_i$ for pilot symbols.

It is shown that the channel estimation error covariance is lower bounded with the pilot placement in (3.9). Thus, this pilot placement is considered in this chapter. Fig. 4.3 shows the effect of the number of pilot symbols and the channel taps on the BER performance when $M_r = M_t = 2$, $K = 64$, $P = 4$, and $\sigma_d^2 = \sigma_p^2$ and $4-QAM$ is used. As shown in this figure, the BER drops steeply when P falls below L. Thus, the number of pilot symbols is required to be grater or equal to the number

of channel taps. Also, using more pilot symbols reduces the available power for data symbols. It will be shown in Section 4.5 that additional pilot symbols above L does not result in better system performance (e.g. spectral efficiency). Thus, once $\mathbf{W}_p^H \mathbf{W}_p$ is a multiple of the identity matrix and $P \geq L$, the minimum possible value L is the optimal number of pilot symbol. With this placement and the number of pilot symbols, the optimal PDPR which minimizes the BER can be found.

With this pilot placement, the LS estimated MIMO-OFDM channel is obtained as follows,

$$\begin{aligned} \hat{\mathbf{h}} &= \mathbf{h} + \tilde{\mathbf{h}} \\ &= \mathbf{h} + \frac{\sqrt{M_t}}{P\sigma_p^2} \left(\mathbf{I}_{M_r} \otimes \mathbf{F}^H \mathbf{S}^H \right) \mathbf{n}, \end{aligned} \tag{4.3}$$

where $\tilde{\mathbf{h}}$ is channel estimation error. Then, the estimation error using LS of the channel between i^{th} transmit antenna and j^{th} receive antenna can be simplified as

$$\tilde{\mathbf{h}}_{i,j} = \frac{\sqrt{M_t}}{P\sigma_p^2} \mathbf{W}_p^H \bar{\mathbf{s}}_{p,i}^H \mathbf{n}_j, \tag{4.4}$$

where $\bar{\mathbf{s}}_{p,i} = \text{diag}(s_i(k))_{k \in \mathcal{P}}$ and $\mathbf{n}_j$ is AWGN vector at j^{th} receive antenna. Then, the error covariance matrix of the LS estimated channel impulse response between i^{th} transmit and j^{th} receive antenna is

$$E\left[\tilde{\mathbf{h}}_{i,j} \tilde{\mathbf{h}}_{i,j}^H \right] = \frac{M_t \sigma_n^2}{P\sigma_p^2}. \tag{4.5}$$

With (4.5), the error covariance matrix of the LS estimated channel frequency response for the data symbols can be obtained as follows,

$$E\left[\tilde{\mathbf{H}}_j \tilde{\mathbf{H}}_m^H \right] = \sum_{i=1}^{M_t} \text{diag}(\mathbf{W}_d \tilde{\mathbf{h}}_{i,j} \tilde{\mathbf{h}}_{i,m}^H \mathbf{W}_d^H),$$

$$= \begin{cases} \frac{M_t^2 L}{P\gamma_p}\mathbf{I}, & j = m \\ \mathbf{0}, & j \neq m \end{cases}, \tag{4.6}$$

where $\gamma_p = \sigma_p^2/\sigma_n^2$ is the SNR of the pilot symbol. Thus,

$$E\left[\tilde{\mathbf{H}}\tilde{\mathbf{H}}^H\right] = \frac{M_t^2 L}{P\gamma_p}\mathbf{I} \tag{4.7}$$

4.2.3 MMSE Channel Estimation

The MMSE estimated channel of MIMO-OFDM is given by

$$\hat{\mathbf{h}} = \frac{1}{\sqrt{M_t}}\mathbf{Z}^H\left(\frac{1}{M_t}\mathbf{Z}\mathbf{Z}^H + L\sigma_n^2\mathbf{I}\right)^{-1}. \tag{4.8}$$

Then, the covariance matrix of the estimation error of the channel impulse response is

$$\begin{aligned} E\left[\tilde{\mathbf{h}}\tilde{\mathbf{h}}^H\right] &= E\left[(\mathbf{h}-\hat{\mathbf{h}})(\mathbf{h}-\hat{\mathbf{h}})^H\right] \\ &= \frac{1}{L}\mathbf{I}_{M_r} \otimes \left(\mathbf{I} - \frac{1}{M_t}\mathbf{F}^H\mathbf{S}^H\left(\frac{1}{M_t}\mathbf{S}\mathbf{F}\mathbf{F}^H\mathbf{S}^H + L\sigma_n^2\mathbf{I}\right)^{-1}\mathbf{S}\mathbf{F}\right) \\ &= \frac{1}{L}\mathbf{I}_{M_r} \otimes \left(\mathbf{I} + \frac{1}{LM_t\sigma_n^2}\mathbf{F}^H\mathbf{S}^H\mathbf{S}\mathbf{F}\right)^{-1}, \end{aligned} \tag{4.9}$$

where the last equality is obtained by using the matrix inversion lemma. Then, with the same pilot placement used in Section 4.2.2, the error covariance matrix of the MMSE estimated channel impulse response between i^{th} transmit and j^{th} receive antenna is

$$\begin{aligned} E\left[\tilde{\mathbf{h}}_{i,j}\tilde{\mathbf{h}}_{i,j}^H\right] &= \bar{\mathbf{I}}_{i,j}E\left[\tilde{\mathbf{h}}\tilde{\mathbf{h}}^H\right]\bar{\mathbf{I}}_{i,j}^T \\ &= \frac{1}{L}\left(\mathbf{I} + \frac{\sigma_p^2}{LM_t\sigma_n^2}\mathbf{W}_p^H\mathbf{W}_p\right)^{-1} \end{aligned}$$

$$= \frac{M_t}{P\gamma_p + LM_t}\mathbf{I}_L, \tag{4.10}$$

where ^{T} is a matrix transpose, $\bar{\mathbf{I}}_{i,j} = [\ \mathbf{0}_{(i-1)L+M_r(j-1)L}\quad \mathbf{I}_L\quad \mathbf{0}\ ]$, the size of $\bar{\mathbf{I}}_{i,j}$ is $(L \times LM_tM_r)$, $\mathbf{0}_{(i-1)L+M_r(j-1)L}$ is an $(L \times ((i-1)L + M_r(j-1)L))$ all zero matrix, and $\mathbf{I}_L$ is a $(L \times L)$ identity matrix. Thus, the error covariance matrix of the MMSE estimated channel frequency response for the data symbols is

$$E\left[\tilde{\mathbf{H}}\tilde{\mathbf{H}}^H\right] = \frac{M_t^2 L}{P\gamma_p + LM_t}\mathbf{I}. \tag{4.11}$$

To analysis the average SER performance of the system, the SNR expression with the derived estimation error of LS and MMSE channel estimation is required.

4.3 SNR Analysis with PDPR

4.3.1 Average SNR of ZF Receiver with LS Channel Estimation

First, a ZF receiver that separates the received signal into its component transmitted streams is considered with LS channel estimation in order to recover the transmitted signal. The received signal is processed by the ZF matrix filter $\mathbf{G}_{ZF}$ given by

$$\mathbf{G}_{ZF} = \sqrt{M_t}\hat{\mathbf{H}}^{\dagger}, \tag{4.12}$$

where † represents the pseudo-inverse. Then, the output of the ZF receiver is given by

$$\mathbf{z} = \sqrt{M_t}\hat{\mathbf{H}}^{\dagger}\left(\frac{1}{\sqrt{M_t}}\mathbf{H}\mathbf{s} + \mathbf{n}\right). \tag{4.13}$$

Since $\hat{\mathbf{H}} = \mathbf{H} + \tilde{\mathbf{H}}$, (4.13) can be expressed as,

$$\mathbf{z} = \sqrt{M_t}\hat{\mathbf{H}}^{\dagger}\left(\frac{1}{\sqrt{M_t}}\left(\hat{\mathbf{H}} - \tilde{\mathbf{H}}\right)\mathbf{s} + \mathbf{n}\right),$$

$$
\begin{aligned}
&= \mathbf{s} - \hat{\mathbf{H}}^{\dagger}\tilde{\mathbf{H}}\mathbf{s} + \sqrt{M_t}\hat{\mathbf{H}}^{\dagger}\mathbf{n} \\
&= \mathbf{s} + \mathbf{e}, \qquad (4.14)
\end{aligned}
$$

where $\mathbf{e}$ is $-\hat{\mathbf{H}}^{\dagger}\tilde{\mathbf{H}}\mathbf{s} + \sqrt{M_t}\hat{\mathbf{H}}^{\dagger}\mathbf{n}$. The ZF receiver has DM_t output data streams. From (4.14), the SNR of the k^{th} ($k = 1, \ldots, DM_t$) output data stream with independent detection can be obtained as follows,

$$
\gamma_k = \frac{\sigma_d^2}{[\mathbf{R_e}]_{k,k}}, \qquad (4.15)
$$

where $\mathbf{R_e}$ is a covariance matrix of $\mathbf{e}$, and is given by

$$
\begin{aligned}
\mathbf{R_e} &= E\left[\mathbf{e}\mathbf{e}^H\right] \\
&= \sigma_d^2 E\left[\hat{\mathbf{H}}^{\dagger}\tilde{\mathbf{H}}\tilde{\mathbf{H}}^H(\hat{\mathbf{H}}^{\dagger})^H\right] + M_t\sigma_n^2 E\left[\hat{\mathbf{H}}^{\dagger}(\hat{\mathbf{H}}^{\dagger})^H\right], \\
&= \left(\sigma_d^2\beta + M_t\sigma_n^2\right)(\hat{\mathbf{H}}^H\hat{\mathbf{H}})^{-1}, \qquad (4.16)
\end{aligned}
$$

where $\beta = \frac{M_t^2 L}{P\gamma_p}$ since $E\left[\tilde{\mathbf{H}}\tilde{\mathbf{H}}^H\right] = \frac{M_t^2 L}{P\gamma_p}\mathbf{I}$. Thus, the SNR of the k^{th} ($k = 1, \ldots, DM_t$) output data stream is given by

$$
\begin{aligned}
\gamma_k &= \frac{\sigma_d^2}{\left(\sigma_d^2\beta + M_t\sigma_n^2\right)\left[(\hat{\mathbf{H}}^H\hat{\mathbf{H}})^{-1}\right]_{k,k}} \\
&= \frac{\gamma_0}{\left[(\check{\mathbf{H}}_k^H\check{\mathbf{H}}_k)^{-1}\right]_{k,k}}, \qquad (4.17)
\end{aligned}
$$

where $\gamma_0 = \frac{\sigma_d^2}{\left(\sigma_d^2\beta + M_t\sigma_n^2\right)}$ and $\check{\mathbf{H}}$ is $(M_r \times M_t)$ modified estimated frequency channel matrix whose elements are the estimated frequency channel on the same subcarrier. For example, in the case of 2×2 MIMO OFDM with K subcarriers,

$$
\hat{\mathbf{H}} = \begin{bmatrix} \mathrm{diag}(\hat{H}_{1,1}(k))_{k\in\mathcal{K}} & \mathrm{diag}(\hat{H}_{2,1}(k))_{k\in\mathcal{K}} \\ \mathrm{diag}(\hat{H}_{1,2}(k))_{k\in\mathcal{K}} & \mathrm{diag}(\hat{H}_{2,2}(k))_{k\in\mathcal{K}} \end{bmatrix} \qquad (4.18)
$$

and

$$\check{\mathbf{H}}_k = \begin{bmatrix} \hat{H}_{1,1}(k) & \hat{H}_{2,1}(k) \\ \hat{H}_{1,2}(k) & \hat{H}_{2,2}(k) \end{bmatrix}. \tag{4.19}$$

Since $\hat{\mathbf{H}}$ is a block diagonal matrix as described in (4.18), each diagonal element of inverse of its hermitian product can be calculated by using only one element in each block of diagonal matrices in $\hat{\mathbf{H}}$. Thus, for convenience in analysis, (4.17) is used instead of the equation above (4.17). Then, it can be easily shown that below is true.

$$\left[(\hat{\mathbf{H}}^H\hat{\mathbf{H}})^{-1}\right]_{k,k} = \left[(\check{\mathbf{H}}_k^H\check{\mathbf{H}}_k)^{-1}\right]_{k,k}. \tag{4.20}$$

Also, The matrix $\check{\mathbf{H}}_k$ is a $(M_R \times M_T)$ MIMO estimated channel matrix composed of the estimated channels on the same subcarrier. Therefore, the distribution of the estimated channel matrix $\check{\mathbf{H}}_k$ is complex Gaussian, $N(\mathbf{0}, \mathbf{\Phi})$. The covariance matrix $\mathbf{\Phi}$ is given by

$$\begin{aligned} \mathbf{\Phi} &= E[\mathrm{vec}(\check{\mathbf{H}}_k)\mathrm{vec}(\check{\mathbf{H}}_k)^H] \\ &= \delta\mathbf{I}_{M_rM_t}, \end{aligned} \tag{4.21}$$

where $\delta = E[\hat{H}_{i,j}(k)\hat{H}_{i,j}(k)^*]$ for $i \in \{1, \ldots, M_t\}$, $j \in \{1, \ldots, M_r\}$, and $k \in \mathcal{K}$. Since

$$\begin{aligned} E[\hat{\mathbf{h}}_{i,j}\hat{\mathbf{h}}_{i,j}^H] &= E[\mathbf{h}_{i,j}\mathbf{h}_{i,j}^H] + E[\tilde{\mathbf{h}}_{i,j}\tilde{\mathbf{h}}_{i,j}^H], \\ &= \frac{P\gamma_p + M_tL}{LP\gamma_p}\mathbf{I}, \end{aligned} \tag{4.22}$$

δ can be obtained as

$$\delta = E[\mathbf{w}_k\hat{\mathbf{h}}_{i,j}\hat{\mathbf{h}}_{i,j}^H\mathbf{w}_k^H]$$

$$= \frac{P\gamma_p + M_t L}{P\gamma_p}. \tag{4.23}$$

Since the estimated channel matrix $\check{\mathbf{H}}_k$ has a matrix-variate Gaussian distribution $N(\mathbf{0}, \mathbf{I}_{M_r} \otimes \delta \mathbf{I}_{M_t})$ with $\delta = \frac{P\gamma_p + M_t L}{P\gamma_p}$, and $M_r \geq M_t$, $\mathbf{Z} = \left(\sqrt{2}\check{\mathbf{H}}_k^H\right)\left(\sqrt{2}\check{\mathbf{H}}_k\right) = 2\check{\mathbf{H}}_k^H\check{\mathbf{H}}_k$ is complex central Wishart distributed, and has the following distribution [40].

$$W_{M_t}(M_r, \mathbf{\Sigma}) = \frac{e^{\mathrm{tr}(-\mathbf{\Sigma}^{-1}\mathbf{Z})}(\det\mathbf{Z})^{M_r - M_t}}{\Gamma_{M_t}(M_r)(\det\mathbf{\Sigma})^{M_r}}, \tag{4.24}$$

where $\Sigma = 2\delta\mathbf{I}_{M_t}$, and the multivariate gamma function $\Gamma_m(\cdot)$ is given by [81]

$$\Gamma_m(a) = \pi^{m(m-1)} \prod_{i=1}^{m} \Gamma\left[a - \frac{1}{2}(i-1)\right], \qquad \mathrm{Re}(a) > \frac{1}{2}(m-1), \tag{4.25}$$

where $\Gamma(\cdot)$ is an ordinary gamma function. Then, with the similar way in [40], the probability density function (p.d.f.) of the SNR on the k^{th} stream γ_k in (4.17) is given by,

$$\begin{aligned} f(\gamma_k) &= \frac{2[\Sigma^{-1}]_{k,k} \exp\left(-\frac{2\gamma_k[\Sigma^{-1}]_{k,k}}{\gamma_0}\right)}{\gamma_0(M_r - M_t)!} \left(\frac{2\gamma_k[\Sigma^{-1}]_{k,k}}{\gamma_0}\right)^{M_r - M_t}, \\ &= \frac{\exp\left(-\frac{\gamma_k}{\delta\gamma_0}\right)}{\delta\gamma_0(M_r - M_t)!} \left(\frac{\gamma_k}{\delta\gamma_0}\right)^{M_r - M_t}. \end{aligned} \tag{4.26}$$

Then, the average SNR of the k^{th} stream can be obtained as following proposition.

Proposition 4.1. *The average SNR of the k^{th} stream of MIMO-OFDM with LS channel estimation and the ZF receiver using the equi-spaced pilot in 4.2.2 is*

$$\begin{aligned} \bar{\gamma_k} &= \delta\gamma_0(M_r - M_t + 1) \\ &= \frac{\sigma_d^2(P\sigma_p^2 + M_t L\sigma_n^2)(M_r - M_t + 1)}{\sigma_n^2 M_t(\sigma_d^2 M_t L + P\sigma_p^2)} \end{aligned} \tag{4.27}$$

Proof. Using the identity [41]

$$\int_0^\infty x^n \exp(-\mu x) dx = n! \mu^{-n-1} \tag{4.28}$$

for $\mathrm{Re}[\mu] > 0$ and the pdf function in (4.26), the average SNR can be obtained. □

4.3.2 Average SNR of MMSE Receiver with MMSE Channel Estimation

The MMSE receiver balances multiple stream interference with noise enhancement and minimizes the total error using the information of noise statistics. The MMSE matrix filter $\mathbf{G}_{MMSE}$ is given by

$$\mathbf{G}_M = \sqrt{M_t}\hat{\mathbf{H}}^H \left(\hat{\mathbf{H}}\hat{\mathbf{H}}^H + \frac{M_t}{\gamma_d}\mathbf{I} \right)^{-1}, \tag{4.29}$$

where $\gamma_d = \frac{\sigma_d^2}{\sigma_n^2}$. Then, as shown in Appendix C.1, the SNR of the k^{th} output data stream of the MMSE receiver using the MMSE estimated channel can be obtained as

$$\gamma_k = \frac{(1 - \mathbf{A}_{k,k})^2}{\mathbf{A}_{k,k} - \mathbf{A}_{k,k}^2 + \frac{\beta_2 \gamma_d}{M_t} \left(\mathbf{A}_{k,k} - (\mathbf{A}^2)_{k,k} \right)}, \tag{4.30}$$

where $\mathbf{A} \triangleq \left(\mathbf{I} + \frac{\gamma_d}{M_t}\hat{\mathbf{H}}^H\hat{\mathbf{H}} \right)^{-1}$ and $\beta_2 = \frac{M_t^2 L}{P\gamma_p + LM_t}$. To get an average SNR of MMSE receiver, the distribution of SNR is required. To my knowledge, the exact statistics of the SNR of MMSE receiver are not yet exactly characterized. However, the distribution of MMSE receiver with correlated Rayleigh fading channel was well approximated using a generalized Gamma distribution in [67]. By using this approximated SNR approach, the average SNR of the MMSE receiver can be found with the channel estimation error according to the PDPR. Since it is hard to find the distribution of $(\mathbf{A}^2)_{k,k}$ in (4.30), the following lemma can be used to find a lower bound of the SNR.

Lemma 4.1. *A tight lower bound of the SNR* (4.30) *can be obtained by using* $\mathbf{A}_{k,k}^2$ *instead of* $(\mathbf{A}^2)_{k,k}$.

Proof. See Appendix C.2. □

The SNR lower bound of (4.30) is given by

$$\begin{aligned}\gamma_{k,lb} &= \frac{(1-\mathbf{A}_{k,k})^2}{\mathbf{A}_{k,k}-\mathbf{A}_{k,k}^2+\frac{\beta_2\gamma_d}{M_t}\left(\mathbf{A}_{k,k}-\mathbf{A}_{k,k}^2\right)} \\ &= \frac{M_t}{M_t+\beta_2\gamma_d}\left(\frac{1}{\mathbf{A}_{k,k}}-1\right) \\ &= \frac{M_t}{M_t+\beta_2\gamma_d}\hat{\gamma}_{k,lb}. \end{aligned} \tag{4.31}$$

Then, the approximated distribution of the SNR lower bound can be obtained in a similar way in [67] by considering $\hat{\mathbf{H}}$ instead of $\mathbf{H}$. The distribution of $\hat{\gamma}_{k,lb} = \frac{1}{\mathbf{A}_{k,k}} - 1$ can be approximated as

$$f(\hat{\gamma}_{k,lb}) = \mathrm{G_g}(\alpha_X, \beta_X, \gamma_X) \tag{4.32}$$

where $\mathrm{G_g}(\alpha_X, \beta_X, \gamma_X)$ is a generalized Gamma distribution [33], and α_X, β_X, and γ_X are defined in Appendix C.3.

Then, the average SNR lower bound of the k^{th} stream can be obtained as following proposition.

Proposition 4.2. *The average SNR lower bound of the* k^{th} *stream of MIMO-OFDM with MMSE channel estimation and the MMSE receiver using the equi-spaced pilot in 4.2.2 is*

$$\bar{\gamma}_{k,lb} = \frac{M_t\delta'\gamma_0'}{M_t+\beta_2\gamma_d}\left(M_r - M_t + 1 - \frac{(M_t-1)(1+\gamma_d-\tau\gamma_d-\xi)}{2\tau\gamma_d}\right). \tag{4.33}$$

Proof. With Lemma 4.1 and the approximated distribution of the SNR lower bound in (4.32), the average SNR lower bound of the k^{th} stream of the MMSE receiver in (4.33) is obtained. □

4.4 Effect of the PDPR on MIMO-OFDM with a Linear Receiver

In this section, the effect of the PDPR on the performance of MIMO-OFDM systems is studied. For the adaptive modulation case, a variable-rate M-QAM system is considered to study the effect of the PDPR, since this is the dominant form of digital modulation in current and proposed systems. The squared M-QAM constellations of size $M_0 = 0$, $M_1 = 2$, and $M_i = 2^{2(i-1)}$ for $i = 2, \ldots, N+1$ are considered.

4.4.1 Optimal PDPR of Minimizing Average SER of Non-adaptive M-QAM Modulation

The closed-form of error probability expressions for M-QAM are presented in [126], and it has been shown that the approximate error rates are within 1∼2 dB for $M = 2 \sim 256$ modulation orders [38, 128]. In order to show the analytical relation between the optimal PDPR and average SER performance, approximate error rates are attractive due to its simplicity to compute the optimization problem. In Section 4.5, the tightness of analysis results with this approximated average SER will be shown by comparing it with simulation results. The approximated average

SER of the M-QAM MIMO-OFDM system in AWGN is given by

$$P_{s,AWGN} = \alpha_M Q(\sqrt{\beta_M \gamma_s}) = \frac{\alpha_M}{\pi} \int_0^{\pi/2} \exp\left(-\frac{\beta_M \gamma_s}{2\sin^2\theta}\right) d\theta \tag{4.34}$$

where α_M and β_M depend on the modulation type [37]. Then, the average SER of the M-QAM MIMO-OFDM with linear receiver under Rayleigh fading channel is

$$\bar{P}_s = \frac{\alpha_M}{\pi} \int_0^{\pi/2} \mathrm{MGF}\left(s; f(\gamma_k)\right) d\theta \tag{4.35}$$

where $s = -\frac{\beta_M}{2\sin^2\theta}$.

4.4.1.1 ZF Receiver

From (4.35), the average SER of the ZF receiver with LS channel estimation can be expressed as follows,

$$\begin{aligned} \bar{P}_s &= \frac{\alpha_M}{\pi} \int_0^{\pi/2} (1 - \delta\gamma_0 s)^{-(M_r - M_t + 1)} \, d\theta & (4.36) \\ &= \alpha_M \left(\frac{1-\nu}{2}\right)^{M_r - M_t + 1} \sum_{k=0}^{M_r - M_t} \binom{M_r - M_t + k}{k} \left(\frac{1+\nu}{2}\right)^k, & (4.37) \end{aligned}$$

where $\nu = \sqrt{\frac{\delta\gamma_0\beta_M}{2+\delta\gamma_0\beta_M}}$. From (4.36), it can be found that $\delta\gamma_0$ should be maximized to minimize the average SER. Then, the optimal PDPR is given by the follow theorem.

Theorem 4.1. *With the equi-spaced pilot in Section 4.2.2, the optimal PDPR that minimizes the average SER of MIMO-OFDM system with LS channel estimation and the ZF receiver is*

$$\eta_{opt} = \begin{cases} \frac{D(P_{tot} - DM_t\sigma_n^2)}{P(P_{tot} + DM_t\sigma_n^2)} & \text{if } LM_t = D \\ \frac{\lambda - DLM_t^2\sigma_n^2}{P(P_{tot} + LM_t^2\sigma_n^2)} & \text{otherwise} \end{cases}. \tag{4.38}$$

Proof. Define α as the fraction of the total transmit power for data symbol as $\sigma_d^2 = \frac{\alpha P_{tot}}{DM_t}, \sigma_p^2 = \frac{(1-\alpha)P_{tot}}{PM_t}$ where P_{tot} is the total transmit power. With α, $\delta\gamma_0$ can be written as

$$\delta\gamma_0 = \frac{\alpha\left((1-\alpha)\,P_{tot} + LM_t^2\sigma_n^2\right)}{M_t^2\sigma_n^2\left(\alpha M_t L + (1-\alpha)\,D\right)} \tag{4.39}$$

Now it can be found the α which maximizes the average SNR over $0 < \alpha < 1$ by differentiating $\delta\gamma_0$ and setting it equal to zero under the power constraints, $DM_t\sigma_d^2 + PM_t\sigma_p^2 = P_{tot}$. If P is a factor of D and $P \geq L$, the optimal fraction of total transmit power that is allocated to data symbols is given by

$$\alpha_{max} = \arg\max_{0<\alpha<1} \delta\gamma_0 = \begin{cases} \frac{P_{tot}+DM_t\sigma_n^2}{2P_{tot}} & \text{if } LM_t = D \\ \frac{DP_{tot}-\lambda}{(D-LM_t)P_{tot}} & \text{otherwise} \end{cases}, \tag{4.40}$$

where $\lambda = \sqrt{DLM_tP_{tot}(P_{tot} + M_t(LM_t - D)\sigma_n^2)}$. The average SER in (4.37) can be minimized with the optimal α_{max} in (4.40). Then, the optimal PDPR can be obtained from its definition in (3.3) with the optimal α_{max}. □

4.4.1.2 MMSE Receiver

Since the distribution of the SNR of the MMSE receiver can be approximated to the generalized Gamma distribution as shown in (4.32), the average SER can be expressed with its moment generating function as follows,

$$\bar{P}_s = \frac{\alpha_M}{\pi}\int_0^{\pi/2} \exp\left(\frac{\alpha_X}{\gamma_X - 1}\left(1 - (1 - \beta_X\gamma_X s)^{\frac{\gamma_X - 1}{\gamma_X}}\right)\right) d\theta \tag{4.41}$$

where $s = -\frac{\beta_M}{2\sin^2\theta}$. The optimal fraction of the total transmit power for data symbol, α_{max}, to minimize the average SER in (4.41) can be obtained numerically.

4.4.2 Optimal PDPR for Adaptive Modulation

In the adaptive modulation scheme, uncertainty in SNR can result in choosing mismatched modulation order. If the modulation order is chosen based on the SNR which includes the channel estimation error $\sigma_{\hat{\mathbf{h}}_e}$, then the modulation order chosen based on this SNR can be different with the correct modulation order. This is because the selected modulation order does not guarantee an instantaneous SNR which is the same as this received SNR due to the variation of the estimated channel error. However, there is no error propagation due to this. Pilot symbols are used for channel estimation, and the modulation order of the pilot symbols is not changed. Adaptive modulation is only used for data symbols. Thus, error propagation does not occur. To include instantaneous channel estimation error, the distribution of SNR with instantaneous channel estimation error instead of its variance is required. However, as shown in my analysis, it is very difficult to find this distribution due to its complicated structure. Moreover, in a practical wireless system, usually modulation order is not changed at every OFDM symbol due to the channel coherence time. Usually, the channel can be considered constant during one OFDM frame which includes several OFDM symbols. During this frame duration, the average channel estimation error (its variance) can be used to support one modulation order for several OFDM symbols. Since it is hard to change modulation order at every OFDM symbol time, this scenario is more acceptable. In this case, the analysis in this chapter is valid.

Moreover, Fig. 4.4 shows the amount of channel estimation error compared with the noise variance. 2×2 MIMO-OFDM, 64 subcarriers, 4 pilot symbols, 4

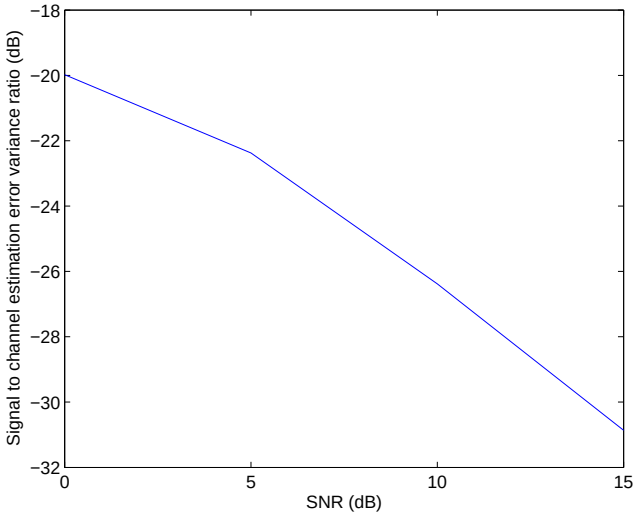

Figure 4.4: Channel estimation error versus noise variance

tap channel, and equal power allocation for pilot and data symbols are considered in this simulation. If the estimated channel gain is very large compared to the actual channel gain, the higher modulation order can be chosen due to the large SNR with estimated channel. Thus, due to this mismatched modulation order, the detection error can be increased in adaptive modulation. However, as shown in this figure, channel estimation error variance is smaller than the noise variance. This shows that the estimated channel well follows the actual channel. Thus, the effect of mismatched modulation order problems on adaptive modulation does not cause significant performance degradation.

If the adaptive modulation with a constant power transmission policy is considered, then the constellation of the data symbol on the k^{th} subcarrier is chosen

according to

$$M = M_i, \text{ when } \gamma_k \in [\epsilon_i, \epsilon_{i+1}), \tag{4.42}$$

where $\{\epsilon_i\}_{i=0}^{N+1}$ is boundary points, $\epsilon_0 = 0$ and $\epsilon_{N+1} = \infty$, γ_k is the received SNR using the estimated channel with the distribution in (4.26). The probability that the constellation M_i is chosen is

$$\Pr(M_i) = \int_{\epsilon_i}^{\epsilon_{i+1}} f(\gamma_k) d\gamma_k, \tag{4.43}$$

where $f(\gamma_k)$ is the distribution of the SNR. The approximate BER of M-QAM ($M \geq 4$) is bounded by [38]

$$BER \leq 0.2 \exp\left(\frac{-1.5\gamma}{(M-1)}\right). \tag{4.44}$$

To maintain a fixed target BER, the boundary points $\{\epsilon_i\}_{i=0}^{N+1}$ can be determined as

$$\epsilon_i = -\frac{2(M_i - 1)}{3} \ln(5\text{BER}_\text{T}), \tag{4.45}$$

where BER_T is the target BER.

Then, using the distributions of the SNR of the ZF and MMSE receivers with the PDPR in (4.26) and (4.32), the probability that the constellation M_i is chosen can be expressed as follows,

- ZF Receiver with LS Channel Estimation:

$$\Pr(M_i)_{ZF} = \frac{1}{(M_r - M_t)!}\left(\text{G}\left(M_r - M_t + 1, \frac{\epsilon_i}{\delta\gamma_0}\right) - \text{G}\left(M_r - M_t + 1, \frac{\epsilon_{i+1}}{\delta\gamma_0}\right)\right), \tag{4.46}$$

  where G is an incomplete gamma function which is defined as

$$\text{G}(a, x) = \int_x^\infty t^{a-1} \exp(-t) dt. \tag{4.47}$$

- MMSE Receiver with MMSE Channel Estimation:

$$\begin{aligned} \Pr(M_i)_{MMSE} &= \int_{\epsilon_i}^{\epsilon_{i+1}} f(\gamma_{k,lb}) d\gamma_{k,lb} \\ &= \int_{\frac{\epsilon_i(M_t+\beta_2\gamma_d)}{M_t}}^{\frac{\epsilon_{i+1}(M_t+\beta_2\gamma_d)}{M_t}} \mathrm{G_g}(\alpha_X, \beta_X, \gamma_X) d\hat{\gamma}_{k,lb}. \end{aligned} \tag{4.48}$$

The average spectral efficiency of the each data stream of the variable-rate system is the sum of the data rates associated with each of the regions multiplied by the probability that γ_k falls in that region. Thus, the average spectral efficiency of the MIMO-OFDM systems with an adaptive modulation considering the PDPR effect is given by

$$S = \sum_{k=1}^{M_t} S_k = \sum_{k=1}^{M_t} \frac{D}{K} \sum_{i=1}^{N} \log_2(M_i) \Pr(M_i), \tag{4.49}$$

where the probability $Pr(M_i)$ for ZF and MMSE receivers are in (4.46) and (4.48), respectively.

The PDPR can be optimally balanced to maximize the average spectral efficiency by solving below problem,

$$\alpha_{opt} = \arg \max_{0<\alpha<1} S \tag{4.50}$$

where α is the fraction of the total transmit power for data symbol. For the ZF receiver case, the second derivative of the average spectral efficiency can be analytically derived. Since it is too long and complicate, it is not worth showing it here. However, this second derivative of the average spectral efficiency of the LS/ZF case is negative for $0 < \alpha < 1$. Thus, S has a maximum value with α^* ($0 < \alpha* < 1$), since it is a concave function over $0 < \alpha < 1$. And this $\alpha*$ maximizing S can be

obtained by finding the α makes the derivative of S to zero. In case of the MMSE receiver case, the optimal solution will be obtained through the numerical search over $0 < \alpha < 1$ by using the obtained final form of the average spectral efficiency. Thus, claiming its concavity is not necessary in here.

4.4.2.1 ZF Receiver

The optimal PDPR maximizing the average spectral efficiency is given by the following theorem.

Theorem 4.2. *With the equi-spaced pilot in Section 4.2.2, the optimal PDPR that maximizes the average spectral efficiency of the adaptive MIMO-OFDM system with ZF receiver is the same as the optimal PDPR that minimizes the average SER shown in* (4.38)*.*

Proof. As shown in Appendix D.1, differentiating S results in

$$\frac{\partial S}{\partial \alpha} = \frac{\partial S}{\partial z}\frac{\partial z}{\partial \alpha}, \tag{4.51}$$

and

$$\frac{\partial S}{\partial z} = \frac{M_t}{(M_r - M_t)!}\sum_{i=1}^{N}\log_2(M_i)\left(-\epsilon_i^{M_r-M_t+1}e^{-\epsilon_i z} + \epsilon_{i+1}^{M_r-M_t+1}e^{-\epsilon_{i+1}z}\right)z^{M_r-M_t}, \tag{4.52}$$

where $z = (\delta\gamma_0)^{-1}$. From Appendix D.2, it is found that α^* cannot be found from $\frac{\partial S}{\partial z}$. Thus, α^* can be found from $\frac{\partial z}{\partial \alpha}$. □

4.4.2.2 MMSE Receiver

The average spectral efficiency of the each data stream is

$$S_k = \sum_{i=1}^{N} \log_2(M_i) \int_{\frac{\epsilon_i(M_t+\beta_2\gamma_d)}{M_t}}^{\frac{\epsilon_{i+1}(M_t+\beta_2\gamma_d)}{M_t}} \mathrm{G_g}(\alpha_X, \beta_X, \gamma_X) d\hat{\gamma}_{k,lb} \tag{4.53}$$

where $f(\gamma_{k,lb})$ is shown in (4.32). The generalized gamma distribution does not have a closed-form density, but its characteristic function can be used to find the probability of each SNR region as follows,

$$\int_{\rho_i}^{\rho_{i+1}} \mathrm{G_g}(\alpha_X, \beta_X, \gamma_X) d\hat{\gamma}_{k,lb} = \frac{1}{2\pi} \int_{-\infty}^{\infty} \frac{\exp(\rho_i) - \exp(\rho_{i+1})}{is} \varphi(s) ds, \tag{4.54}$$

where $\rho_i = \frac{\epsilon_i(M_t+\beta_2\gamma_d)}{M_t}$ and $\varphi(s) = \exp\left(\frac{\alpha_X}{\gamma_X - 1}\left(1 - (1 - \beta_X\gamma_X is)^{\frac{\gamma_X - 1}{\gamma_X}}\right)\right)$. The average spectral efficiency is given by

$$S_k = \sum_{i=1}^{N} \log_2(M_i) \frac{1}{2\pi} \int_{-\infty}^{\infty} \frac{\exp(-is\rho_i) - \exp(-is\rho_{i+1})}{is} \varphi(s) ds. \tag{4.55}$$

Then, the optimal PDPR for maximizing the spectral efficiency of MIMO-OFDM with MMSE receiver can be readily obtained numerically.

4.5 Numerical Results

In this section, the effect of the PDPR on the average SER and the spectral efficiency of the MIMO-OFDM system is demonstrated by using the analysis in Section 4.3 and 4.4. For the simulation, $L = 4$, $P = 4$, and $K = 64$.

4.5.1 Effect of the PDPR on the Average SER of M-QAM MIMO-OFDM

Fig. 4.5 shows the effect of the PDPR on the average SER of M-QAM MIMO-OFDM systems for both ZF and MMSE receiver cases. 4-QAM and 2

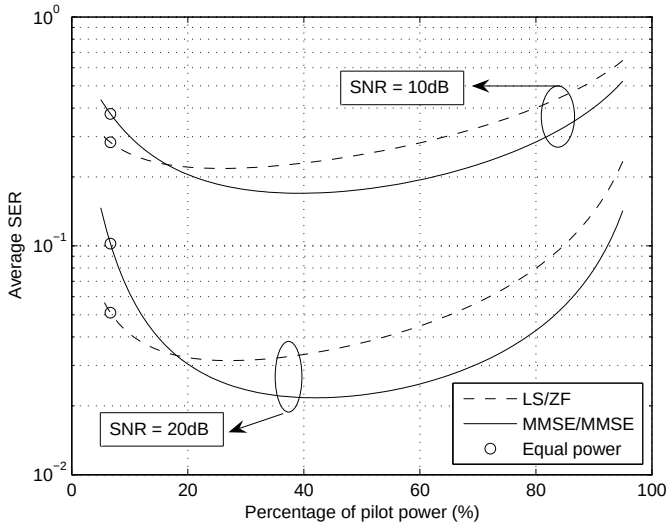

Figure 4.5: SER versus percentage of pilot power for 2×2 QPSK MIMO-OFDM with LS/ZF and MMSE/MMSE cases.

transmit and receive antennas are used. At each SNR, there is an optimal point where the average SER is minimized, and this optimal point depends on the channel estimation and receiver type. The average SER is minimized when about 25% of the total transmit power is allocated to the pilot symbol for LS/ZF case. For each SNR case, the average SER when same power is allocated to the pilot and data symbols is marked with a circle. By using the optimal PDPR, the average SER can be reduced compared with the equal power policy.

In Fig. 4.6 and Fig. 4.7, the average SER from analysis and simulation with two different PDPR cases are compared for different modulations (M=2,4) with a 2x2 MIMO-OFDM system. For each modulation order, the solid line shows the results from the analysis in Section 4.4, and the dashed line shows the results from

simulation. The simulation results are well matched with the analytical results, and show that SER can be lowered by using the optimal PDPR without using any additional resource. Especially, in the MMSE/MMSE case, the gain from optimal PDPR is higher than LS/ZF case.

4.5.2 Effect of the PDPR on Adaptive Modulation

Fig. 4.8 and Fig. 4.9 show the effect of the PDPR on the adaptive modulation in the MIMO-OFDM system. The highest modulation order M_{max} is 256, e.g. M=0, 2, 4, 16, 64, 256, and the target BER for adaptive modulation is 10^{-3}. Fig. 4.8 and Fig. 4.9 show the effect of the PDPR on the achievable spectral efficiency of the 2x2 MIMO-OFDM system with adaptive modulation. Fig. 4.8 shows the average spectral efficiency versus SNR for LS/ZF case. The ideal case is when the transmitter has perfect channel knowledge. Thus, the whole available transmit power is allocated to data symbols only. The achievable spectral efficiency of the adaptive M-QAM MIMO-OFDM system highly depends on the PDPR. In Fig. 4.9, the achievable spectral efficiency (lower bound) of MMSE/MMSE case is shown. It is shown that about 4dB gain can be obtained with the optimal PDPR in MMSE/MMSE case when it is compared with the equal power allocation case.

Fig. 4.10 shows the effect of using more number of pilots than the number of channel taps in LS/ZF case. $L = 4$, and 2x2 MIMO-OFDM system is considered. As shown in this figure, the spectral efficiency loss by using more number of pilot symbols than L is larger than the improvement in spectral efficiency by more accurate channel estimation.

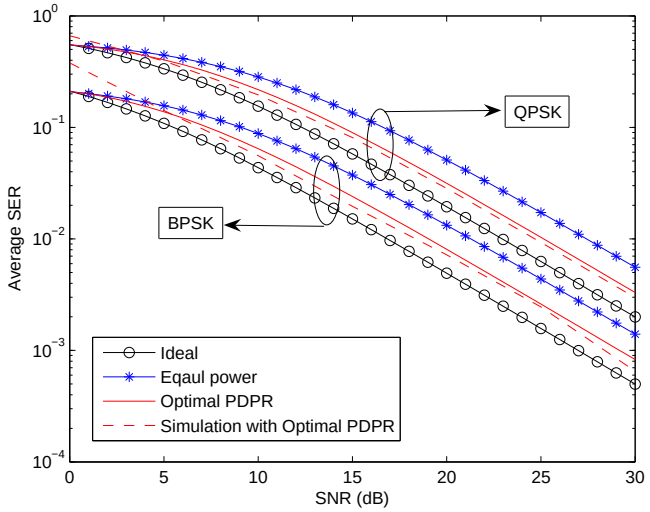

Figure 4.6: SER versus SNR with optimal PDPR and equal power of 2×2 MIMO-OFDM with LS/ZF. Comparison between the analysis and simulation.

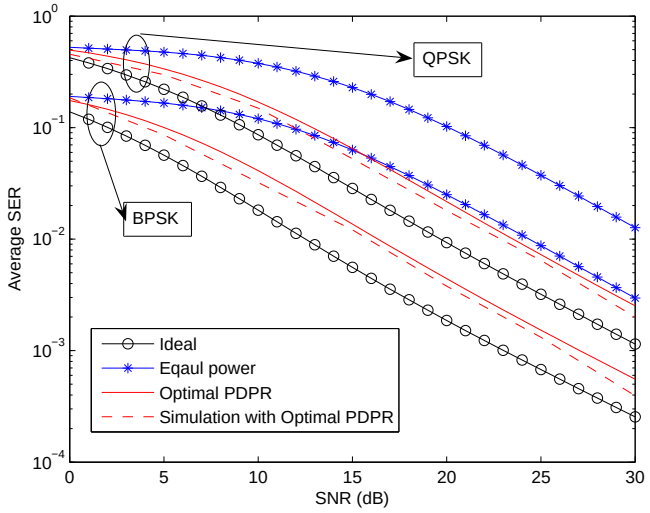

Figure 4.7: SER versus SNR with optimal PDPR and equal power of 2×2 MIMO-OFDM with MMSE/MMSE. Comparison between the analysis and simulation.

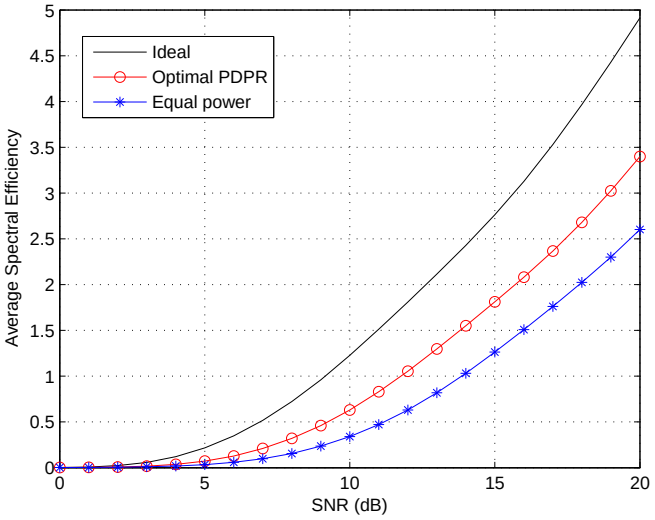

Figure 4.8: Average spectral efficiency versus SNR of 2×2 MIMO-OFDM with LS/ZF.

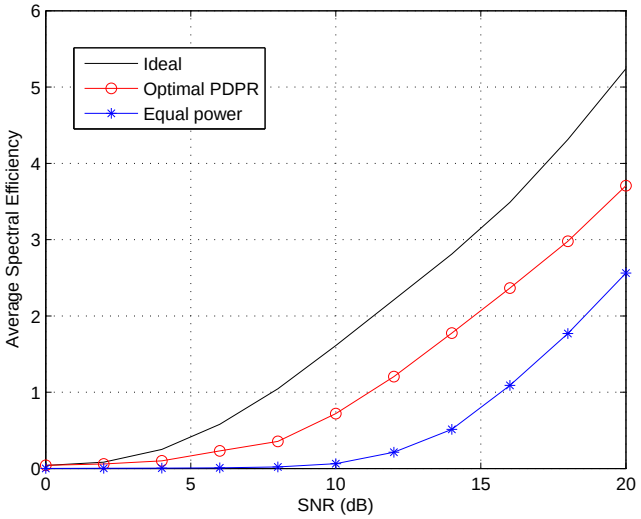

Figure 4.9: Average spectral efficiency versus SNR of 2×2 MIMO-OFDM with MMSE/MMSE.

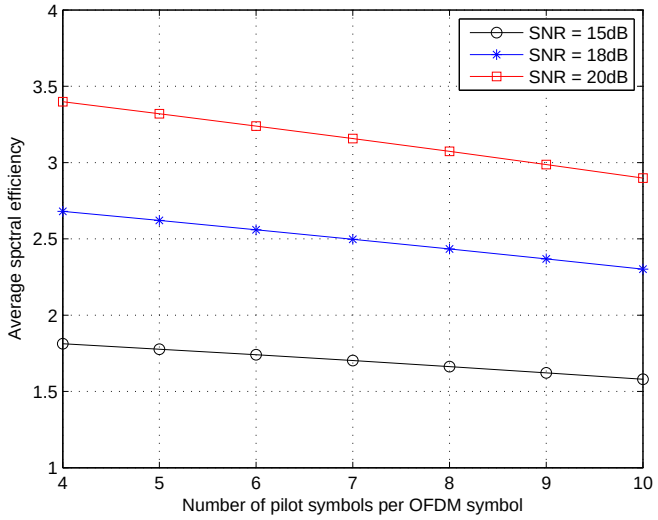

Figure 4.10: Average spectral efficiency versus the number of pilot symbols ($P \geq L$) for 2×2 MIMO-OFDM with LS/ZF.

4.5.3 Validating the Optimal PDPR in a Practical Channel Model

In this chapter, the practically used system structure is considered with a complex Gaussian channel having an uniform distributed power delay profile (PDP). However, there are many channel models that can be used for evaluating practical system performance, for example, typical urban (TU), Stanford University Interim (SUI), pedestrian A, and pedestrian B.

Usually, when system developers and researchers design channel estimation schemes and pilot signals, uniform distributed PDP can be considered due to unknown channel statistics. To verify the results from my analysis, the proposed optimal PDPR is compared with the optimal PDPR obtained by simulation for the TU channel model, which is one of practical channel models used for evaluating

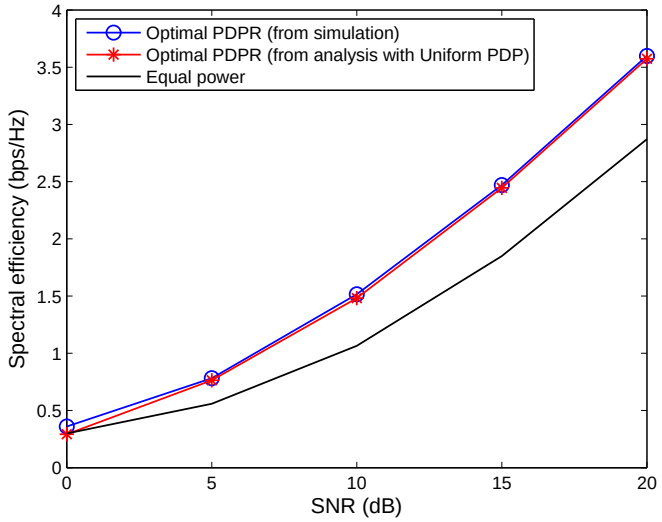

Figure 4.11: Comparison between the analysis and simulation results with TU channels: spectral efficiency vs. SNR (TU channel)

system performance in emerging standards. For the LS/ZF system case, the closed form solution of the optimal PDPR has been obtained, so this system model is considered in this simulation. For simulation, the TU channel model is used, channel bandwidth is 1.25Mhz, carrier frequency is 2GHz, the system is 2×2 MIMO-OFDM with 128 subcarriers (these system parameters are selected from 3GPP-LTE standard). The number of pilot symbols is 8, target BER is 10^{-3}, and modulation order is chosen from $\{2, 4, 16, 64, 256\}$.

Figs. 4.11 and 4.12 show the simulation results of the optimal PDPR with the TU channel model. Figs. 4.11 and 4.12 compare the average spectral efficiency of two different cases. One is the average spectral efficiency under the TU channel model with the optimal PDPR obtained from my research. This PDPR is obtained

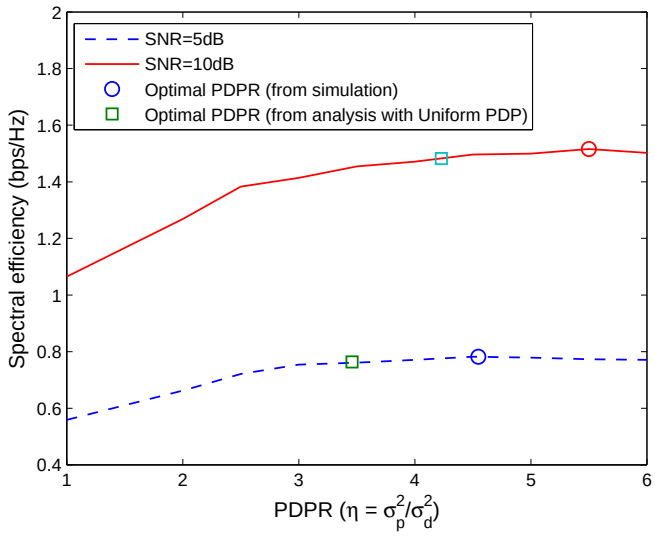

Figure 4.12: Comparison between the analysis and simulation results with TU channels: spectral efficiency vs. PDPR (TU channel)

by assuming the uniform distributed PDP with the same channel taps as the TU channel model. The other is the maximum average spectral efficiency obtained from the simulation over different PDPR values (0< α <1) for the TU channel model. Equal power allocation case is shown as a reference. Fig. 4.11 shows the average spectral efficiency vs. SNR for three different PDPR cases. As shown in this figure, even though the analysis result is obtained from the uniform distributed PDP assumption, it shows the performance which is very close to the optimal PDPR obtained by simulation. Moreover, by comparing the results of those two PDPR cases with the equal power case, it can be shown that we can get higher average spectral efficiency under practical channel (TU channel) by simple power allocation between pilot and data symbols.

The similar performance between the proposed optimal PDPR and the one obtained by simulation can be explained by Fig. 4.12. It shows the achievable spectral efficiency versus PDPR (linear scale) for two different SNR cases (i.e. 5dB and 10dB). The spectral efficiency is obtained by simulation with TU channel. The circle marks show the optimal PDPR which maximizes the spectral efficiency, and the square marks represent the optimal PDPR obtained from the analysis. As shown in this figure, those two PDPR values are different, but their achievable spectral efficiency is similar. This is because there is a broad range of PDPR which shows similar spectral efficiency near the optimal PDPR and those two PDPR values are located in this range. Moreover, if pilot power is too high, then there can be a peak power problem at the transmit power amplifier. Therefore, it is better to use lower pilot power if similar spectral efficiency can be obtained. Also, it can be shown that the spectral efficiency with the optimal PDPR obtained from the analysis is higher than the equal power allocation case.

4.6 Chapter Summary

In this chapter, the optimal PDPR for minimizing the average SER and maximizing the spectral efficiency of adaptive MIMO-OFDM systems was derived for two different channel estimation and linear receivers. The analysis with LS and MMSE channel estimation and ZF and MMSE receivers shows that by balancing between channel estimation accuracy (high pilot power) and high signal power (high data power), the spectral efficiency of adaptive modulation systems can be substantially increased without consuming any additional resources. For example,

it is shown that the optimal PDPR provides 4dB of gain for 2x2 MIMO-OFDM with MMSE channel estimation and MMSE receiver compared to allocating equal power to the pilot and data symbols.

Chapter 5

Conclusion

Designing a system in order to maximize its achievable throughput and robustness is related to how the system can exploit various resources such as the achievable spreading and diversity gain, and the amount of transmit power. The system can exploit these resources according to trading off the need for robust communication versus the desire for high data rate in dynamic and challenging wireless channels. Thus, in multicarrier wireless communications, the rate-robustness tradeoff has a strong impact on system design.

This dissertation studied the rate-robustness tradeoff in three different aspects for multicarrier wireless communication systems: the variable data rate and interference robustness tradeoff, the pilot-data power allocation tradeoff in MIMO multicarrier systems from a theoretical capacity perspective, and the pilot-data power allocation tradeoff in M-QAM MIMO multicarrier systems from a practical performance viewpoint.

First, when MC-CDMA is combined with multi-code techniques to support variable data rates, there is a tradeoff between the number of supportable subscribers and the per subscriber data rate due to the interference scaling problem. In Chapter 2, we proposed a novel multi-code multicarrier CDMA system to efficiently ad-

dress this problem with enhanced robustness to multipath fading channels [63, 64]. Moreover, the proposed system gains in both the time and frequency domains to exploit the diversity and interference averaging properties of multicarrier modulation and CDMA. The proposed MC-MC-CDMA system shows that data rate flexibility can be achieved in a multicarrier CDMA system without any sacrifice in performance, and to the contrary, can actually allow improved robustness, flexibility, and capacity. Hence this system outperforms multicarrier CDMA and single carrier multi-code CDMA in terms of bit error probability and user capacity in a frequency selective Rayleigh fading channel with the same total bandwidth.

Another rate-robustness tradeoff in multicarrier systems can be found in the pilot and data symbol power allocation problem. Since pilot symbols consume both bandwidth and energy, the power budget is reduced for data symbols per OFDM symbol when the total transmit power is fixed. This suggests a tradeoff, especially, when OFDM is used in conjunction with MIMO. In MIMO-OFDM it is crucial to system performance due to the necessity of CSI at the receiver. This power allocation problem is studied in theoretically in Chapter 3 and from a practical performance perspective in Chapter 4.

In Chapter 3, the optimal PDPR in MIMO-OFDM for maximizing a capacity lower bound was formed and analyzed for two different channel conditions and four likely pilot patterns [58–60]. In MIMO-OFDM systems, pilot symbols can be transmitted in various ways to avoid spatial interference when estimating the channel. For dynamic channels, the optimal PDPR is obtained by considering both channel estimation and interpolation error over the Doppler spectrum, since

in emerging standards pilot symbols are transmitted periodically, and interpolation techniques are used over two pilot-inserted OFDM symbols. From the analysis, it is shown that the SPP-2 pilot pattern can achieve a higher capacity lower bound than other schemes, and the capacity lower bound of a typical MIMO-OFDM system can be increased about 10%∼30% compared with the case of equal power allocation by simply using the optimal PDPR. Moreover, the optimal PDPR varies with vehicle speed, but the variation is small.

As shown in Chapter 3, the optimal PDPR results in improved system performance without using additional resources, and the optimal pilot power is higher than the data power. This pilot power boost has been shown empirically to provide substantial improvement in system performance, and explains why pilot power boosting is considered in many emerging high data rate standards. In Chapter 4, the effect of the PDPR on the performance of adaptive M-QAM based MIMO-OFDM systems with ZF and MMSE linear receivers was analytically shown, and the optimal PDPR, in terms of minimizing the average SER and maximizing the spectral efficiency, was derived [61, 62]. Since, the performance of MIMO-OFDM with adaptive modulation depends on the distribution of the SNR and the receiver type, our results find the optimal PDPR by deriving the distribution of the output SNR of different linear receivers including the effect of the pilot-based channel estimation, which has not been done previously. The analysis shows that by appropriately balancing pilot power and data power, the spectral efficiency of adaptive modulation systems can be substantially increased without consuming any additional resources. For example, it is shown that the optimal PDPR provides 4dB of gain for

2x2 MIMO-OFDM with MMSE channel estimation and an MMSE receiver compared to allocating equal power to the pilot and data symbols. The key insights are that pilot power boosting to improve system performance should be optimized by considering system structures such as pilot structure, modulation order, and receiver type.

The various fundamental tradeoffs in multicarrier communications presented in this dissertation can be applied to the design of the PHY layer of high data rate systems. It will provide guidelines to the system designer on how to exploit numerous available features to maximize performance while balancing the rate-robustness tradeoffs.

5.1 Future Research

In this section, I propose several future research topics for the rate-robustness tradeoff in wireless communication systems, potentially for other researchers interested in this area.

- *Optimal PDPR with a non-uniform power delay profile (PDP)*

  The results for finding the optimal PDPR in this dissertation assume uniform PDP. In many scenarios, a uniform PDP provides a good approximation of the delay profile. However, in some wireless environments, an exponential PDP may be more appropriate. In the case of exponential PDP, the channel coefficients are non-identically distributed, and an equally spaced exponential profile might be substituted [26]. The feasibility of finding optimal PDPR

with exponential PDP analytically can be further studied, and the results of a uniform PDP case addressed in this dissertation can be used for comparison.

- *Maximizing system capacity in a multi-cell environment with the PDPR trade-off*

  In multi-cell MIMO-OFDM systems, pilot symbols from other cells can result in interference to data signals in a desired cell and vice versa. Therefore, the effective SNR includes other cell interference (which might either be pilot or data signals from other cells). In this case, the optimal PDPR obtained in this dissertation does not guarantee maximum system capacity. Higher PDPR than the optimal PDPR implies lower capacity in this work. However, since the number of data symbols is usually greater than the number of pilot symbols, the effect of other cell interference due to data symbols can be more significant than pilot symbols. In an interference-limited case, higher PDPR than the optimal PDPR found here can result in higher system capacity due to lower out-of-cell interference. Simply put, a key question to consider is: "How does the PDPR affect out-of-cell interference in capacity analysis?" Thus, in a multi-cell environment, a framework needs to be developed where the effect of the PDPR could be accounted for a capacity analysis.

- *Applying the optimal PDPR to practical system design*

  The optimal PDPR addressed in this dissertation can be better applied to practical system design with more investigation on channel and system models

such as cell structure, power constraints, and system configurations as follows.

- *A multi-cell environment:* As noted previously, in a multi-cell environment, the optimal PDPR is related to the amount of interference.
- *Channel models:* The PDPR depends on the channel model while more detailed channel models are difficult to apply analytically. Thus, the optimal PDPR under numerous channel models can be obtained from simulation using the PDPR analysis framework developed in this work.
- *Power constraints:* The limited average power constraint is assumed here. However, other power constraints such as a peak power constraint can be considered. For a peak power constraint, the pilot power is limited by the peak power constraint of the power amplifier. Also, it is related to the PAPR problem in multicarrier modulation systems.
- *System configurations:* Since the channel estimation and interpolation methods are directly related to the effect of the PDPR as shown in my work, the structure of these methods used in systems should be included for finding optimal PDPR.

Appendices

Appendix A

Derivation of the Decision Variable: the Output of the Matched Filter

For the analysis of the BER performance of the proposed system, the matched filter output can be written as (2.11). From (2.8) and (2.11), due to the orthogonality between subcarriers, the desired signal $D_{1,m}$ can be written as

$$\begin{aligned} D_{1,m} &= \frac{1}{T_b}\sum_{n=0}^{N_c-1} \nu_m(n)\nu_{b_{1,0}}(n) \\ &\qquad \times \int_{nT_b}^{(n+1)T_b} \sum_{q=1}^{K} g_{1,q}(n) f_r(t-nT_b) c_{1,q}^2(n)\cos^2(\omega_q t + \phi_{1,q}(n))dt \\ &= \frac{1}{2}\sum_{n=0}^{N_c-1} \nu_m(n)\nu_{b_{1,0}}(n)\sum_{q=1}^{K} g_{1,q}(n). \end{aligned} \tag{A.1}$$

The interference term $I_{1,m} + J_{1,m}$ is given by

$$\begin{aligned} I_{1,m} + J_{1,m} = \frac{1}{T_b}\sum_{j=0}^{N_c-1} \nu_m(j) \int_{jT_b}^{(j+1)T_b} \sum_{u=2}^{N_u}\sum_{k=1}^{K}\sum_{n=0}^{N_c-1} g_{u,k}(n)\nu_{b_{u,0}}(n) f_r(t-nT_b) c_{u,k}(n) \\ \times \cos(\omega_k t + \phi_{u,k}(n)) \sum_{q=1}^{K} c_{1,q}(j)\cos(\omega_q t + \phi_{1,q}(j))dt, \end{aligned} \tag{A.2}$$

where $I_{1,m}$ corresponds to the interference from the other $N_u - 1$ users on the same subcarrier and $J_{1,m}$ corresponds to the interference from the other $N_u - 1$ users on

the other subcarriers. Both $I_{1,m}$ and $J_{1,m}$ can be simplified as

$$\begin{aligned} I_{1,m} &= \frac{1}{T_b}\sum_{j=0}^{N_c-1}\nu_m(j)\sum_{u=2}^{N_u}\sum_{k=1}^{K}\sum_{n=0}^{N_c-1} g_{u,k}(n)\nu_{b_{u,0}}(n)c_{u,k}(n)c_{1,k}(j) \\ &\qquad \times \int_{jT_b}^{(j+1)T_b} f_r(t-nT_b)\cos\left(\omega_k t+\phi_{u,k}(n)\right)\cos(\omega_k t+\phi_{1,k}(j))dt \\ &= \frac{1}{2}\sum_{u=2}^{N_u}\sum_{k=1}^{K}\sum_{n=0}^{N_c-1} g_{u,k}(n)\nu_m(n)\nu_{b_{u,0}}(n)c_{u,k}(n)c_{1,k}(n)\cos\left(\phi_{u,k}(n)-\phi_{1,k}(n)\right), \end{aligned} \tag{A.3}$$

$$\begin{aligned} J_{1,m} &= \frac{1}{T_b}\sum_{j=0}^{N_c-1}\nu_m(j)\sum_{u=2}^{N_u}\sum_{n=0}^{N_c-1}\sum_{k=1}^{K}\sum_{\substack{q=1\\q\neq k}}^{K} g_{u,k}(n)\nu_{b_{u,0}}(n)c_{u,k}(n)c_{1,q}(j) \\ &\qquad \times \int_{jT_b}^{(j+1)T_b} f_r(t-nT_b)\cos(\omega_k t+\phi_{u,k}(n))\cos(\omega_q t+\phi_{1,q}(j))dt \\ &= \frac{1}{2T_b}\sum_{u=2}^{N_u}\sum_{n=0}^{N_c-1}\sum_{k=1}^{K}\sum_{\substack{q=1\\q\neq k}}^{K} g_{u,k}(n)\nu_m(n)\nu_{b_{u,0}}(n)c_{u,k}(n) \\ &\qquad \times c_{1,q}(n)\int_0^{T_b}\cos\Big((\omega_k-\omega_q)t+\phi_{u,k}(n)-\phi_{1,q}(n)\Big)dt. \end{aligned} \tag{A.4}$$

As shown in (A.1)-(A.4), the matched filter output is expressed in terms of correlation functions of the code sequences. Now the variance of the term $I_{1,m}$ and $J_{1,m}$ for the EGC case is derived. All cross terms are uncorrelated due to the random phase, and $I_{1,m}$ and $J_{1,m}$ are zero mean. Therefore, with the fact that $E[g_{u,k}^2] = 2\sigma^2$, the variance of $I_{1,m}$ and $J_{1,m}$ can be simplified as

$$\begin{aligned} \mathrm{var}[I_{1,m}] &= \frac{1}{4}\sum_{u=2}^{N_u}\sum_{k=1}^{K}\sum_{n=0}^{N_c-1} E[g_{u,k}^2(n)]E[\nu_m^2(n)\nu_{b_{u,0}}^2(n)c_{u,k}^2(n)c_{1,k}^2(n)] \\ &\qquad \times E[\cos^2\left(\phi_{u,k}(n)-\phi_{1,k}(n)\right)] \\ &= \frac{1}{4}(N_u-1)KN_c\sigma^2, \end{aligned} \tag{A.5}$$

$$\begin{aligned}
\mathrm{var}[J_{1,m}] &= \frac{1}{2T_b^2}\sum_{u=2}^{N_u}\sum_{n=0}^{N_c-1}\sum_{k=1}^{K}\sum_{\substack{q=1\\q\neq k}}^{K} E[g_{u,k}^2(n)]E[\nu_m^2(n)\nu_{b_{u,0}}^2(n)c_{u,k}^2(n)c_{1,q}^2(n)] \\
&\qquad\qquad \times E\left[\left(\int_0^{T_b}\cos\Big((\omega_k-\omega_q)t+\phi_{u,k}(n)-\phi_{1,q}(n)\Big)\,dt\right)^2\right] \\
&= \frac{\sigma^2}{4T_b^2}\sum_{u=2}^{N_u}\sum_{n=0}^{N_c-1}\sum_{k=1}^{K}\sum_{\substack{q=1\\q\neq k}}^{K} E\Bigg[\Bigg(\frac{T_b}{2\pi(k-q)}\{\sin((\omega_k-\omega_q)t+\phi_{u,k}(n)-\phi_{1,q}(n)) \\
&\qquad\qquad - \sin(\phi_{u,k}(n)-\phi_{1,q}(n))\}\Bigg)^2\Bigg] \\
&= \frac{\sigma^2 N_c(N_u-1)}{8\pi^2}\sum_{k=1}^{K}\sum_{\substack{q=1\\q\neq k}}^{K}\frac{1}{(k-q)^2}. \qquad \text{(A.6)}
\end{aligned}$$

Appendix B

Channel Estimation and Interpolation Error Analysis

B.1 MMSE Time Interpolation

The time interpolated k^{th} subcarrier channel response of N OFDM symbols can be obtained as

$$\begin{aligned}\hat{\mathbf{H}}_{FT,k}^{m_r,m_t} &= \mathbf{R}_{C\hat{C}_P}\mathbf{R}_{\hat{C}_P\hat{C}_P}^{-1}\hat{\mathbf{C}}_{P,k} \\ &= \mu P\mathbf{R}_{CC_P}\left(\mu^2P^2\mathbf{R}_{C_PC_P}+\frac{\mu^2\omega_k}{\gamma_P}\mathbf{I}\right)^{-1}\hat{\mathbf{C}}_{P,k}, \end{aligned} \tag{B.1}$$

where $\omega_k = \left[\mathbf{F}\mathbf{F}_P^H\mathbf{F}_P\mathbf{F}^H\right]_{k,k}$ $\hat{\mathbf{C}}_{P,k} = \left[\begin{array}{cc} \hat{H}_{F,k}^{m_r,m_t}(1) & \hat{H}_{F,k}^{m_r,m_t}(N) \end{array}\right]^T$ is a vector of the frequency interpolated k^{th} subcarrier estimated channel response of two consecutive pilot inserted OFDM symbols, $\mathbf{C}(k) = \left[\begin{array}{ccc} H_{F,k}^{m_r,m_t}(1) & \cdots & H_{F,k}^{m_r,m_t}(N) \end{array}\right]^T$ is a channel vector composed of the k^{th} subcarrier channel response of N OFDM symbols. Since the time correlation of channel is expressed by the bessel function with the Doppler frequency. $\mathbf{R}_{CC_P}$ and $\mathbf{R}_{C_PC_P}$ are ($N\times2$) and (2×2) size covariance matrices as below.

$$\begin{aligned}\mathbf{R}_{C_PC_P} &= \left[\begin{array}{cc} 1 & \mathrm{J}_0(2\pi f_d(N-1)T_s) \\ \mathrm{J}_0(-2\pi f_d(N-1)T_s) & 1 \end{array}\right], \\ \mathbf{R}_{CC_P} &= \left[\begin{array}{cc} 1 & \mathrm{J}_0(2\pi f_d(N-1)T_s) \\ \mathrm{J}_0(-2\pi f_dT_s) & \mathrm{J}_0(2\pi f_d(N-2)T_s) \\ \vdots & \vdots \\ \mathrm{J}_0(-2\pi f_d(N-2)T_s) & \mathrm{J}_0(2\pi f_dT_s) \\ \mathrm{J}_0(-2\pi f_d(N-1)T_s) & 1 \end{array}\right], \end{aligned} \tag{B.2}$$

where $J_0(\cdot)$ is a 0^{th} order bessel function. Then, the time interpolated k^{th} subcarrier channel response of N OFDM symbols can be obtained as (3.31).

B.2 Channel Estimation Error Covariance of the Dynamic Channel Case

The channel estimation error covariance matrix is

$$\mathbf{R}_{\mathbf{y}_{E,n}} = \sigma_d^2 E\left[\tilde{\mathbf{H}}(n)\tilde{\mathbf{H}}^H(n)\right] + \sigma_n^2 \mathbf{I}, \tag{B.3}$$

and the channel estimation error of k^{th} subcarrier of n^{th} OFDM symbol between m_r^{th} receive and m_t^{th} transmit antenna is given by

$$\tilde{H}_k^{m_r,m_t}(n) \quad = \quad H_k^{m_r,m_t}(n) - (g_{n,1}\hat{H}_{F,k}^{m_r,m_t}(1) + g_{n,2}\hat{H}_{F,k}^{m_r,m_t}(N)). \tag{B.4}$$

Assuming that there is no spatial correlation, $E\left[\tilde{\mathbf{H}}(n)\tilde{\mathbf{H}}^H(n)\right]$ is a block diagonal matrix as below,

$$E\left[\tilde{\mathbf{H}}(n)\tilde{\mathbf{H}}^H(n)\right] = \mathrm{diag}\left(\sum_{m_t=1}^{M_t} E\left[\tilde{\mathbf{H}}^{m_r,m_t}(n)(\tilde{\mathbf{H}}^{m_r,m_t}(n))^H\right]\right)_{m_r=1}^{M_r}, \tag{B.5}$$

where $\tilde{\mathbf{H}}^{m_r,m_t}(n)$ is a diagonal matrix, and its diagonal elements is

$$\begin{aligned} & E\left[\tilde{H}_k^{m_r,m_t}(n)(\tilde{H}_k^{m_r,m_t}(n))^H\right] \\ & \quad = 1 - 2g_{n,1}\mu P\mathrm{J}(n,1) - 2g_{n,2}\mu P\mathrm{J}(n,N) + 2g_{n,1}g_{n,2}\mu^2 P^2\mathrm{J}(1,N) \\ & \qquad\qquad + g_{n,1}^2\mu^2 P^2 + g_{n,2}^2\mu^2 P^2 + (g_{n,1}^2 + g_{n,2}^2)\frac{\mu^2\omega_k}{\gamma_P}, \\ & \quad \triangleq \xi_k(n) \end{aligned} \tag{B.6}$$

$$\mathrm{J}(a,b) = \mathrm{J}_0(2\pi f_d(a-b)T_s). \tag{B.7}$$

Then, the channel estimation error covariance matrix can be expressed as

$$\mathbf{R}_{\mathbf{y}_{E,n}} = \text{diag}(\mathbf{\Lambda}_{m_r,n})_{m_r=1}^{M_r}, \tag{B.8}$$

where

$$\mathbf{\Lambda}_{m_r,n} = (M_t\sigma_d^2\xi_k(n) + \sigma_n^2)_{k=1}^{K}. \tag{B.9}$$

Appendix C

SNR Lower Bound of MMSE Receiver with MMSE Channel Estimation

C.1 Derivation of the k^{th} Stream SNR of the MMSE Receiver

The output of the MMSE receiver is given by

$$\mathbf{z} = \mathbf{G}_M\mathbf{y} = \frac{1}{\sqrt{M_t}}\mathbf{G}_M\hat{\mathbf{H}}\mathbf{s} - \frac{1}{\sqrt{M_t}}\mathbf{G}_M\tilde{\mathbf{H}}\mathbf{s} + \mathbf{G}_M\mathbf{n}. \tag{C.1}$$

Then, the SNR of the k^{th} stream of the MMSE receiver with the MMSE channel estimation is given by,

$$\gamma_k = \frac{\frac{\sigma_d^2}{M_t}\left(\left[\mathbf{G}_M\hat{\mathbf{H}}\right]_{k,k}\right)^2}{\left[\frac{\sigma_d^2}{M_t}\mathbf{G}_M\hat{\mathbf{H}}\hat{\mathbf{H}}^H\mathbf{G}_M^H + \frac{\sigma_d^2}{M_t}\beta_2\mathbf{G}_M\mathbf{G}_M^H + \sigma_n^2\mathbf{G}_M\mathbf{G}_M^H\right]_{k,k} - \frac{\sigma_d^2}{M_t}\left(\left[\mathbf{G}_M\hat{\mathbf{H}}\right]_{k,k}\right)^2}, \tag{C.2}$$

where $\beta_2 = E\left[\tilde{\mathbf{H}}\tilde{\mathbf{H}}^H\right] = \frac{M_t^2 L}{P\gamma_p + LM_t}$ as derived in (4.11). Since

$$\begin{aligned}
\mathbf{G}_M\hat{\mathbf{H}} &= \sqrt{M_t}\left(\hat{\mathbf{H}}^H\hat{\mathbf{H}} + \frac{M_t}{\gamma_d}\mathbf{I}\right)^{-1}\left(\hat{\mathbf{H}}^H\hat{\mathbf{H}} + \frac{M_t}{\gamma_d}\mathbf{I} - \frac{M_t}{\gamma_d}\mathbf{I}\right) \\
&= \sqrt{M_t}\left(\mathbf{I} - \left(\mathbf{I} + \frac{\gamma_d}{M_t}\hat{\mathbf{H}}^H\hat{\mathbf{H}}\right)^{-1}\right), \qquad \text{(C.3)} \\
\mathbf{G}_M\hat{\mathbf{H}}\hat{\mathbf{H}}^H\mathbf{G}_M^H &= M_t\left(\hat{\mathbf{H}}^H\hat{\mathbf{H}} + \frac{M_t}{\gamma_d}\mathbf{I}\right)^{-1}\hat{\mathbf{H}}^H\hat{\mathbf{H}}\hat{\mathbf{H}}^H\hat{\mathbf{H}}\left(\hat{\mathbf{H}}^H\hat{\mathbf{H}} + \frac{M_t}{\gamma_d}\mathbf{I}\right)^{-1} \\
&= M_t\left(\mathbf{I} - \left(\mathbf{I} + \frac{\gamma_d}{M_t}\hat{\mathbf{H}}^H\hat{\mathbf{H}}\right)^{-1}\right)^2, \qquad \text{(C.4)}
\end{aligned}$$

$$\begin{aligned}\mathbf{G}_M\mathbf{G}_M^H &= M_t\left(\hat{\mathbf{H}}^H\hat{\mathbf{H}}+\frac{M_t}{\gamma_d}\mathbf{I}\right)^{-1}\hat{\mathbf{H}}^H\hat{\mathbf{H}}\left(\hat{\mathbf{H}}^H\hat{\mathbf{H}}+\frac{M_t}{\gamma_d}\mathbf{I}\right)^{-1}\\ &= \gamma_d\left[\mathbf{I}-\left(\mathbf{I}+\frac{\gamma_d}{M_t}\hat{\mathbf{H}}^H\hat{\mathbf{H}}\right)^{-1}\right]\left(\mathbf{I}+\frac{\gamma_d}{M_t}\hat{\mathbf{H}}^H\hat{\mathbf{H}}\right)^{-1}, \qquad \text{(C.5)}\end{aligned}$$

the SNR γ_k can be obtained as

$$\gamma_k = \frac{(1-\mathbf{A}_{k,k})^2}{\mathbf{A}_{k,k}-\mathbf{A}_{k,k}^2+\frac{\beta_2\gamma_d}{M_t}\left(\mathbf{A}_{k,k}-(\mathbf{A}^2)_{k,k}\right)}, \qquad \text{(C.6)}$$

where $\mathbf{A} \triangleq \left(\mathbf{I}+\frac{\gamma_d}{M_t}\hat{\mathbf{H}}^H\hat{\mathbf{H}}\right)^{-1}$.

C.2 Proof of Lemma 4.1 in Section 4.3.2

$\mathbf{A}_{k,k}$ is k^{th} diagonal element of $\mathbf{A}$, and $(\mathbf{A}^2)_{k,k}$ is k^{th} diagonal element of $\mathbf{A}^2$. Moreover, $\mathbf{A}_{k,k}^2 := (\mathbf{A}_{k,k})^2$. Then, since $\mathbf{A} \triangleq \left(\mathbf{I}+\frac{\gamma_d}{M_t}\hat{\mathbf{H}}^H\hat{\mathbf{H}}\right)^{-1}$ is a Hermitian matrix,

$$\begin{aligned}(\mathbf{A}^2)_{k,k} &= (\mathbf{A}_{k,k})^2+\sum_{i,i\neq k}(\mathbf{A}_{k,i})^2\\ &= \mathbf{A}_{k,k}^2+\sum_{i,i\neq k}\mathbf{A}_{k,i}^2\\ &> \mathbf{A}_{k,k}^2 \qquad (\text{since } \mathbf{A}_{k,i}^2 \geq 0) \qquad \text{(C.7)}\end{aligned}$$

Then, the SNR with $\mathbf{A}_{k,k}^2$ instead of $(\mathbf{A}^2)_{k,k}$ is

$$\underline{\gamma}_k = \frac{(1-\mathbf{A}_{k,k})^2}{\mathbf{A}_{k,k}-\mathbf{A}_{k,k}^2+\frac{\beta_2\gamma_d}{M_t}\left(\mathbf{A}_{k,k}-\mathbf{A}_{k,k}^2\right)} < \gamma_k. \qquad \text{(C.8)}$$

Thus, $\underline{\gamma}_k$ is a lower bound of the exact SNR γ_k. Moreover,

$$\begin{aligned}\mathbf{A}_{k,k} &< \lambda_{max}(\mathbf{A})\\ &= \frac{1}{\lambda_{min}(\mathbf{I}+\frac{\gamma_d}{M_t}\hat{\mathbf{H}}^H\hat{\mathbf{H}})}\end{aligned}$$

$$= \frac{1}{1 + \frac{\gamma_d}{M_t}\lambda_{min}(\hat{\mathbf{H}}^H\hat{\mathbf{H}})} < 1. \tag{C.9}$$

$$\begin{aligned}\left(\mathbf{A}^2\right)_{k,k} &< \lambda_{max}(\mathbf{A}^2) \\ &\leq \lambda^2_{max}(\mathbf{A}) < 1. \end{aligned} \tag{C.10}$$

where $\lambda_{max}(\cdot)$ and $\lambda_{min}(\cdot)$ are the maximum and minimum singular value of $(\cdot)$.

Since the scalar exponential function can be represented by the power series and $\mathbf{A}_{k,k} < 1$, $\exp(\mathbf{A}_{k,k})$ can be approximated as

$$\exp(\mathbf{A}_{k,k}) \approx 1 + \mathbf{A}_{k,k} + \frac{\mathbf{A}^2_{k,k}}{2!}. \tag{C.11}$$

From the definition of the matrix exponential [66],

$$\exp(\mathbf{A}) = \sum_{n=0}^{\infty} \frac{\mathbf{A}^n}{n!} = \mathbf{I} + \mathbf{A} + \frac{\mathbf{A}^2}{2!} + \frac{\mathbf{A}^3}{3!} + \cdots . \tag{C.12}$$

Since $\mathbf{A} = (\mathbf{I} + \frac{\gamma_d}{M_t}\hat{\mathbf{H}}^H\hat{\mathbf{H}})^{-1}$ is a Hermitian matrix, its singular value decomposition (SVD) is $\text{SVD}(\mathbf{A}) = \mathbf{U}\mathbf{\Lambda}\mathbf{U}^H$, where $\mathbf{\Lambda}$ is a diagonal matrix and its entries are the singular values of $\mathbf{A}$, and $\mathbf{U}$ a unitary matrix. Because $\lambda_{max}(\mathbf{A}) < 1$ as shown in (C.9), the diagonal element of the matrix exponential of $\mathbf{A}$ can be expressed as

$$\begin{aligned}[\exp(\mathbf{A})]_{k,k} &= \left[\mathbf{U}\mathbf{U}^H + \mathbf{U}\mathbf{\Lambda}\mathbf{U}^H + \frac{1}{2}\mathbf{U}\mathbf{\Lambda}^2\mathbf{U}^H + \frac{1}{3!}\mathbf{U}\mathbf{\Lambda}^3\mathbf{U}^H + \cdots\right]_{k,k} \\ &= \mathbf{u}_k \exp(\mathbf{\Lambda})\mathbf{u}_k^H \\ &= \mathbf{u}_k \text{diag}(\exp(\mathbf{\Lambda}_{1,1}), \cdots, \exp(\mathbf{\Lambda}_{M_t,M_t}))\mathbf{u}_k^H \\ &\approx \mathbf{u}_k \text{diag}\left((1 + \mathbf{\Lambda}_{1,1} + \frac{\mathbf{\Lambda}^2_{1,1}}{2}), \cdots, (1 + \mathbf{\Lambda}_{M_t,M_t} + \frac{\mathbf{\Lambda}^2_{M_t,M_t}}{2})\right)\mathbf{u}_k^H \\ &= 1 + \mathbf{A}_{k,k} + \frac{(\mathbf{A}^2)_{k,k}}{2}. \end{aligned} \tag{C.13}$$

Then, the difference between $(\mathbf{A}^2)_{k,k}$ and $\mathbf{A}^2_{k,k}$ is given by

$$\begin{aligned}(\mathbf{A}^2)_{k,k} - \mathbf{A}^2_{k,k} &\approx ([\exp(\mathbf{A})]_{k,k} - 1 - \mathbf{A}_{k,k}) - (\exp(\mathbf{A}_{k,k}) - 1 - \mathbf{A}_{k,k}) \\ &= [\exp(\mathbf{A})]_{k,k} - \exp(\mathbf{A}_{k,k}) \end{aligned} \tag{C.14}$$

Since the dominant terms in (C.11) and (C.13) are the same with $(1 + \mathbf{A}_{k,k})$, the difference is very small. Moreover, in (C.9) and (C.10), as γ_d increases, the upper bound becomes more smaller than 1. Then, $[\exp(\mathbf{A})]_{k,k} \approx \exp(\mathbf{A}_{k,k}) \approx 1 + \mathbf{A}_{k,k}$, and $(\mathbf{A}^2)_{k,k} \approx \mathbf{A}^2_{k,k}$.

C.3 α_X, β_X, and γ_X Values for the Approximated Distribution of the SNR Lower Bound in Section 4.3.2

$$\alpha_X = \frac{\xi(2M_r\tau\gamma_d - (M_t-1)(1-\xi+(1+\tau)\gamma_d))^2}{2\tau\gamma_d^2(2\xi M_r\tau + (M_t-1)(1+\tau-\xi(1+\tau)+(\tau-1)^2\gamma_d))}, \tag{C.15}$$

$$\beta_X = \delta'\gamma_0'\left(\frac{\gamma_d(\xi(1+\tau+2M_r\tau-M_t(1+\tau))+(M_t-1)(1+\tau+(\tau-1)^2\gamma_d))}{\xi(1+\xi(M_t-1)+(1+\tau+2M_r\tau)\gamma_d - M_t(1+\gamma_d+\tau\gamma_d))}\right), \tag{C.16}$$

$$\gamma_X = -1 + \gamma_{X1}\gamma_{X2}, \tag{C.17}$$

$$\gamma_{X1} = \frac{\xi(M_t-1)+2M_r\tau\gamma_d+\tau\gamma_d+\gamma_d-M_t(\tau\gamma_d+\gamma_d+1)+1}{\xi\gamma_d\left(\xi(M_t+(-2M_r+M_t-1)\tau-1)-(M_t-1)\left(\gamma_d(\tau-1)^2+\tau+1\right)\right)^2},$$

$$\gamma_{X2} = (1-M_t+(1+2M_r-M_t)\tau)\xi^3 + (M_t-1)(1+(\tau-1)^2\gamma_d)\xi^2 + (M_t-1)\tau(1+2\tau\gamma_d+(\tau-1)^2\gamma_d^2),$$

$$\xi = \sqrt{1+2(1+\tau)\gamma_d+(1-\tau)^2\gamma_d^2}, \qquad \delta' = \frac{P\gamma_p+2LM_t}{P\gamma_p+LM_t}, \tag{C.18}$$

$$\gamma_0' = \frac{\sigma_d^2}{\left(\sigma_d^2\beta_2+M_t\sigma_n^2\right)}, \qquad \tau = \frac{M_t}{M_r}. \tag{C.19}$$

Appendix D

Differentiation of S and Finding the Optimal α

D.1 Differentiation of S

S is shown in (4.49). Then,

$$\begin{aligned}\frac{\partial S}{\partial \alpha} &= \frac{\partial S}{\partial z}\frac{\partial z}{\partial \alpha} \\ &= \frac{\partial}{\partial z}\Bigg(\frac{M_t}{(M_r - M_t)!}\sum_{i=1}^{N}\log_2(M_i)(\mathrm{G}(M_r - M_t + 1, \epsilon_i z) \\ &\qquad - \mathrm{G}(M_r - M_t + 1, \epsilon_{i+1} z))\Bigg)\frac{\partial z}{\partial \alpha} \end{aligned} \tag{D.1}$$

where $z = \frac{1}{\delta\gamma_0}$. Differentiation of an incomplete gamma function is given by

$$\frac{\partial \mathrm{G}(a, x)}{\partial x} = -\exp(-x)x^{a-1}. \tag{D.2}$$

Then,

$$\begin{aligned}&\frac{\partial}{\partial z}\left(\mathrm{G}\left(M_r - M_t + 1, \epsilon_i z\right) - \mathrm{G}\left(M_r - M_t + 1, \epsilon_{i+1} z\right)\right) \\ &\qquad = \left(-\epsilon_i e^{-\epsilon_i z}(\epsilon_i z)^{M_r - M_t} + \epsilon_{i+1} e^{-\epsilon_{i+1} z}(\epsilon_{i+1} z)^{M_r - M_t}\right) \\ &\qquad = \left(-\epsilon_i^{M_r - M_t + 1} e^{-\epsilon_i z} + \epsilon_{i+1}^{M_r - M_t + 1} e^{-\epsilon_{i+1} z}\right) z^{M_r - M_t}. \end{aligned} \tag{D.3}$$

With (D.1) and (D.3), $\partial S/\partial \alpha$ can be obtained as

$$\frac{\partial S}{\partial \alpha} = \frac{M_t}{(M_r - M_t)!}\sum_{i=1}^{N}\log_2(M_i)\left(-\epsilon_i^{M_r - M_t + 1} e^{-\epsilon_i z} + \epsilon_{i+1}^{M_r - M_t + 1} e^{-\epsilon_{i+1} z}\right) z^{M_r - M_t}\frac{\partial z}{\partial \alpha}. \tag{D.4}$$

D.2 Finding α^* from $\partial S/\partial z$

$\partial S/\partial z$ is given by

$$\frac{\partial S}{\partial z} = \frac{M_t}{(M_r - M_t)!} \sum_{i=1}^{N} \log_2(M_i) \left(-\epsilon_i^{M_r - M_t + 1} e^{-\epsilon_i z} + \epsilon_{i+1}^{M_r - M_t + 1} e^{-\epsilon_{i+1} z} \right) z^{M_r - M_t}. \quad \text{(D.5)}$$

Since $\delta\gamma_0 > 0$ for $0 < \alpha < 1$, $z > 0$. Then,

$$\begin{aligned} &\sum_{i=1}^{N} \log_2(M_i) \left(-\epsilon_i^{M_r - M_t + 1} e^{-\epsilon_i z} + \epsilon_{i+1}^{M_r - M_t + 1} e^{-\epsilon_{N+1} z} \right) \\ &= \log_2 M_N \epsilon_{N+1}^{M_r - M_t + 1} e^{-\epsilon_{i+1} z} + \sum_{i=2}^{N} \left(\log_2 M_{i-1} - \log_2 M_i \right) \epsilon_i^{M_r - M_t + 1} e^{-\epsilon_i z} \\ &\qquad - \log_2 M_1 \epsilon_1^{M_r - M_t + 1} e^{-\epsilon_1 z}. \end{aligned} \quad \text{(D.6)}$$

The first term $\log_2 M_N \epsilon_{N+1} e^{-\epsilon_{i+1} z}$ goes to zero due to the definition of $\epsilon_{N+1} = \infty$. Since $(\log_2 M_{i-1} - \log_2 M_i)$ is negative for all i and $\epsilon_i > 0$ for $i \geq 2$, z (and α) which makes $\partial S/\partial z$ equal to zero cannot be found.

Bibliography

[1] S. R. 3GPP2, "High speed data enhancement for CDMA2000 1x-data only," June 2000.

[2] S. Adireddy, L. Tong, and H. Viswanathan, "Optimal placement of training for frequency-selective block-fading channels," *IEEE Transactions on Information Theory*, vol. 48, no. 8, pp. 2338–2353, Aug. 2002.

[3] D. Agarwal, V. Tarokh, A. F. Naguib, and N. Seshadri, "Space-time coded OFDM for high data rate wireless communication over wideband channels," *Proc., IEEE Vehicular Technology Conference*, vol. 3, pp. 2232–2236, May 1998.

[4] J. G. Andrews and T. H. Meng, "Performance of multicarrier CDMA with successive interference cancellation in a multipath fading channel," *IEEE Transactions on Communications*, vol. 52, pp. 811–822, May 2004.

[5] E. Baccarelli, M. Biagi, and C. Pelizzoni, "On the information throughput and optimized power allocation for MIMO wireless systems with imperfect channel estimation," *IEEE Transactions on Signal Processing*, vol. 53, pp. 2335–2347, July 2005.

[6] I. Barhumi, G. Leus, and M. Moonen, "Optimal training design for MIMO-OFDM systems in mobile wireless channels," *IEEE Transactions on Signal Processing*, vol. 51, no. 6, pp. 1615–1624, June 2003.

[7] P. Bender, P. Black, M. Grob, R. Padovani, N. Sindhushayana, and A. Viterbi, "CDMA/HDR: a bandwidth-efficient high-speed wireless data service for

nomadic users," *IEEE Communications Magazine*, vol. 38, pp. 70–77, July 2000.

[8] J. A. C. Bingham, "Multicarrier modulation for data transmission: an idea whose time has come," *IEEE Communications Magazine*, vol. 28, pp. 5–14, May 1990.

[9] H. Bolcskei, D. Gesbert, and A. J. Paulraj, "On the capacity of OFDM-based spatial multiplexing systems," *IEEE Transactions on Communications*, vol. 50, pp. 225–234, Feb. 2002.

[10] X. Cai and G. B. Giannakis, "Error probability minimizing pilots for OFDM with M-PSK modulation over Rayleigh-fading channels," *IEEE Transactions on Vehicular Technology*, vol. 53, no. 1, pp. 146–155, Jan. 2004.

[11] ——, "Adaptive PSAM accounting for channel estimation and prediction errors," *IEEE Transactions on Wireless Communications*, vol. 4, no. 1, pp. 246–256, Jan. 2005.

[12] Y. W. Cao, C. C. Ko, and T. T. Tjhung, "A new multi-code/multi-carrier DS-CDMA system," *Proc., IEEE Global Telecommunications Conference*, vol. 1, pp. 543–546, Nov. 2001.

[13] E. Casas and C. Leung, "OFDM for data communication over mobile radio FM channels. I. Analysis and experimental results," *IEEE Transactions on Communications*, vol. 39, no. 5, pp. 783–793, May 1991.

[14] S. Catreux, V. Erceg, D. Gesbert, and R. W. Heath, "Adaptive modulation and MIMO coding for broadband wireless data networks," *IEEE Communications Magazine*, vol. 40, no. 6, pp. 108–115, June 2002.

[15] R. W. Chang, "Synthesis of band limited orthogonal signlas for multichannel data transmission," *Bell System Technical Journal*, vol. 45, pp. 1775–1796, Dec. 1966.

[16] A. Chouly, A. Brajal, and S. Jourdan, "Orthogonal multicarrier techniques applied to direct sequence spread spectrum cdma systems," *Proc., IEEE Global Telecommunications Conference*, vol. 3, pp. 1723–1728, Nov. 1993.

[17] S. Chung and A. J. Goldsmith, "Degrees of freedom in adaptive modulation: a unified view," *IEEE Transactions on Communications*, vol. 49, no. 9, pp. 1561–1571, Sept. 2001.

[18] S. T. Chung and J. Cioffi, "Rate and power control in a two-user multicarrier channel with no coordination: the optimal scheme versus a suboptimal method," *IEEE Transactions on Communications*, vol. 51, no. 11, pp. 1768–1772, Nov. 2003.

[19] J. Cimini, L., "Analysis and simulation of a digital mobile channel using orthogonal frequency division multiplexing," *IEEE Transactions on Communications*, vol. 33, no. 7, pp. 665–675, July 1985.

[20] V. DaSilva and E. S. Sousa, "Performance of orthogonal CDMA codes for quasi-synchronous communication systems," *IEEE International Conference on Universal Personal Communications*, vol. 2, pp. 995–999, Oct. 1993.

[21] A. Dowler and A. Nix, "Performance evaluation of channel estimation techniques in a multiple antenna OFDM system," *Proc., IEEE Vehicular Technology Conference*, vol. 2, pp. 1214–1218, Oct. 2003.

[22] D. V. Duong, B. Holter, and G. E. Oien, "Optimal pilot spacing and power in rate-adaptive MIMO diversity systems with imperfect transmitter CSI," *IEEE Workshop on Signal Processing Advances in Wireless Communications*, pp. 47–51, June 2005.

[23] D. V. Duong, G. E. Oien, and K. J. Hole, "Adaptive coded modulation with receive antenna diversity and imperfect channel knowledge at receiver and

transmitter," *IEEE Transactions on Vehicular Technology*, vol. 55, pp. 458–465, Mar. 2006.

[24] H. Ekstrom, A. Furuskar, J. Karlsson, M. Meyer, S. Parkvall, J. Torsner, and M. Wahlqvist, "Technical solutions for the 3g long-term evolution," *IEEE Communications Magazine*, vol. 44, no. 3, pp. 38–45, Mar. 2006.

[25] H. El Gamal, G. Caire, and M. Damen, "The MIMO ARQ channel: Diversity-multiplexing-delay tradeoff," *IEEE Transactions on Information Theory*, vol. 52, no. 8, pp. 3601–3621, Aug. 2006.

[26] T. Eng and L. B. Milstein, "Coherent DS-CDMA performance in Nakagami multipath fading," *IEEE Transactions on Communications*, vol. 43, no. 234, pp. 1134–1143, Feb.-Mar.-Apr. 1995.

[27] European Telecommunication Standard, "Digital audio broadcasting (DAB) to mobile, portable, and fixed receiver, ETS 300 401," Feb. 1995.

[28] European Telecommunications Standards Institute, "Digital video broadcasting (DVB); interaction channel for digital terrestrial television (RCT) incorporating multiple access OFDM, ETSI EN 301 958," Mar. 2002.

[29] K. Fazel and S. Kaiser, *Multi-carrier and spread spectrum systems*. England: John Wiley and Sons, 2003.

[30] G. J. Foschini, "Layered space-time architecture for wireelss communication in a fading environment when using multielement antennas," *Bell Labs Technical Journal*, vol. 1, pp. 41–59, 1996.

[31] P. W. Fu and K. C. Chen, "Multi-rate MC-DS-CDMA with multi user detections for wireless multimedia communications," *Proc., IEEE Wireless Communications and Networking Conference*, vol. 3, pp. 1536–1540, May 2002.

[32] ——, "Multi-rate multi-carrier CDMA with multiuser detection for wireless multimedia communications," *Proc., IEEE Wireless Communications and Networking Conference*, vol. 1, pp. 385–390, Mar. 2003.

[33] H. U. Gerber, "From the generalized gamma to the generalized negative binomial distribution," *Insurance: Mathematics and Economics*, vol. 10, pp. 303–309, 1991.

[34] D. Gesbert, M. Shafi, D. Shiu, P. J. Smith, and A. Naguib, "From theory to practice: An overview of MIMO space-time coded wireless systems," *IEEE Journal on Selected Areas in Communications*, vol. 21, pp. 281–302, Apr. 2003.

[35] A. Ghosh, D. R. Wolter, J. G. Andrews, and R. Chen, "Broadband wireless access with WiMax/802.16: Current performance benchmarks and future potential," *IEEE Communications Magazine*, vol. 43, pp. 129–136, Feb. 2005.

[36] A. Glavieux, P. Cochet, and A. Picart, "Orthogonal frequency division multiplexing with BFSK modulation in frequency selective Rayleigh and Rician fading channels," *IEEE Transactions on Communications*, vol. 42, no. 234, pp. 1919–1928, Feb./Mar./Apr. 1994.

[37] A. Goldsmith, *Wireless Communications*. Cambridge university press, 2005.

[38] A. J. Goldsmith and S.-G. Chua, "Variable-rate variable-power MQAM for fading channels," *IEEE Transactions on Communications*, vol. 45, no. 10, pp. 1218–1230, Oct. 1997.

[39] A. J. Goldsmith and L. Greenstein, "Effect of average power estimation error on adaptive MQAM modulation," *Proc., IEEE International Conference on Communications*, vol. 2, pp. 1105–1109, June 1997.

[40] D. A. Gore, R. W. Heath, and A. J. Paulraj, "Transmit selection in spatial multiplexing systems," *IEEE Communications Letters*, vol. 6, no. 11, pp. 491–493, Nov. 2002.

[41] I. S. Gradshteyn and I. M. Ryzhik, *Table of Integrals, Series, and Products*, 1st ed. NY: Academic Press Inc., 1994.

[42] X. Gui and T. S. Ng, "Performance of asynchronous orthogonal multicarrier CDMA system in a frequency selective fading channel," *IEEE Transactions on Communications*, vol. 47, no. 7, pp. 1084–1091, July 1999.

[43] S. Hara and R. Prasad, "Overview of multicarrier CDMA," *IEEE Communications Magazine*, vol. 35, pp. 126–133, Dec. 1997.

[44] B. Hassibi and B. M. Hochwald, "How much training is needed in multiple-antenna wireless links?" *IEEE Transactions on Information Theory*, vol. 49, no. 4, pp. 951–963, Apr. 2003.

[45] B. Hassibi and B. Hochwald, "High-rate codes that are linear in space and time," *IEEE Transactions on Information Theory*, vol. 48, no. 7, pp. 1804–1824, July 2002.

[46] R. W. Heath and D. J. Love, "Multimode antenna selection for spatial multiplexing systems with linear receivers," *IEEE Transactions on Signal Processing*, vol. 53, no. 8, pp. 3042–3056, Aug. 2005.

[47] R. W. Heath and A. J. Paulraj, "Switching between diversity and multiplexing in mimo systems," *IEEE Transactions on Communications*, vol. 53, pp. 962–968, June 2005.

[48] D. Hong, T. Kim, D. Hong, and C. Kang, "Pilot to data channel power allocation for PCA-DS/CDMA with interference canceler," *IEEE Communications Letters*, vol. 5, pp. 331–333, Aug. 2001.

[49] Z. Hong, K. Liu, R. W. Heath, and A. M. Sayeed, "Spatial multiplexing in correlated fading via the virtual channel representation," *IEEE Journal on Selected Areas in Communications*, vol. 21, pp. 856–866, June 2003.

[50] C. L. I and R. D. Gitlin, "Multi-code CDMA wireless personal communications networks," *Proc., IEEE International Conference on Communications*, vol. 2, pp. 1060–1064, June 1995.

[51] C. L. I, G. P. Pollini, L. Ozarow, and R. D. Gitlin, "Performance of multi-code CDMA wireless personal communications networks," *Proc., IEEE Vehicular Technology Conference*, vol. 2, pp. 907–911, July 1995.

[52] IEEE Std 802.16e-2005, "IEEE Standard for local and metropolitan area networks - Part 16: Air interface for fixed broadband wireless access systems - Amendment 2: medium access control modifications and additional physical layer specifications for 2-11 GHz," Feb. 28 2006.

[53] J. Jang and K. B. Lee, "Transmit power adaptation for multiuser OFDM systems," *IEEE Journal on Selected Areas in Communications*, vol. 21, no. 2, pp. 171–178, Feb. 2003.

[54] I. Kalet, "The multitone channel," *IEEE Transactions on Communications*, vol. 37, no. 2, pp. 119–124, Feb. 1989.

[55] A. P. Kannu and P. Schniter, "Reduced-complexity decision-directed pilot-aided tracking of doubly-selective channels," *Proc. Conference on Information Sciences and Systems, (Princeton, NJ)*, pp. 915–920, Mar. 2004.

[56] ——, "Capacity analysis of mmse pilot-aided transmission for doubly selective channels," *Signal Processing Advances in Wireless Communications, 2005 IEEE 6th Workshop on*, pp. 801–805, June 2005.

[57] T. Keller and L. Hanzo, "Adaptive multicarrier modulation: a convenient framework for time-frequency processing in wireless communications," *Proceedings of the IEEE*, vol. 88, no. 5, pp. 611–640, May 2000.

[58] T. Kim and J. G. Andrews, "Optimal pilot-to-data power ratio for MIMO-OFDM," *Proc., IEEE Global Telecommunications Conference*, vol. 3, pp. 1481–1485, Dec. 2005.

[59] ——, "Optimal Pilot-to-Data Power Ratio Simulator for MIMO-OFDM Using NI LabVIEW 7.1," *NIWeek 2005 Paper Contest*, Aug. 2005.

[60] ——, "Optimal pilot-to-data power ratio for MIMO-OFDM in mobile channels," *IEEE Transactions on Vehicular Technology*, Sept. 2006, Submitted.

[61] ——, "Optimally balancing data and pilot power for adaptive MIMO-OFDM systems," *IEEE Transactions on Wireless Communications*, Aug. 2006, Submitted.

[62] ——, "Balancing pilot and data power for adaptive MIMO-OFDM systems," *Proc., IEEE Global Telecommunications Conference*, Dec. 2006, to appear.

[63] T. Kim, J. G. Andrews, J. Kim, and T. S. Rappaport, "Multi-code Multicarrier CDMA: Performance Analysis," *Journal of Communications Software and Systems (JCOMSS), special issue on Future Wireless Systems*, vol. 2, no. 1, pp. 12–19, Mar. 2006.

[64] T. Kim, J. Kim, J. G. Andrews, and T. S. Rappaport, "Multi-code multicarrer CDMA: Performance analysis," *Proc., IEEE International Conference on Communications*, vol. 2, pp. 973–977, June 2004.

[65] I. Koffman and V. Roman, "Broadband wireless access solutions based on OFDM access in IEEE 802.16," *IEEE Communications Magazine*, vol. 40, no. 4, pp. 96–103, Apr. 2002.

[66] I. E. Leonard, "The matrix exponential," *SIAM Review*, vol. 38, no. 3, pp. 507–512, Sept. 1996.

[67] P. Li, D. Paul, R. Narasimhan, and J. Cioffi, "On the distribution of SINR for the MMSE MIMO receiver and performance analysis," *IEEE Transactions on Information Theory*, vol. 52, no. 1, pp. 271–286, Jan. 2006.

[68] Y. G. Li, "Simplified channel estimation for OFDM systems with multiple transmit antennas," *IEEE Transactions on Wireless Communications*, vol. 1, pp. 67–75, Jan. 2002.

[69] Y. G. Li, N. Seshadri, and S. Ariyavisitakul, "Channel estimation for OFDM systems with transmitter diversity in mobile wireless channels," *IEEE Journal on Selected Areas in Communications*, vol. 17, pp. 461–470, Mar. 1999.

[70] Y. G. Li and N. R. Sollenberger, "Clustered OFDM with channel estimation for high rate wireless data," *IEEE Transactions on Communications*, vol. 49, no. 12, pp. 2071–2076, Dec. 2001.

[71] Y. G. Li, J. H. Winters, and N. R. Sollenberger, "MIMO-OFDM for wireless communications: signal detection with enhanced channel estimation," *IEEE Transactions on Communications*, vol. 50, pp. 1471–1477, Sept. 2002.

[72] S. Lin and D. J. Costello, *Error control coding*, 2nd ed. Upper Saddle River, New Jersey: Pearson Prentice Hall, 2004.

[73] L. Litwin, "An introduction to multicarrier modulation," *IEEE Potentials*, vol. 19, no. 2, pp. 36–38, Apr.-May 2000.

[74] Z. Liu, Y. Xin, and G. B. Giannakis, "Space-time-frequency coded OFDM over frequency-selective fading channels," *IEEE Transactions on Signal Processing*, vol. 50, pp. 2465–2476, Oct. 2002.

[75] X. Ma, G. B. Giannakis, and S. Ohno, "Optimal training for block transmissions over doubly-selective wireless fading channels," *IEEE Transactions on Signal Processing*, vol. 51, pp. 1351–1366, May 2003.

[76] X. Ma, L. Yang, and G. B. Giannakis, "Optimal training for MIMO frequency-selective fading channels," *Proc., IEEE Asilomar*, vol. 2, pp. 1107–1111, Nov. 2002.

[77] X. Ma, L. Yang, and G. Giannakis, "Optimal training for MIMO frequency-selective fading channels," *IEEE Transactions on Wireless Communications*, vol. 4, no. 2, pp. 453–466, Mar. 2005.

[78] U. Mitra, "Comparison of maximum-likelihood-based detection for two multi-rate access schemes for CDMA signals," *IEEE Transactions on Communications*, vol. 47, pp. 64–67, Jan. 1999.

[79] A. F. Molisch, M. Z. Win, and J. H. Winters, "Space-time-frequency (STF) coding for MIMO-OFDM systems," *IEEE Communications Letters*, vol. 6, pp. 370–372, Sept. 2002.

[80] Motorola, "Technical overview of 1xEV-DV," White paper, Motorola Inc., Sept. 2002, version G1.4. [Online]. Available: http://www.cdg.org

[81] R. J. Muirhead, *Aspects of multivariate statistical theory*. Wiley-Interscience, 1982.

[82] S. A. Mujtaba, "TGn Sync proposal technical specification, IEEE802.11-04/0889r6," May 2005.

[83] R. Narasimhan, "Finite-SNR diversity&ultiplexing tradeoff for correlated Rayleigh and rician MIMO channels," *IEEE Transactions on Information Theory*, vol. 52, no. 9, pp. 3965–3979, Sept. 2006.

[84] C. Nassar, B. Natarajan, Z. Wu, D. Wiegandt, S. A. Zekavat, and S. Shattil, *Multi-carrier technolobies for wireless communication*. Boston: Kluwer Academic Publishers, 2002.

[85] R. Negi and J. Cioffi, "Pilot tone selection for channel estimation in a mobile OFDM system," *IEEE Transactions on Consumer Electronics*, vol. 44, pp. 1122–1128, Aug. 1998.

[86] S. Ohno and G. B. Giannakis, "Capacity maximizing MMSE-optimal pilots for wireless OFDM over frequency-selective block Rayleigh fading channel," *IEEE Transactions on Information Theory*, vol. 50, pp. 2138–2145, Sept. 2004.

[87] T. Ottosson and A. Svensson, "Multi-rate schemes in DS/CDMA systems," *Proc., IEEE Vehicular Technology Conference*, vol. 2, pp. 1006–1010, Jan. 1995.

[88] J. F. Paris, M. C. Aguayo-Torres, and J. T. Entrambasaguas, "Impact of channel estimation error on adaptive modulation performance in flat fading," *IEEE Transactions on Communications*, vol. 52, no. 5, pp. 716–720, May 2004.

[89] T. Park, J. Jang, O.-S. Shin, and K. B. Lee, "Transmit power allocation for a downlink two-user interference channel," *IEEE Communications Letters*, vol. 9, no. 1, pp. 13–15, Jan. 2005.

[90] A. Paulraj, D. A. Gore, R. U. Nabar, and H. Bolcskei, "An overview of MIMO communications - a key to gigabit wireless," *Proceedings of the IEEE*, vol. 92, no. 2, pp. 198–218, Feb. 2004.

[91] A. Paulraj and T. Kailath, "Increasing capacity in wireless broadcast systems using distributed transmission/directional reception (DTDR)," U.S. Patent 5345599, Sept. 6 1994.

[92] A. J. Paulraj and C. B. Papadias, "Space-time processing for wireless communications," *IEEE Signal Processing Magazine*, vol. 14, pp. 49–83, Nov. 1997.

[93] J. G. Proakis, *Digital communications*, 4th ed. New York, NY: 4th edition, New York : McGraw-Hill, 2001.

[94] T. S. Rappaport, *Wireless communications, principles and practice*, 2nd ed. Upper Saddle River, NJ: Prentice Hall PTR, 2002.

[95] T. S. Rappaport, A. Annamalai, R. M. Buehrer, and W. H. Tranter, "Wireless communications: Past events and a future perspective," *IEEE Communications Magazine*, vol. 40, pp. 148–161, May 2002.

[96] D. Samardzija and N. Mandayam, "Pilot-assisted estimation of MIMO fading channel response and achievable data rates," *IEEE Transactions on Signal Processing*, vol. 51, no. 11, pp. 2882–2890, Nov. 2003.

[97] H. Sampath, S. Talwar, J. Tellado, V. Erceg, and A. J. Paulraj, "A fourth-generation MIMO-OFDM broadband wireless system: design, performance, and field trial results," *IEEE Communications Magazine*, vol. 40, pp. 143–149, Sept. 2002.

[98] P. Schniter, "Low-complexity estimation of doubly-selective channels," *IEEE Workshop on Signal Processing Advances in Wireless Communications, SPAWC*, pp. 200–204, June 2003.

[99] H. D. Schotten, H. Elders-Boll, and A. Busboom, "Multi-code CDMA with variable sequence-sets," *Proc., IEEE International Conference on Universal Personal Communications*, vol. 2, pp. 628–631, Oct. 1997.

[100] ——, "Adaptive multi-rate multi-code CDMA systems," *Proc., IEEE Vehicular Technology Conference*, vol. 2, pp. 782–785, May 1998.

[101] P. Schramm, "Analysis and optimization of pilot-channel-assisted BPSK for DS/CDMA systems," *IEEE Transactions on Communications*, vol. 46, pp. 1122–1124, Sept. 1998.

[102] S. Sfar, L. Dai, and K. Letaief, "Optimal diversity-multiplexing tradeoff with group detection for mimo systems," *IEEE Transactions on Communications*, vol. 53, no. 7, pp. 1178–1190, July 2005.

[103] Z. Shen, J. G. Andrews, and B. L. Evans, "Adaptive resource allocation in multiuser ofdm systems with proportional rate constraints," *IEEE Transactions on Wireless Communications*, vol. 4, no. 6, pp. 2726–2737, Nov. 2005.

[104] S. Simoens, P. Pellati, J. Gosteau, K. Gosse, and C. Ware, "The evolution of 5GHz WLAN toward higher throughputs," *IEEE Wireless Communications*, vol. 10, no. 6, pp. 6–13, Dec. 2003.

[105] E. A. Sourour and M. Makagawa, "Performance of orthogonal multicarrier CDMA in a multipath fading channel," *IEEE Transactions on Communications*, vol. 44, no. 3, pp. 356–367, Mar. 1996.

[106] G. L. Stuber, J. R. Barry, S. W. McLaughlin, Y. G. Li, M. A. Ingram, and T. G. Pratt, "Broadband MIMO-OFDM wireless communications," *Proceedings of the IEEE*, vol. 92, pp. 271–294, Feb. 2004.

[107] Y. Sun, "Bandwidth-efficient wireless OFDM," *IEEE Journal on Selected Areas in Communications*, vol. 19, no. 11, pp. 2267–2278, Nov. 2001.

[108] V. Tarokh, H. Jafarkhani, and A. R. Calderbank, "Space-time block codes from orthogonal designs," *IEEE Transactions on Information Theory*, vol. 45, pp. 1456–1467, July 1999.

[109] V. Tarokh, N. Seshadri, and A. R. Calderbank, "Space-time codes for high data rate wireless communication: Performance criterion and code construc-

tion," *IEEE Transactions on Information Theory*, vol. 44, pp. 744–765, Mar. 1998.

[110] D. Tse, P. Viswanath, and L. Zheng, "Diversity-multiplexing tradeoff in multiple-access channels," *IEEE Transactions on Information Theory*, vol. 50, pp. 1859–1874, Sept. 2004.

[111] J.-J. van de Beek, P. Borjesson, M.-L. Boucheret, D. Landstrom, J. Arenas, P. Odling, C. Ostberg, M. Wahlqvist, and S. Wilson, "A time and frequency synchronization scheme for multiuser OFDM," *IEEE Journal on Selected Areas in Communications*, vol. 17, no. 11, pp. 1900–1914, Nov. 1999.

[112] L. Vandendorpe, "Multitone spread spectrum multiple access communications system in a multipath rician fading channel," *IEEE Transactions on Vehicular Technology*, vol. 44, no. 2, pp. 327–337, May 1995.

[113] D. Vassis, G. Kormentzas, A. Rouskas, and I. Maglogiannis, "The IEEE 802.11g standard for high data rate WLANs," *IEEE Network*, vol. 19, no. 3, pp. 21–26, May-June 2005.

[114] H. Vikalo, B. Hassibi, B. Hochwald, and T. Kailath, "On the capacity of frequency-selective channels in training-based transmission schemes," *IEEE Transactions on Signal Processing*, vol. 52, pp. 2572–2583, Sept. 2004.

[115] S. Vishwanath and A. Goldsmith, "BER bounds for turbo coded modulation and their application to adaptive modulation," *IEEE International Symposium on Information Theory*, p. 193, June 2000.

[116] ——, "Adaptive turbo-coded modulation for flat-fading channels," *IEEE Transactions on Communications*, vol. 51, no. 6, pp. 964–972, June 2003.

[117] Z. Wang and G. B. Giannakis, "Wireless multicarrier communications," *IEEE Signal Processing Magazine*, vol. 17, pp. 29–48, May 2000.

[118] S. Weinstein and P. Ebert, "Data transmission by frequency-division multiplexing using the discrete fourier transform," *IEEE Transactions on Communications*, vol. 19, no. 5, pp. 628–634, Oct. 1971.

[119] C. Y. Wong, R. S. Cheng, K. B. Lataief, and R. Murch, "Multiuser OFDM with adaptive subcarrier, bit, and power allocation," *IEEE Journal on Selected Areas in Communications*, vol. 17, no. 10, pp. 1747–1758, Oct. 1999.

[120] J. Xie and P. Fan, "Throughput maximization of adaptive MQAM and the effects of inaccurate feedback channel estimation," *Proceedings of the Fourth International Conference on Parallel and Distributed Computing, Applications and Technologies*, pp. 404–407, Aug. 2003.

[121] H. Yang, "A road to future broadband wireless access: MIMO-OFDM-based air interface," *IEEE Communications Magazine*, vol. 43, no. 1, pp. 53–60, Jan. 2005.

[122] L. Yang and L. Hanzo, "Multicarrier DS-CDMA: a multiple access scheme for ubiquitous broadband wireless communications," *IEEE Communications Magazine*, vol. 41, pp. 116–124, Oct. 2003.

[123] N. Yee, J.-P. Linnartz, and G. Fettweis, "Multi-carrier CDMA in indoor wireless radio networks," *Proc., IEEE International Symposium on Personal, Indoor and Mobile Radio Communications*, pp. 109–113, Sept. 1993.

[124] D. Yoo and W. E. Stark, "Characterization of WSSUS channels: Normalized mean square covariance," *IEEE Transactions on Wireless Communications*, vol. 4, pp. 1575–1584, 2005.

[125] ——, "Stochastic degree of freedom and WSSUS channel diversity," *IEEE Transactions on Wireless Communications*, Submitted.

[126] D. Yoon and K. Cho, "General bit error probability of rectangular quadrature amplitude modulation," *Electronics Letters*, vol. 38, pp. 131–133, Jan. 2002.

[127] L. Zheng and D. Tse, "Diversity and multiplexing: A fundamental tradeoff in multiple antenna channels," *IEEE Transactions on Information Theory*, vol. 49, no. 5, pp. 1073–1096, May 2003.

[128] S. Zhou and G. B. Giannakis, "Adaptive modulation for multiantenna transmissions with channel mean feedback," *IEEE Transactions on Wireless Communications*, vol. 3, no. 5, pp. 1626–1636, Sept. 2004.

[129] ——, "How accurate channel prediction needs to be for transmit-beamforming with adaptive modulation over Rayleigh MIMO channels?" *IEEE Transactions on Wireless Communications*, vol. 3, no. 4, pp. 1285–1294, July 2004.

[130] Z. Zhou, B. Vucetic, M. Dohler, and Y. Li, "MIMO systems with adaptive modulation," *IEEE Transactions on Vehicular Technology*, vol. 54, no. 5, pp. 1828–1842, Sept. 2005.

Vita

Tae Yoon Kim received his B.S. in Electronic Engineering and M.S. in Electrical and Computer Engineering from Yonsei University, Seoul, South Korea in 1998 and 2000, respectively. During the summers of 2005 and 2006, He interned as a research engineer at Freescale Semiconductor in Austin, Texas. Taeyoon was awarded a fellowship from the South Korean Ministry of Information and Communication from 2002 to 2006. He also received the David Bruton, Jr. Graduate Fellowship for the 2004-2005 academic year by The Office of Graduate Studies at The University of Texas at Austin. Taeyoon has been a member of the Institute of Electrical and Electronics Engineers (IEEE) since 2003.

Permanent address: 6800 Austin Center Blvd. #1322,
Austin, TX 78731, USA

This dissertation was typeset with LaTeX[†] by the author.

[†]LaTeX is a document preparation system developed by Leslie Lamport as a special version of Donald Knuth's TeX Program.